Technical Report

454

H. M. Heggestad

Optical Communication Through Multiple-Scattering Media

22 November 1968

Lincoln Laboratory

MASSACHUSETTS INSTITUTE OF TECHNOLOGY

Lexington, Massachusetts

MASSACHUSETTS INSTITUTE OF TECHNOLOGY

LINCOLN LABORATORY

OPTICAL COMMUNICATION
THROUGH MULTIPLE-SCATTERING MEDIA

H. M. HEGGESTAD

Group 45

LEXINGTON   MASSACHUSETTS

OPTICAL COMMUNICATION THROUGH MULTIPLE-SCATTERING MEDIA[*]

ABSTRACT

A model is developed for the effects of multiple scattering upon optical-frequency radiation. Attention is focused upon situations in which the scattering particles are large compared to the carrier wavelength, so that forward-scattering predominates. This is the case for atmospheric clouds at visible-light wavelengths, the physical framework within which the analysis is carried out. The objectives served by the model are those of a communications engineer desiring to design a system for optical communication through clouds.

Light traversing optically dense clouds suffers dispersion in space, time and frequency. These effects are considered both separately and in a compact unified formulation. The spatial variation of the intensity of light beneath a cloud subjected to continuous-wave illumination is modeled as the output of a multidimensional linear system. The approximate impulse response of the system is determined, in two complementary forms, and the approximate response below the cloud under arbitrary illumination is shown to be given by a linear superposition integral. In general, the spatial behavior is representable as a joint function of angle of arrival and horizontal coordinates over the ground.

The field on the ground is shown to be representable in terms of a complex Gaussian random process. A complete statistical description of the process is therefore provided by its mean (which is zero) and its correlation function. The time-space correlation function $K(t_1, t_2, \vec{r}_1, \vec{r}_2)$ is written in terms of a generalized scattering function $\sigma(\tau, f, \vec{v}')$, combining all the time, frequency and spatial information. The spatial impulse responses are shown to be special cases of the scattering function. Expressions are derived for the spatial correlation function of the received field over the ground, for both omnidirectional and directive antennas. The conventional range-Doppler scattering function $\sigma(\tau, f)$ is derived for an upward-pointing narrow-beam antenna. Polarization effects are not included in any of the analyses.

Some of the implications of these results are considered with respect to communications system design and performance. A system is proposed and analyzed to provide an indication of the rates and error performance that can be achieved with optical signaling through a cloud.

---

[*] This report is based on a thesis of the same title submitted to the Department of Electrical Engineering at the Massachusetts Institute of Technology on 24 October 1968 in partial fulfillment of the requirements for the degree of Doctor of Science.

CONTENTS

ACKNOWLEDGMENTS

OPTICAL COMMUNICATION
THROUGH MULTIPLE-SCATTERING MEDIA

CHAPTER 1
INTRODUCTION

Clouds and fog are common enough in most regions of the earth to present a serious problem to the designer of an optical communication system whose transmission path includes the atmosphere. One alternative is simply to agree that the link will not be usable when these obstructions are present. In many applications one might be unable to accept such a constraint, but willing to trade receiver complexity and diminished communication rates for more nearly constant channel availability. This possibility motivated the research reported in this paper. The chief objective was the development of a realistic model for a cloud layer as an optical-frequency communication channel.

A small particle suspended in the atmosphere absorbs a portion of the light incident on it, in general, and scatters the remainder in all directions. The particles in clouds are droplets composed mainly of liquid water, and their diameters[1] range from about 10 to 40 microns. Since they are large compared with the wavelengths of visible light, they tend to scatter most of the incident energy at these wavelengths in the forward direction. Also, their absorption at visible-light frequencies is small. Thus a large fraction of the light entering a cloud emerges at the other side. A beam of light traversing a cloud will suffer dispersion in angle of arrival and degradation of spatial coherence, while any modulating signal which may have been carried by the beam will experience dispersion in time and frequency. These deleterious effects become progressively more severe as the particle concentration increases. For typical clouds, one finds that most of the emerging light has been scattered more than once. All the results reported here account for the presence of this multiple scattering.

We take the point of view that an observer standing beneath a cloud illuminated from above is interested only in the light emerging from the bottom of the cloud. We do not attempt to calculate intensity distributions or other characteristics of the backscattered light. All the energy which is lost from the forward-directed signal in this manner is treated as though it were lost by absorption in the cloud.

The analysis in this report depends heavily upon the condition that most of the light incident on each individual particle is scattered in a generally forward direction. This is demonstrably true for clouds at visible wavelengths, as we have already indicated; in general, it is true for any situation in which the particle diameter is large compared with the wavelength of the incident radiation. Although all our analyses are couched in terms of a somewhat idealized model for a cloud, most of our results can be applied for communication through fog as well by simply letting both the transmitter and the receiver be located right at the cloud boundaries. Although natural fog particles tend to be somewhat smaller than those of clouds (their diameter distributions[2] tend to peak up in the neighborhood of 4 to 6 microns), they are still quite large compared with visible wavelengths. Thus the light scattered by fog particles is also quite strongly forward-directed.

The applicability of our results to optical communication through atmospheric hazes is somewhat questionable, and has not yet been investigated in any detail. Hazes generally contain many particles roughly comparable in size to visible-light wavelengths,[3] which scatter substantial amounts of light through large angles. This tends to violate our assumption that any light which is scattered through an accumulated total angle of about 2π radians is so attenuated as to be negligible compared with the forward-scattered light.

Section 1.1 describes the effects of a cloud upon the angular and spatial properties of the transmitted light. Section 1.2 provides a brief description of the generalized space-time-frequency scattering function presented in Chapter 4, which is the most general form of our cloud-channel communication model. Section 1.3 outlines the body of this report.

1.1 SPATIAL DISPERSION OF LIGHT TRAVERSING A CLOUD

Chapter 3 of this report is an analysis of the angular and spatial distributions of light beneath optically thick clouds. The topic is treated separately, and an entire section of this introductory chapter is devoted to it, because it is potentially of interest in areas outside of communications theory. The incident light is assumed to have constant intensity, and the results are derived without reference to communications-oriented concepts such as bandwidth and modulation.

We define a simplified representation for both the incident and the scattered light as a superposition of elementary waves, specifying the distribution of light intensity in angle and in position on the horizontal plane. By using the ideas and techniques of linear system theory, we show how this mathematical function is modified as the light traverses the cloud. We find that the intensity distribution below a cloud with arbitrary illumination incident on its upper surface is given by a multidimensional linear superposition integral.

The results are obtained in two complementary forms. One of them is appropriate for incident illumination which is uniform over the entire horizontal plane, while the other must be used for beams of finite cross-sectional area. We show that the first result is simply a special case of the second.

As an example of the utility of these results, suppose that one illuminates the top of a cloud with a group of constant-intensity uniform plane waves, having angles of arrival distributed over some range. By application of the first kind of superposition integral, we immediately obtain the distribution of intensity as a function of angle of arrival over the ground below the cloud. As another example, suppose the top of the cloud is illuminated with a pencil beam incident at horizontal coordinates (x_o, y_o). The second form of the superposition integral yields the distribution of intensity over the ground as a joint function of angle of arrival and the horizontal coordinates x and y.

1.2 CHARACTER OF CHANNEL

As one might well expect, the field incident on the ground beneath a cloud can be represented as a complex Gaussian random process. The arguments leading to this conclusion are presented in detail in Appendix A. Since a signal traversing the cloud suffers time and frequency dispersion as well, we anticipate that a signal detected on the ground will be qualitatively similar to one which was transmitted over a classical fading dispersive channel. The problem is complicated, however, by the fact that the spatial and angular variation of the arriving field are both important and useful. In Chapter 4 we present a generalized scattering function $\sigma(\tau, f, \vec{v}')$, first suggested by Kennedy,[4] which combines all this information about the channel in a useful, compact

form. The vector argument $\vec{v}'$ may be thought of as a unit vector pointing in some direction, drawn through some point (x, y) on the ground plane. The function $\sigma(\ )$ is defined in such a way that the quantity $\sigma(\tau, f, \vec{v}')\, d\tau\, df\, d\vec{v}'$ is the fraction of total received signal energy at the point (x, y) on the ground borne by rays which experienced time delay and Doppler shift in the ranges $(\tau, \tau + dt)$ and $(f, f + df)$, and had angles of arrival in the range $d\vec{v}'$ about $\vec{v}'$. We derive the function from basic assumptions, and present a brief discussion of the manner in which one would proceed to a mathematical description of the optimum communication receiver from knowledge of $\sigma(\ )$ and the transmitted signal.

Declining to carry the general treatment any further, we proceed to derivations and discussions of various special cases of the scattering function and signal correlation functions. We show that the spatial superposition integrals of Chapter 3 are in fact special cases of $\sigma(\tau, f, \vec{v}')$. The other specialized functions based on $\sigma(\ )$ that we discuss include a time-independent spatial correlation function of the field over the ground, angular and spatial correlation functions for signals received by directive antennas, the range scattering function $\sigma(\tau)$ for an antenna aimed in a given direction, and the range-Doppler scattering function $\sigma(\tau, f)$ for the same antenna.

1.3 OUTLINE OF REPORT

A large body of literature exists on the subject of electromagnetic scattering by particles. Chapter 2 is devoted to a brief survey of some of this material, with particular emphasis on those results which will be exploited in the remainder of the report. Chapters 3 and 4 have just been discussed. Because their contents are thought to be of particular interest, they have each been accorded an entire section of this chapter for introductory comments.

In Chapter 5 we propose a sub-optimum communication system which could be realized with techniques and components which are available or readily visualized as being available in the future. Since it falls within the purview of classical fading dispersive channel analyses, we can readily analyze its performance. The results give us some feeling for the performance one might expect with the optimum system.

Chapter 6 summarizes the conclusions we have reached in this report, and outlines areas of potentially fruitful future research on optical cloud communication. The appendices deal with matters which are peripheral to the main issues in the body of the report, and with long and complicated derivations.

3

CHAPTER 2
AVAILABLE RESULTS OF SCATTERING THEORY

The scattering of electromagnetic radiation by particles has been studied extensively for many years. The scattering behavior of collections of particles has been thoroughly analyzed for situations in which single scattering predominates. For a particle suspension so dense that a substantial fraction of the light traversing it has been scattered more than once, however, the problem becomes far more complex. A number of books and papers have been written about specialized aspects of multiple scattering (of which this thesis report is an example), but the status of research on the general problem is still very fluid.

The first section of this chapter is a brief survey of the literature on both single and multiple scattering of light. In Sec. 2.2 we review those results of single-scattering theory which will be utilized in the development of our linear-system model for multiple scattering.

2.1 HISTORICAL DEVELOPMENT

A concise review of the early history of the subject of electromagnetic scattering by particles is given by van de Hulst[5] in his Sec. 1.3. The problem of the scattering of electromagnetic waves by a single homogeneous sphere was first solved in complete generality by Mie.[6] His approach was to represent the fields in space as a superposition of spherical waves which were concentric with the scatterer. The solution of the boundary-value problem in this coordinate system was straightforward. He obtained completely accurate and general formulas for the scattered field in the presence of a sphere of arbitrary radius and arbitrary complex refractive index, for incident radiation of arbitrary wavelength.

Virtually all electromagnetic scattering research since that time has been based upon the fundamental work of Mie. The first logical extension of his results was the analysis of light scattering by low-density suspensions of particles. By assumption, the volume density of particles in such suspensions is small enough that light scattered more than once can be neglected compared to unscattered and single scattered light. Many authors have attacked this problem; excellent treatments of the subject are provided by, for example, van de Hulst[1] and Newton.[7] The usual approach has been to show that the angular distribution of light traversing such a medium is simply a superposition of unscattered light and the scattering pattern of a single particle, averaged over the distribution of particle sizes in the medium.

For denser suspensions of particles, however, a significant fraction of the emerging light has been scattered more than once. The mathematical complexity of the multiple scattering problem is enormous, compared to the simpler results described above. The first successful treatment of the problem was that of Chandrasekhar,[8] who attacked light propagation through multiple-scattering media as a transport phenomenon. He derived an elegant diffusion equation (his "Equation of Radiative Transfer") for the angular distribution of scattered intensity. His work has been widely applied in such areas as the study of planetary atmospheres in radio astronomy. In practice, his equation is extremely difficult to solve, except when the particles scatter isotropically, or nearly so. His ideas have been extended, and additional results of the same general nature have been obtained by Sobolev.[9] Like those of Chandrasekhar, his equations for angular intensity distributions of diffuse scattered radiation are very difficult to solve except in a few special cases.

Certain other multiple-scattering results have been obtained by Fritz.[10-12] He modeled the scattering pattern of an individual cloud droplet as a superposition of forward-scattered

and isotropically scattered intensities; the latter were smaller by a factor of several hundred. His main results were angular distributions of luminance and illuminance below an overcast sky, which he obtained by the approximate solution of a diffusion equation. Like the work described in the preceding paragraph, Fritz's techniques do not have enough versatility to provide the additional information (such as spatial correlation functions and time and frequency spreading of signals) required for a useful optical communications model.

A substantial number of papers have appeared in recent literature, reporting experimental work on single and multiple scattering of light. For example, Carrier and Nugent[13] and Reisman, et al.,[14] have carried out measurements of light scattered by fogs in air as a function of angle. Smart, et al.,[15] Woodward[16,17] and a number of other workers have made angular intensity distribution measurements of light scattered by water suspensions of polystyrene latex spheres, where the particle concentration was high enough that multiple scattering was important.

Certain other results have recently been obtained which are more directly applicable to the questions of interest in optical communication. Dell-Imagine[18] used numerical integration of Chandrasekhar's equation of radiative transfer to obtain the transient response of a cloud illuminated from above by a plane wave which was turned on at some instant of time. In a series of four articles, Plass and Kattawar[19-22] have reported on a Monte Carlo technique which accurately follows the multiple scattered paths of photons through thick clouds. They have obtained numerical simulations of the cloud albedo and of the angle dependence of reflected and transmitted light, as functions of various parameters of the clouds and the particles, the wavelength and incident angle of the incoming light, and the albedo of the planetary surface. They have also obtained information about the optical path lengths traversed by photons penetrating clouds.

In Appendix G we carry out explicit comparisons of our results with some of those of Dell-Imagine and of Plass and Kattawar.

2.2 BASIC DESCRIPTION OF SINGLE SCATTERING

The study of multiple scattering must begin with an understanding of the mechanism of plane-wave scattering by a single particle. Thorough expositions of the theory of electromagnetic scattering by homogeneous spheres are contained in the original paper of Mie,[6] in the classical book by Stratton,[23] and in the cited works of van de Hulst[1] and Newton.[7] In general, the amplitude, phase, state of polarization and direction of propagation of the scattered wave can be precisely determined as functions of the parameters of the sphere and the incident wave. Although the formulas of Mie are elegant in their generality, their application to specific cases involves a great deal of computational labor. Our task is somewhat simpler, because we choose to ignore polarization effects. Furthermore, as we show in Appendix A, we need not retain phase information, since phase coherence is lost in the multiple-scattering process. Thus the only result we need from the Mie theory is the sum of the intensity scattering patterns for the two orthogonal polarization components, for a spherical particle of radius a at a given wavelength. We shall call it $F_a(\Theta)$. Its argument is the angle between the incident-wave propagation vector and the direction of propagation of scattered radiation. The function is conventionally defined in such a way that the intensity of light scattered into the solid angle

$$d\omega = \sin \Theta \, d\Theta \, d\varphi$$

is given by $F_a(\Theta) \, d\omega$, when the particle is illuminated by a unit-intensity plane wave. Assumptions and approximations to be used in the present study will be developed in Chapter 3.

It is convenient to describe the behavior of a scattering particle in a cloud in terms of its cross sections. Suppose a particle intercepts P_i watts of power from an incident plane wave of intensity I_i. Let P_{sca} watts of this power be scattered, while P_{abs} watts are absorbed. By definition, we have

$$C_{sca} = P_{sca}/I_i \quad , \tag{2-1a}$$

$$C_{abs} = P_{abs}/I_i \quad , \tag{2-1b}$$

and

$$C_{ext} = P_i/I_i \quad . \tag{2-1c}$$

These quantities are the cross sections (in square meters) of the particle for scattering, absorption and extinction, respectively. By virtue of energy conservation, we have

$$C_{ext} = C_{sca} + C_{abs} \quad . \tag{2-2}$$

The extinction cross section of a particle is not necessarily equal to its geometrical cross section. For a spherical particle of radius a which is large compared to a wavelength, C_{ext} is roughly equal to $2\pi a^2$ (see the discussion of the "extinction paradox" on pp. 107-108 of van de Hulst[1]).

Within a medium containing scattering particles, a wave of initial intensity I_o traversing a distance z suffers the well-known "extinction" attenuation

$$I(z) = I_o \exp[-\gamma z] \quad , \tag{2-3}$$

where $I(z)$ is just the unscattered and unabsorbed residue of the original wave. For a so-called "monodisperse" suspension containing d_v identical particles of radius a per unit volume, we have

$$\gamma = d_v C_{ext}(a) \quad . \tag{2-4}$$

In a "polydisperse" suspension the particle radii obey some probability density function $p(a)$ If the average volume density of particles is d_v, we have

$$\gamma = d_v \int_0^\infty C_{ext}(a) \, p(a) \, da \quad . \tag{2-5}$$

The coefficient γ is frequently expressed as D_e^{-1}, where D_e is defined as the "extinction distance" of the medium. When distance within the cloud is normalized to D_e, it is called "optical distance." In particular, the "optical thickness" of a cloud is

$$N_c = \frac{\tau}{D_e} \tag{2-6}$$

where τ is its physical thickness.

As a general rule of thumb, one assumes that a single-scattering analysis is adequate for a particular cloud when its optical thickness is about 0.1 or less. Thus the extinction attenuation $\exp(-0.1)$ for propagation all the way through the cloud is very nearly unity. The single-scattered intensity emerging from the cloud is very small, being roughly $[1 - \exp(-0.1)]$ times the unscattered intensity, and higher-order scattered radiation is of a higher order of smallness.

Now, we shall direct our attention in the present study to clouds whose optical thicknesses range from perhaps 5 to 100. Thus the importance of multiple scattering in analyzing the behavior of these clouds is manifest.

These few concepts comprise all the background that is necessary for the idealized cloud model described in Chapter 3.

CHAPTER 3
SPATIAL IMPULSE RESPONSES

We begin this chapter with a description of an idealized physical model for a cloud and the particles comprising it. We then define two complementary forms of a simplified elementary-wave representation, which gives us an adequate mathematical description of the angular and spatial variation of the intensity of the incident and scattered light. It is demonstrated that the average effect of the cloud upon the function representing the incident illumination is analogous to the effect of a linear system upon its input. We define impulses in each of the two forms of the elementary-wave representation, and obtain the response of the cloud to each of the impulses. We show that the effects of the cloud upon an arbitrary incident distribution can be determined by means of a superposition integral involving the appropriate impulse response.

In this chapter we consider only the intensity of the scattered light beneath a cloud. Moreover, we restrict our attention to the average behavior of the intensity. We argue in Sec. 3.1 that the intensity of the scattered light measured by an antenna is a random variable with extremely small variance, so that it is always very nearly equal to its statistical average.

3.1 IDEALIZED CLOUD

The physical configuration of the idealized cloud to be analyzed is illustrated in Fig. 3-1. Its boundaries are infinite parallel planes separated by τ meters; it is parallel to the earth, which is represented as an infinite plane h meters below the lower boundary of the cloud. The statistical properties of the cloud (e. g., particle density and size distribution) are uniform everywhere within its boundaries. The receiving antenna on the ground has some aperture size and beamwidth associated with it.

We shall assume that the particles in the cloud are spherical and that all have the same complex refractive index m. Their radii are assumed to obey a probability density function $p(a)$, $0 < a < \infty$, and the average volume density of particles is taken to be d_v per cubic meter. As we pointed out in Chapter 2, the extinction cross section $C_{ext}(a)$ and the intensity scattering pattern $F_a(\theta)$ are precisely specified by the Mie theory for each individual particle, at a given wavelength. The average extinction cross section over all the particles in the cloud is

Fig. 3-1. Physical configuration of idealized cloud.

$$\overline{C_{ext}} = \int_0^\infty C_{ext}(a) \, p(a) \, da \quad . \tag{3-1}$$

We shall find it expedient to depart from conventional practices to a degree, with respect to the particle scattering pattern. For calculations involving polydisperse suspensions, one would normally use the average scattering pattern defined by the relation
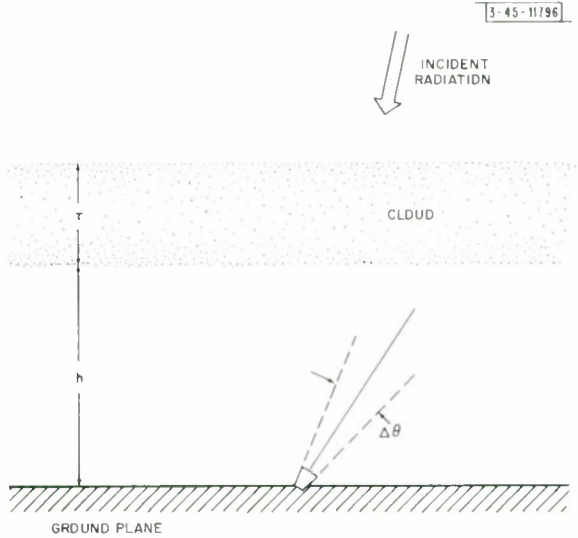
$$\overline{F(\Theta)} = \int_0^\infty F_a(\Theta)\, p(a)\, da \quad .$$

This is a spatial average, in the following sense: a small volume of the scattering particle suspension, illuminated by a plane wave, will look like a point source of scattered radiation if observed from a sufficient distance. As we shall show later in this section, it is reasonable to imagine a volume large enough to contain an enormous number of scatterers, but small enough (and having its scatterers far enough from each other) that each particle scatters the incident light independently. The above definition of $\overline{F(\Theta)}$ then follows.

In the present case, however, the particle diameters (roughly 10 to 40 microns in typical clouds[24]) are much larger than visible-light wavelengths. The scattering pattern at a given wavelength is therefore strongly peaked in the forward direction. The intensity of radiation scattered through π radians is roughly 50 to 60 times smaller than the forward-scattered intensity, for large spherical particles.[25] We shall assume that backscattered light is lost, for our purposes, exactly as though it had been absorbed. (If it were to contribute to the effects of light scattered forward by a given particle, the backscattered light must undergo a second reversal of direction. Such rays will then be attenuated relative to the forward-scattered rays by a factor of perhaps 2500.) Thus we restrict our attention to the forward-scattering pattern $F_{f,\,a}(\Theta)$, which we define for a given wavelength as

$$F_{f,\,a}(\Theta) \triangleq \begin{cases} F_a(\Theta) \quad , & |\Theta| \leqslant \frac{\pi}{2} \quad ; \\ 0 \quad , & \text{elsewhere} \quad . \end{cases} \tag{3-2}$$

The average forward-scattering pattern for the particles in the cloud is

$$\overline{F_f(\Theta)} \triangleq \int_0^\infty F_{f,\,a}(\Theta)\, p(a)\, da \quad . \tag{3-3}$$

The average total power scattered through angles less than $\pi/2$ by a particle illuminated by a unit-intensity plane wave will be called the <u>average forward-scattering cross section</u>

$$\begin{aligned}
\overline{C_f} &\triangleq \int \overline{F_f(\Theta)}\, d\omega \\
&= \int_0^{2\pi} d\varphi \int_0^{\pi/2} d\Theta \, \sin\Theta \, \overline{F_f(\Theta)} \\
&= 2\pi \int_0^{\pi/2} d\Theta \, \sin\Theta \, \overline{F_f(\Theta)} \quad .
\end{aligned} \tag{3-4}$$

We lump the average total backscattered light together with the absorption loss, describing the result in terms of the <u>average loss cross section $\overline{C_\ell}$</u>. By virtue of energy conservation, we have

$$\overline{C_{\text{ext}}} = \overline{C_\ell} + \overline{C_f} \quad . \tag{3-5a}$$

We define the <u>average forward-scattering efficiency</u>

$$\gamma_f \triangleq \frac{\overline{C_f}}{\overline{C_{\text{ext}}}} \quad , \tag{3-5b}$$

the average fraction of the incident power which is scattered forward. For convenience in the thin-layer model analysis to follow, we define a normalized average single-particle forward scattering pattern

$$f(\Theta) \triangleq (\overline{C_f})^{-1} \overline{F_f(\Theta)} \quad .$$ (3-6)

Neglecting near-field effects, we see that the average scattered intensity at a point at spherical coordinates (r, Θ, φ) relative to a particle is

$$\overline{I_s(r, \Theta)} = \begin{cases} I_i \dfrac{\overline{C_f}}{r^2} f(\Theta) \quad , & |\Theta| \leqslant \dfrac{\pi}{2} \\ 0 \quad , & \text{elsewhere} \quad , \end{cases}$$ (3-7)

independent of the azimuth angle φ. The incident illumination is a plane wave of intensity I_i, and Θ is measured from its propagation vector.

We remark in passing that the Mie theory does not hold for incident illumination other than a uniform plane wave. Thus Eq. (3-7) is not strictly correct in a multiple-scattering environment, where some components of the light incident on a particle are approximately spherical waves that result from scattering by other particles. As a practical matter, however, this problem may be ignored. For a very dense cloud,[26] d_v is on the order of 10^{10} per cubic meter. The corresponding average particle separation is roughly

$$d_v^{-1/3} \cong 5 \times 10^{-4} \text{ meter} \quad .$$ (3-8)

At this distance, a spherical phase front is flat over a region the size of a particle (say, 5 microns) to within about 6.2×10^{-9} meter, which is roughly 0.012λ at a wavelength of 0.5 micron.

We assume that the locations of the scattering particles within the cloud obey a Poisson distribution. This follows from the assumption that individual particle locations are statistically independent of each other, and that the location of each of them is a uniformly distributed random variable over the volume of the cloud. Specifically, let there be

$$n = Vd_v$$

particles in a large but finite volume V in the cloud, and let a given particle be present in a given region δv of V with probability $\delta v/V$. Let all n particles obey the same probability law, independently of each other. Then the population k of δv obeys a binomial distribution, with

$$\Pr[k \text{ particles in } \delta v] = \binom{n}{k} \left(\frac{\delta v}{V}\right)^k \left(1 - \frac{\delta v}{V}\right)^{n-k} \quad .$$ (3-9)

Now, if n becomes large and $\delta v/V$ becomes small, while their product

$$n \frac{\delta v}{V} = d_v \delta v$$ (3-10)

remains moderate, the Poisson approximation[27] holds. Thus

$$\lim_{V \to \infty} \Pr[k \text{ particles in } \delta v] = \frac{(d_v \delta v)^k}{k!} e^{-d_v \delta v} \quad .$$ (3-11)

The exponential extinction of waves traversing the cloud follows from the Poisson assumption. Suppose a plane wave of intensity $I(x)$ within the cloud progapates through a layer of thickness dx whose boundaries are parallel to the phase fronts of the wave. On the average, each particle in the layer removes $\overline{C_{ext}}I(x)$ watts of power from the plane wave (we visualize the averaging process as a spatial average over a large area of phase front). We assume that the resulting local perturbations in the wave become smoothed out rapidly enough that its plane wave character is preserved everywhere. Now, a section of this layer with unit-area faces contains $d_v dx$ particles, on the average. The average intensity of the unscattered remnant of the plane wave at $x + dx$ is therefore given by

$$I(x + dx) = I(x) - \overline{C_{ext}}d_v I(x)\, dx \quad , \tag{3-12}$$

which we integrate to obtain

$$I(x) = I_o\, e^{-\overline{C_{ext}}d_v x} \quad . \tag{3-13}$$

By similar reasoning, we find that the extinction losses of a spherical wave traversing a shell of thickness dr are represented by the equation

$$(r^2 + 2rdr)\, I(r + dr) = r^2 I(r) - r^2 \overline{C_{ext}}d_v I(r)\, dr \quad , \tag{3-14}$$

which we integrate to yield

$$I(r) = \frac{I_o}{r^2}\, e^{-\overline{C_{ext}}d_v r} \quad . \tag{3-15}$$

Throughout this chapter we consider the average intensity of the scattered light traversing a cloud. In Appendix A and Chapter 4, we study the statistics of the light in greater generality. It is meaningful and useful to study only the average behavior of the intensity, as we do here, because the variance of the intensity is extremely small. Thus it is always very nearly equal to its average value. An heuristic argument in support of this assertion is now given, with particular reference to the total intensity I measured by an antenna on the ground aimed at the underside of the cloud. Because of their independent random phases, the contributions arriving at the antenna from each particle in its beam add incoherently. Let the intensity contributed by the ith particle be the random variable ϵ_i. Now, the contributions from two particles will be statistically decoupled if the light rays illuminating one of them have no effect on the other. This will be true when the distance r between the two particles obeys the condition

$$r \ll D_e \quad , \tag{3-16}$$

so that the probability of double scattering within a distance r is very small. Thus the cloud particles in a volume V of dimensions small compared to the extinction distance D_e will provide a set of signal contributions at the antenna which are essentially statistically independent of each other. The total intensity received from the volume V is a random variable

$$I_V = \sum_k \epsilon_k \tag{3-17}$$

where k ranges over the particles in V. Let the number of such particles be K; assume that

the variance of ϵ_k is σ_k^2, and that its mean is

$$m = \frac{\overline{I_V}}{K} \tag{3-18}$$

for every k. Let us make the intuitively satisfying assumption that each ϵ_k varies over a reasonably small range, so that its standard deviation is no larger than a number roughly comparable to its mean. Thus

$$\sigma_k = C_k m = C_k \frac{\overline{I_V}}{K} \quad , \tag{3-19}$$

where C_k is a factor of fairly modest magnitude (possibly even less than unity). Let us upper-bound the quantities C_k by the relation

$$C_k \leqslant \max_k \{C_k\} \triangleq C_{max} \quad . \tag{3-20}$$

Then

$$\operatorname{var}(I_V) = \sum_{k=1}^{K} \sigma_k^2$$

$$= \sum_{k=1}^{K} C_k^2 \frac{(\overline{I_V})^2}{K^2} \leqslant C_{max}^2 \frac{(\overline{I_V})^2}{K} \quad . \tag{3-21}$$

Under these assumptions, then, the ratio of the standard deviation of I_V to its mean goes as $K^{-1/2}$. Now, the dimensions of V are on the order of, say, $0.1\,D_e$. Thus a very conservative estimate for the volume of V would be a few cubic meters, so that K is of the order of the particle density, a huge number. We conclude that I_V is always very nearly equal to its average value. The same statement holds for the total intensity I measured by the antenna, which is a superposition of a number of nearly-constant components similar to I_V.

3.2 PLANE WAVE SUPERPOSITIONS

An essential feature of the analyses in this chapter is the representation of the intensities of arbitrary propagating fields as superpositions of elementary waves. We require the user of our results first to represent the incident illumination in accordance with the techniques we shall define below. The scattered illumination that we predict beneath the cloud is to be interpreted in the same way.

Now, it is possible in principle to obtain a complete and precise representation for a general propagating field in the form of a superposition of uniform plane waves (see, for example, Stratton[28]). Such a technique is more general than is necessary for the representation of the scattered light within and below clouds. Because of uncertainty in our knowledge of the locations of cloud particles, we take all the scattered wavelets to have statistically independent random phases, uniformly distributed over $(-\pi, \pi)$, as we explain in Appendix A. Thus all the wavelets at a point in space, including any unscattered residue of the incident radiation, add in an incoherent fashion (i.e., their intensities add). For our purposes, then, an adequate description of the field at each point in space (even for the incident radiation, before it enters the cloud) need specify

13

only the intensities and directions of propagation of all rays passing through the point. We shall define two different kinds of simplified plane wave distributions which provide this information in a convenient form. The first of these is appropriate for wave configurations which are uniform over any plane parallel to the ground, while the second must be used to represent finite beams whose intensity varies with the lateral coordinates x and y.

The first plane wave distribution function we shall employ depends only upon angles of arrival. It will be called the <u>angular intensity distribution function</u> $I(\alpha, \beta)$, with dimensions of watts-meter^{-2}-radian^{-2}. Its arguments are the orthogonal angular coordinates defined in Appendix B by the relations

$$\alpha = \Theta \cos \varphi \quad ,$$
$$\beta = \Theta \sin \varphi \quad , \tag{3-22}$$

where Θ and φ are the polar and azimuthal angles in spherical coordinates. As we explain in detail in Appendix B, the transformation is approximate in roughly the same sense as the statement that

$$\frac{\sin \Theta}{\Theta} \cong 1 \quad . \tag{3-23}$$

Thus Eq. (3-22) is precisely correct at $\Theta = 0$ and is good within 20 percent for

$$\Theta \leqslant 1.03 \text{ radians} \quad . \tag{3-24}$$

The resulting restricted angular range of $I(\alpha, \beta)$ causes no real problems. For the situations we shall consider, the condition (3-24) is satisfied by that portion of the scattered light beneath a cloud which is intense enough to be of value for optical communication. Thus the approximation is valid for our objective, which is the development of a useful approximate analysis of the cloud as a communication channel, not a precise description of the physical phenomena involved. We define $I(\alpha, \beta)$ by means of the statement that $I(\alpha, \beta) \, d\alpha \, d\beta$ is the total intensity borne by those plane waves whose angles of arrival lie in the intervals $(\alpha, \alpha + d\alpha)$ and $(\beta, \beta + d\beta)$. Thus a hypothetical antenna with unit aperture area whose power gain is unity over a solid angle

$$d\omega = d\alpha \, d\beta \tag{3-25}$$

and zero elsewhere simply reproduces the intensity distribution incident upon it. When it is illuminated by $I(\alpha, \beta)$ the antenna measures a total power level

$$P_{rec} (\alpha, \beta) = I(\alpha, \beta) \, d\omega \quad . \tag{3-26}$$

A more general antenna, with power gain pattern $g(\alpha, \beta)$ and aperture A, aimed in direction (α_1, β_1) and illuminated by $I(\alpha, \beta)$, receives a total power level

$$P_{rec} (\alpha_1, \beta_1) = \iint A I(\alpha, \beta) \, g(\alpha_1 - \alpha, \beta_1 - \beta) \, d\alpha \, d\beta \quad . \tag{3-27}$$

The double-impulse intensity distribution

$$I(\alpha, \beta) = u_0(\alpha - \alpha_0) \, u_0(\beta - \beta_0) \tag{3-28}$$

is taken to be a single unit-intensity uniform plane wave whose angle of arrival is (α_0, β_0).

14

The second type of plane wave distribution we utilize will be called the power distribution function $P(\alpha, \beta, x, y)$. Its dimensions are also watts-meter^{-2}-radian^{-2}. We define this function by the statement that $P(\alpha, \beta, x, y)\, d\alpha\, d\beta\, dx\, dy$ is the total power borne by those rays of light with angles of arrival in a solid angle $d\alpha\, d\beta$ at the angular position (α, β), which fall on an area $dx\, dy$ at the point (x, y) on a plane parallel to the ground. This situation is illustrated in Fig. 3-2. The indicated angle

$$\Theta = \sqrt{\alpha^2 + \beta^2} \tag{3-29}$$

is the polar angle in conventional spherical coordinates which corresponds to the position (α, β).

Fig. 3-2. Geometry for definition of P ( ).
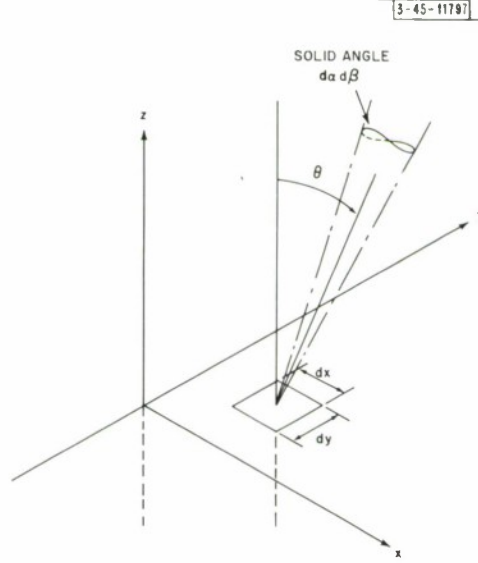
The interpretation of P( ) in terms of plane waves is complicated by the fact that the phase fronts of an arriving plane wave are not parallel to the x-y plane. Referring to Fig. 3-2, we observe that the area $dx\, dy$ projects into an area $dx\, dy \cos \Theta$ on a plane parallel to the phase fronts of a plane wave having angle of arrival (α, β). Thus the power distribution function

$$P(\alpha, \beta, x, y) = u_o(\alpha - \alpha_o)\, u_o(\beta - \beta_o) \tag{3-30}$$

must correspond to a uniform plane wave with angle of arrival (α_o, β_o) whose intensity is

$$I_p = \sec \Theta_o$$

$$= \sec \left(\sqrt{\alpha_o^2 + \beta_o^2} \right) \quad . \tag{3-31}$$

Suppose that a plane wave arriving from (α_o, β_o) had some nonuniform intensity given as a function of the x- and y-coordinates by the expression $I_p(x, y)$. Clearly the corresponding power distribution function would be

$$P(\alpha, \beta, x, y) = I_p(x, y) \cos \Theta_o\, u_o(\alpha - \alpha_o)\, u_o(\beta - \beta_o) \quad . \tag{3-32}$$

The quadruple-impulse power distribution function

$$P(\alpha, \beta, x, y) = u_o(\alpha - \alpha_o)\, u_o(\beta - \beta_o)\, u_o(x - x_o)\, u_o(y - y_o) \tag{3-33}$$

15

corresponds to a "plane wave" arriving from (α_o, β_o) whose intensity is

$$I_p(x, y) = \sec \Theta_o u_o(x - x_o) u_o(y - y_o) \quad . \tag{3-34}$$

This can be envisioned as, for example, the limiting case of a plane wave whose intensity is Gaussian in both x and y and is multiplied by $\sec \Theta_o$. In another sense we may think of it as an individual ray, carrying unit power. An idealization, like the familiar impulse in linear system theory, Eq. (3-33) will be used only as a mathematical artifice in studying the behavior of waves which could exist physically.

A hypothetical antenna which reproduces a power distribution function P( ) incident upon it must have an aperture dx dy which remains fixed in the x-y-plane, rather than the plane perpendicular to the antenna boresight axis. The power gain of the reproducing antenna must be unity over an incremental solid angle $d\omega$ and zero elsewhere. Let the location of the antenna be denoted by (x_1, y_1), while its pointing angle is (α_1, β_1). Then the power received by the antenna when it is illuminated by $P(\alpha, \beta, x, y)$ is given by

$$p_{rec}(\alpha_1, \beta_1, x_1, y_1) = P(\alpha_1, \beta_1, x_1, y_1) \, d\omega \, dx \, dy \quad . \tag{3-35}$$

In order to write an expression for the power received by an arbitrary antenna, we require that its aperture be described by an aperture function $A(\alpha, \beta, x, y)$ defined over the x-y-plane,
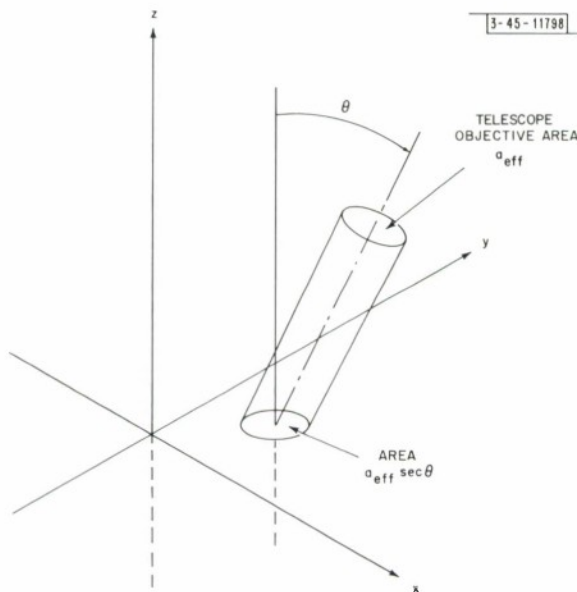
Fig. 3-3. Aperture function geometry.

which includes any variation of the aperture with the antenna pointing angle (α, β). As an example of what we mean by this statement, consider a conventional telescope pointed at some angle (α, β) whose effective aperture area (on a plane perpendicular to the axis of the telescope) has a constant value a_{eff}. For this antenna, the function A( ) that we require is a function of x and y whose area is $a_{eff} \sec(\sqrt{\alpha^2 + \beta^2})$; that is, it is the region on the x-y-plane which projects into a_{eff} on the aperture plane. The situation is illustrated in Fig. 3-3. In addition to the aperture function, we require knowledge of the power gain pattern $g(\alpha, \beta)$ of the arbitrary antenna. When illuminated by a power distribution function $P(\alpha, \beta, x, y)$, this antenna receives a power level

16

$$P_{rec}(\alpha_1, \beta_1, x_1, y_1) = \int\int\int_{-\infty}^{\infty}\int d\alpha \, d\beta \, dx \, dy \, P(\alpha, \beta, x, y)$$

$$\cdot \, g(\alpha_1 - \alpha, \beta_1 - \beta) \, A(\alpha_1 - \alpha, \beta_1 - \beta, x_1 - x, y_1 - y) \quad . \qquad (3\text{-}36)$$

One final comment about the function $P(\ )$ is in order. It is obvious that the function depends upon the vertical coordinate z in addition to the four arguments listed. In our development we are able to suppress explicit indication of this dependence, however, because the vertical location is clearly specified in the context at each step of the analysis.

3.3 THIN-LAYER MODEL

We consider a subdivision of the cloud into parallel layers of thickness ℓ_0, each of which is treated independently. Since the particles are assumed to scatter only in the forward direction, we can consider each layer successively from the top of the cloud downward. The desired results are obtained in the limit as ℓ_0 goes to zero. While our analysis appears to be new, the thin layer idea itself is not. Hartel,[29] for example, calculated the angular distribution of diffuse scattered light intensity in a thick cloud by computing the effects of successive layers of scatterers. He used an exceedingly complicated approach, involving the expansion of both the single-particle scattering pattern and the scattered light intensity distribution in associated Legendre polynomials. Another approach was used by Fritz in the work mentioned in Chapter 2, in which he divided the cloud into layers of fixed optical thickness 0.25. By adding the contributions of diffuse scattered light "generated" independently in each of the layers, he derived a diffusion equation for the angular distributions of transmitted and reflected light.

Fig. 3-4. Layer model of the cloud.
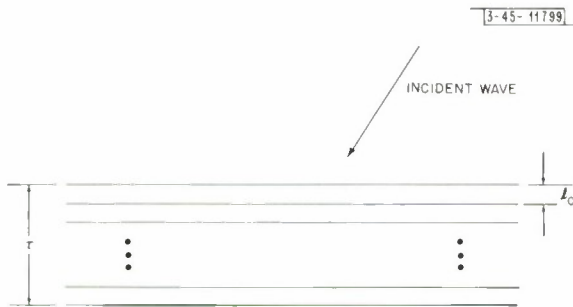
We assume that the thickness ℓ_0 of the layers in our model is small enough at the outset that the probability of multiple scattering within a layer is vanishingly small. Thus most of the light rays traversing a layer emerge without having been scattered, and a few undergo a single scattering, but virtually none of them is scattered more than once. An alternate statement of this assumption is the condition that

$$\ell_0 \ll D_e \qquad (3\text{-}37)$$

whence the extinction attenuation $\exp[-\ell_0/D_e]$ is very nearly unity. Here we implicitly interpret the extinction attenuation as the probability that a light ray traverses a distance ℓ_0 without being scattered. This and related ideas will be discussed in detail in Chapter 4. Now, since ℓ_0 is so small and will be driven to zero in a later step anyway, we will not be changing the gross behavior of the model if we assume that all the particles in each layer are physically located on a plane at the center of the layer. Thus we arrive at the simple model illustrated in Fig. 3-4, in which each particle in the cloud is located on one of the N parallel planes in the region occupied by the cloud. For a cloud thickness of τ meters, we have

17

$$N = \frac{\tau}{\ell_o} \quad . \tag{3-38}$$

Since we assumed the particles were Poisson-distributed over the volume of the cloud with average density d_v meter^{-3}, it is appropriate to let them be Poisson-distributed over each of the parallel planes with average density

$$\rho = \ell_o d_v \text{ meter}^{-2} \tag{3-39}$$

and to let the distribution on each plane be statistically independent of all the others.

For the present we shall assume that each particle has zero velocity. The inclusion of questions of Doppler dispersion at this point in the layer-model analysis leads to excessive complexity without changing the results. This issue will be addressed by means of an alternate technique in Chapter 4.

The determination of the average impulse responses of the cloud involves averaging over all possible sets of particle locations in the cloud. This problem resolves itself into averaging separately over the Poisson distributions of particles on the plane at the center of each layer, since they are assumed to be statistically independent of each other. Each layer is considered successively in the analyses to follow, from the top of the cloud downward, and an implicit averaging process is carried out for each layer in turn.

For the sake of convenience, we shall use the term "layer" somewhat loosely hereafter, to refer to the plane and its Poisson-distributed particles at the center of the actual cloud layer.

3.4 ANGULAR IMPULSE RESPONSE $h_I(\alpha, \beta; \alpha_o, \beta_o)$

When a cloud is illuminated from above by a uniform plane wave, the light emerging below it will be spread out over a range of angles of arrival. In terms of the angular intensity distribution function $I(\alpha, \beta)$ defined in Sec. 3.2, the incident plane wave is equivalent to a two-dimensional impulse. The average angular dispersion of the light emerging below the cloud in response to this illumination is shown to be equivalent to the double-impulse response of a two-dimensional linear filter. We show that the response of the cloud to an arbitrary plane wave illumination is given by a linear superposition integral with the impulse response as its kernel.

The angular impulse response $h_I(\alpha, \beta; \alpha_o, \beta_o)$ is defined as the angular intensity distribution at coordinates (α, β) below a cloud in response to a unit double impulse at coordinates (α_o, β_o) incident on the top of the cloud. We derive $h_I(\ )$ by finding the impulse response $h_I(\alpha_1, \beta_1; \alpha_o, \beta_o)$ of a single layer of thickness ℓ_o, and writing an $(N-1)$-fold two-dimensional superposition integral to obtain the response of an array of N layers. We then solve the integral in the limit as N goes to infinity and the layer separation ℓ_o goes to zero, while the cloud thickness

$$\tau = N\ell_o \tag{3-40}$$

remains constant.

We begin by transforming the normalized average single-particle forward scattering pattern $f(\Theta)$ of Eq. (3-6) into a function $f_1(\alpha, \beta)$ defined over the $\alpha - \beta$ domain. As we explain in Appendix B, the result is

$$f_1(\alpha, \beta) = \frac{\sin\left(\sqrt{\alpha^2 + \beta^2}\right)}{\sqrt{\alpha^2 + \beta^2}} \ f\left(\sqrt{\alpha^2 + \beta^2}\right) \quad . \tag{3-41}$$

Fig. 3-5. Average single-particle scattering pattern $f_1(\alpha,\beta)$.
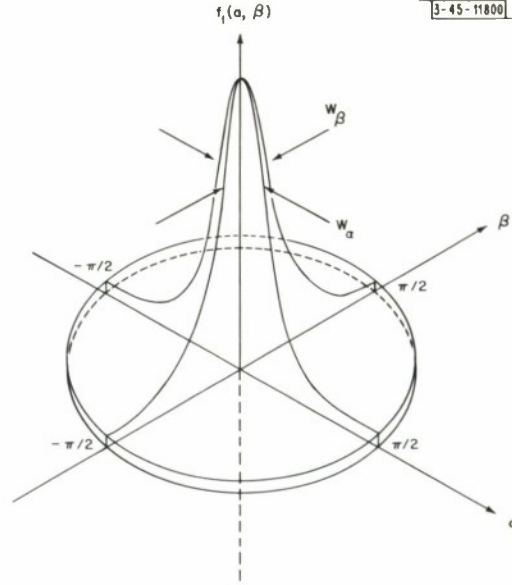
A typical $f_1(\alpha, \beta)$ is illustrated in Fig. 3-5, where we have indicated that the function peaks up sharply near $\alpha = \beta = 0$ and is zero for $\Theta > \pi/2$. We shall find that $f_1(\ )$ affects the angular impulse response $h_1(\ )$ only through the width parameters W_α and W_β. They are defined for convenience as

$$W_\alpha = \left[\int_{-\infty}^{\infty} d\alpha \int_{-\infty}^{\infty} d\beta\, \alpha^2 f_1(\alpha, \beta) \right]^{1/2} \tag{3-42a}$$

and

$$W_\beta = W_\alpha = \left[\int_{-\infty}^{\infty} d\alpha \int_{-\infty}^{\infty} d\beta\, \beta^2 f_1(\alpha, \beta) \right]^{1/2} \quad , \tag{3-42b}$$

by analogy with the marginal standard deviations of a joint probability density function. We remark that the "covariance" $\overline{\alpha\beta}$ is zero, because of the circular symmetry of $f_1(\alpha, \beta)$.

In accordance with our discussions in Sec. 3.2 and Appendix B, we shall replace the metric coefficient

$$\frac{\sin\left(\sqrt{\alpha^2 + \beta^2}\right)}{\sqrt{\alpha^2 + \beta^2}} = \frac{\sin\Theta}{\Theta}$$

by unity. Thus we use the approximate single-particle scattering pattern

$$f_1(\alpha, \beta) \cong f\left(\sqrt{\alpha^2 + \beta^2}\right) \tag{3-43}$$

in most of the work to follow. As we point out in Appendix B, it is necessary to include the metric coefficient in the variance calculations [Eq. (3-42)] because the integrand is weighted heavily at larger values of Θ by the factor α^2 or β^2. We shall improve the accuracy of our results by including the factor $(\sin\Theta)/\Theta$ when we transform our ultimate answers back into polar coordinates. In all the intermediate calculations in the analysis below, however, we shall assume that the metric coefficient is unity.

19
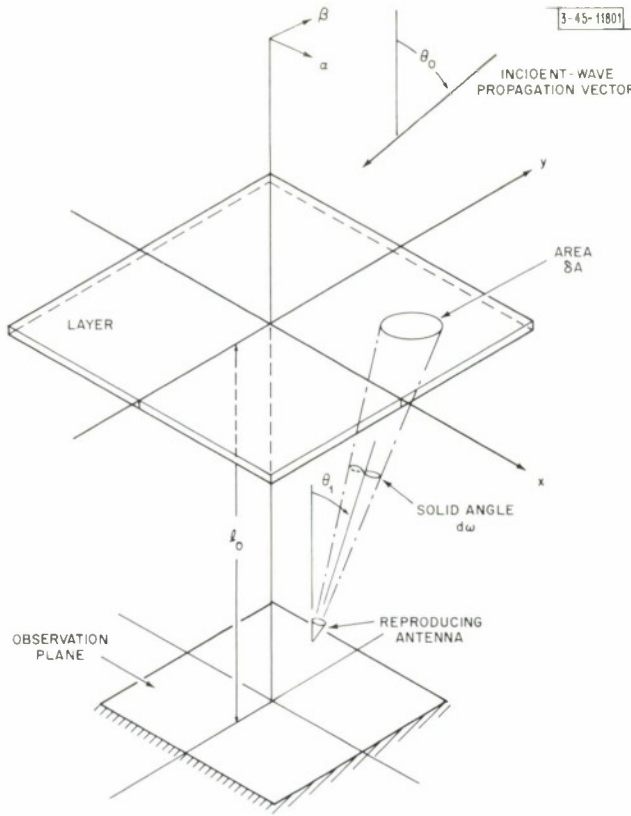
Fig. 3-6. Geometry for single-layer impulse response.

The geometry for the derivation of the single-layer impulse response $h_1(\alpha_1, \beta_1; \alpha_o, \beta_o)$ is shown in Fig. 3-6. The antenna in the figure is the hypothetical reproducing antenna defined in connection with Eq. (3-26) in Sec. 3.2. At its indicated location ℓ_o meters below the layer, it measures the average angular intensity distribution function which will illuminate the second cloud layer when we add it to the model. The antenna is aimed in the direction (α_1, β_1), where α_1 and β_1 are measured in the directions indicated at the top of the figure, and

$$\Theta_1 = \sqrt{\alpha_1^2 + \beta_1^2} \quad . \tag{3-44}$$

The distance from the antenna to the layer, measured along the axis of its receiving "beam," is $\ell_o \sec \Theta_1$. At that distance, the cross-sectional area of the beam is $\ell_o^2 \sec^2 \Theta_1 \, d\omega$. Since this cross section is inclined at angle Θ_1 to the layer, the region on the layer which lies in the beam of the antenna has area

$$\delta A = \ell_o^2 \sec^3 \Theta_1 \, d\omega \quad . \tag{3-45}$$

The incident plane wave illumination, represented as an angular intensity distribution, is the unit double impulse $u_o(\alpha - \alpha_o) \, u_o(\beta - \beta_o)$; the polar angle indicated in the figure is

$$\Theta_o = \sqrt{\alpha_o^2 + \beta_o^2} \quad . \tag{3-46}$$

The antenna in Fig. 3-6 receives scattered radiation from the layer if and only if a particle is present in the region δA. Given that a particle is there, we use Eqs. (3-7) and (3-43) to write the conditional average scattered power

20

$$P_{rec,sca}(\alpha_1, \beta_1; \alpha_o, \beta_o) = \frac{\overline{C_f}}{\ell_o^2 \sec^2 \Theta_1} f_1(\alpha_1 - \alpha_o, \beta_1 - \beta_o) \qquad (3-47)$$

received by the antenna. (Recall that both $\overline{C_f}$ and $f_1(\alpha, \beta)$ are averaged over the distribution of particle sizes in the cloud.) Now, by the Poisson assumption, a particle is present in the incremental area δA with probability

$$\rho \delta A = \rho \ell_o^2 \sec^3 \Theta_1 d\omega \quad , \qquad (3-48)$$

where ρ is the average particle density [Eq. (3-33)]. Thus the average scattered power received by the antenna in Fig. 3-6 is given by

$$\overline{P_{rec,sca}}(\alpha_1, \beta_1; \alpha_o, \beta_o) = \frac{\overline{C_f} \rho \ell_o^2 \sec^3 \Theta_1 d\omega}{\ell_o^2 \sec^2 \Theta_1} f_1(\alpha_1 - \alpha_o, \beta_1 - \beta_o)$$

$$= \rho \overline{C_f} \sec \Theta_1 f_1(\alpha_1 - \alpha_o, \beta_1 - \beta_o) d\omega \quad . \qquad (3-49)$$

The unscattered light emerging below the layer is assumed to be a plane wave propagating in the same direction as the incident wave. Its average intensity is reduced because of the extraction of $\overline{C_{ext}}$ watts of power from the wave by each particle in the layer, where $\overline{C_{ext}}$ is the average extinction cross section over all particles in the cloud. Now, an area $\sec \Theta_o$ in the layer projects into unit area on a phase front of the incident wave. Thus each unit area of phase front has its path obscured by $\rho \sec \Theta_o$ particles, on the average. The average intensity of the unscattered plane wave emerging below the layer is therefore $[1 - \rho \overline{C_{ext}} \sec \Theta_o]$. Since the antenna can receive this plane wave only when $\alpha_1 = \alpha_o$ and $\beta_1 = \beta_o$, the average unscattered power received by the antenna is given by

$$P_{rec,unsc}(\alpha_1, \beta_1; \alpha_o, \beta_o) = (1 - \rho \overline{C_{ext}} \sec \Theta_1) u_o(\alpha_1 - \alpha_o) u_o(\beta_1 - \beta_o) d\omega \quad , \qquad (3-50)$$

in which we were able to write $\sec \Theta_1$ in place of $\sec \Theta_o$ because the impulses constrain the two angles to be equal. We observe, however, that the unbounded growth of $\sec \Theta_1$ as Θ_1 approaches $\pm \pi/2$ will cause the coefficient in Eq. (3-50) to become negative whenever

$$|\Theta_1| > \sec^{-1} \frac{1}{\rho \overline{C_{ext}}} \quad . \qquad (3-51)$$

We cannot permit this to occur, since it would violate the law of conservation of energy. A negative coefficient in Eq. (3-50) would correspond to the absorption by the particles of more power than is incident on them. The difficulty arises because, although ℓ_o is small enough to preclude double scattering, $\ell_o \sec \Theta_1$ is not. We avoid the problem by replacing $\sec \Theta_1$ in Eq. (3-50) by

$$\widehat{\sec \Theta_1} \triangleq \begin{cases} \sec \Theta_1 & , \quad |\Theta_1| \leqslant \sec^{-1} \frac{1}{\rho \overline{C_{ext}}} \\[2ex] \frac{1}{\rho \overline{C_{ext}}} & , \quad \text{elsewhere} \quad . \end{cases} \qquad (3-52)$$

This artifice becomes unnecessary in the limit as ℓ_o (and hence ρ) goes to zero. Upon a moment's reflection, we see that the same substitution should be made in the expression (3-49) for

the average scattered power. When the inequality (3-51) holds, Eq. (3-52) actually expresses the fact that the path of the plane wave is completely obscured by particles, on the average. Thus all its power is removed by the particles, and a fraction $\overline{C_f}/\overline{C}_{ext}$ is re-radiated as forward-scattered light. This behavior is expressed precisely by the replacement of $\sec \Theta_1$ by $\widehat{\sec} \Theta_1$ in Eq. (3-49).

These substitutions having been made, the sum of Eqs. (3-49) and (3-50) is the total power received by the reproducing antenna in Fig. 3-6. In view of Eq. (3-22), the average angular intensity distribution incident on the observation plane is

$$[d\omega]^{-1} [\overline{p_{rec,unsc}}( ) + \overline{p_{rec,sca}}( )] \quad .$$ (3-53)

This distribution is, by definition, the average single-layer unit double-impulse response. Writing it out in full, we have

$$h_1(\alpha_1, \beta_1;\ \alpha_o, \beta_o) = (1 - \rho \overline{C}_{ext} \widehat{\sec} \Theta_1)\, u_o(\alpha_1 - \alpha_o)\, u_o(\beta_1 - \beta_o)$$
$$+ \rho \overline{C}_f \widehat{\sec} \Theta_1\, f_1(\alpha_1 - \alpha_o, \beta_1 - \beta_o) \quad .$$ (3-54)

The response below many layers follows from an argument which is familiar from linear system theory. Let us think of an arbitrary incident distribution $I(\alpha_o, \beta_o)$ as a sum of very narrow rectangular pulses. Because of the linearity of Maxwell's equations, the scattering process is linear. In a straightforward fashion, then, we construct a linear superposition integral

$$R(\alpha_1, \beta_1) = \int d\alpha_o \int d\beta_o\, I(\alpha_o, \beta_o)\, h_1(\alpha_1, \beta_1;\ \alpha_o, \beta_o)$$ (3-55)

to calculate the average response $R(\alpha_1, \beta_1)$ below a single layer to the arbitrary illumination $I(\alpha_o, \beta_o)$. It follows that the double-impulse response $h_N(\alpha_N, \beta_N;\ \alpha_o, \beta_o)$ of an array of N parallel cloud layers ℓ_o meters apart is given by the $(N - 1)$-fold two-dimensional superposition integral

$$h_N(\alpha_N, \beta_N;\ \alpha_o, \beta_o) = \iint \cdots \int d\alpha_{N-1} \cdots d\alpha_1 \iint \cdots \int d\beta_{N-1} \cdots d\beta_1$$
$$\cdot h_1(\alpha_N, \beta_N;\ \alpha_{N-1}, \beta_{N-1}) \cdots h_1(\alpha_1, \beta_1;\ \alpha_o, \beta_o) \quad .$$ (3-56)

The impulse response of the actual cloud is

$$h_I(\alpha, \beta;\ \alpha_o, \beta_o) = \lim_{\substack{N \to \infty \\ \ell_o \to 0}} h_N(\alpha, \beta;\ \alpha_o, \beta_o) \quad .$$ (3-57)

The question of the limits of integration in Eq. (3-56) requires a certain amount of discussion. Within the context of our thin-layer model, a problem arises whenever α and β lie outside the region

$$\Theta = \sqrt{\alpha^2 + \beta^2} \leqslant \frac{\pi}{2} \quad .$$ (3-58)

This would correspond to scattering through accumulated total angles large enough that some light was propagating upward toward the top of the cloud. Our model will account for the loss of this light by simply setting $h_N( )$ equal to zero outside the region [Eq. (3-58)], whenever it

extends that far. One way to do this analytically is to let the integration limits in Eq. (3-56) be such that $(\alpha_i^2 + \beta_i^2) \leqslant (\pi/2)^2$ for all i. The other alternative is to let all the limits be $\pm\infty$, and then truncate the final result outside Eq. (3-58). Both schemes were studied in some detail during the course of this research. Attention was focused upon the analogs of Eqs. (3-56) and (3-57) for a two-dimensional cloud, which were similar except that all the β-variables were absent. Appendix C describes the results of a numerical solution obtained by Zaborowski,[30] who programmed an (N − 1)-fold one-dimensional integral equation similar to Eq. (3-56) which had the limits $\pm\pi/2$ on all integrals. He simulated the solutions for a range of optical thicknesses, using values of N such that ℓ_o was equal to $0.5\,D_e$. Another approximate solution was obtained by letting

$$\widehat{\sec\Theta}_i \simeq 1 \tag{3-59}$$

everywhere in the integral, using the integration limits $\pm\infty$ on all integrals, and applying the Central Limit Theorem. The two solutions were essentially identical over the central region (specifically, the region $|\alpha| \lesssim 2\sigma_\alpha$, which includes 95 percent of the area under the curve). A more detailed discussion of the two solutions is presented in Appendix C.

We carry out a Central Limit Theorem approach to the solution of Eqs. (3-56) and (3-57) here, with integration limits $\pm\infty$. The factors $h_1(\ )$ in the integrand must fulfill three requirements in order that this technique be applicable:

(a) $h_1(\ ) \geqslant 0$

(b) $\displaystyle\iint\limits_{-\infty}^{\infty} d\alpha\, d\beta\, h_1(\alpha, \beta;\ 0, 0) = K_h < \infty$

(c) $h_1(\alpha_k, \beta_k;\ \alpha_{k-1}, \beta_{k-1}) = h_1(\alpha_k - \alpha_{k-1},\ \beta_k - \beta_{k-1})$. $\hfill$ (3-60)

Requirements (a) and (b) are clearly satisfied. We meet condition (c) by setting

$$\widehat{\sec\Theta}_i = 1 \hspace{4cm} [\text{Eq. (3-59)}]$$

everywhere. We note that this approximation is accurate within 10 percent for

$$|\Theta_i| \leqslant 0.42 \text{ radian} \quad , \tag{3-61a}$$

and within 20 percent for

$$|\Theta_i| \leqslant 0.58 \text{ radian} \quad , \tag{3-61b}$$

and that these numbers are roughly comparable to the other angular restrictions on our analysis. Thus we expect that, like the effects of our earlier approximations, errors due to Eq. (3-59) will become important only out in the tails of the final result. Making use of Eq. (3-59), then, we approximate $h_1(\ )$ of Eq. (3-54) as

$$h_1(\alpha_k, \beta_k;\ \alpha_{k-1}, \beta_{k-1}) \simeq (1 - \rho\,\overline{C_{ext}})\, u_o(\alpha_k - \alpha_{k-1})\, u_o(\beta_k - \beta_{k-1})$$
$$+ \rho\,\overline{C_f}\, f_1(\alpha_k - \alpha_{k-1},\ \beta_k - \beta_{k-1}) \quad . \tag{3-62}$$

It will be convenient for the kernels in the integrand of the multiple integral equation to be normalized to unit volume. Integrating the right side of (3-62) to find the total volume under the function, we have

$$K_{ha} = \int\int_{-\infty}^{\infty} d\alpha \, d\beta \, [(1 - \rho\overline{C_{ext}}) \, u_o(\alpha) \, u_o(\beta) + \rho\overline{C_f}f_1(\alpha,\beta)]$$

$$= 1 - \rho(\overline{C_{ext}} - \overline{C_f})$$

$$= 1 - \rho\overline{C_\ell} \quad . \tag{3-63}$$

The quantity $\overline{C_\ell}$ is the average loss cross section per particle defined by Eq. (3-5) in Sec. 3.1. Defining the normalized function

$$h_{1a}(\alpha_k - \alpha_{k-1}, \beta_k - \beta_{k-1}) = K_{ha}^{-1} \, [(1 - \rho\overline{C_{ext}}) \, u_o(\alpha_k - \alpha_{k-1}) \, u_o(\beta_k - \beta_{k-1})$$

$$+ \rho\overline{C_f}f_1(\alpha_k - \alpha_{k-1}, \beta_k - \beta_{k-1})] \quad , \tag{3-64}$$

we write

$$h_1(\alpha_k, \beta_k; \alpha_{k-1}, \beta_{k-1}) \cong K_{ha}h_{1a}(\alpha_k - \alpha_{k-1}, \beta_k - \beta_{k-1}) \quad . \tag{3-65}$$

The integral equation (3-56) then becomes

$$h_N(\alpha_N, \beta_N; \alpha_o, \beta_o) \cong K_{ha}^N \int\int_{-\infty}^{\infty} \cdots \int d\alpha_{N-1}\cdots d\alpha_1 \cdot \int\int_{-\infty}^{\infty} \cdots \int d\beta_{N-1}\cdots d\beta_1$$

$$\cdot h_{1a}(\alpha_N - \alpha_{N-1}, \beta_N - \beta_{N-1})\cdots h_{1a}(\alpha_1 - \alpha_o, \beta_1 - \beta_o) \quad . \tag{3-66}$$

The approximate solution of this equation for large N follows immediately from the Central Limit Theorem for two dimensions.[31] We have

$$h_N(\alpha_N, \beta_N; \alpha_o, \beta_o) \cong \frac{K_{ha}^N}{2\pi N\sigma_{h\alpha}\sigma_{h\beta}} \cdot \exp\left[-\frac{(\alpha_N - \alpha_o)^2}{2N\sigma_{h\alpha}^2} - \frac{(\beta_N - \beta_o)^2}{2N\sigma_{h\beta}^2}\right] \quad , \tag{3-67}$$

in which

$$N\sigma_{h\alpha}^2 = N \int_{-\infty}^{\infty} \int_{-\infty}^{\infty} d\alpha \, d\beta \, \alpha^2 h_{1a}(\alpha,\beta)$$

$$= NK_{ha}^{-1} \, \rho\overline{C_f} \, W_\alpha^2 = \frac{N\ell_o \, d_v\overline{C_f}W_\alpha^2}{1 - \ell_o \, d_v\overline{C_\ell}} \tag{3-68}$$

and $N\sigma_{h\beta}^2$ is given by a similar expression involving W_β^2. The quantities W_α and W_β are the single-particle scattering beamwidth parameters defined by Eq. (3-42). Since they are equal, $N\sigma_{h\alpha}^2$ is equal to $N\sigma_{h\beta}^2$. We recall that the cloud thickness

24

$$\tau = N\ell_o$$

and that

$$\overline{C_f} = \gamma_f \overline{C_{ext}} \quad ,$$

in terms of the average forward-scattering efficiency γ_f defined by Eq. (3-5b). The extinction distance in the cloud is

$$D_e = [d_v \overline{C_{ext}}]^{-1} \quad ,$$

and the optical thickness of the cloud is

$$N_c = \frac{\tau}{D_e} \quad .$$

Using these relations we reduce Eq. (3-68) to

$$N\sigma_{h\alpha}^2 = N\sigma_{h\beta}^2 = \frac{\gamma_f N_e W_\alpha^2}{1 - \ell_o d_v \overline{C_\ell}} \quad . \tag{3-69}$$

In the limit as N goes to infinity (while $\ell_o = \tau/N$ goes to zero) Eq. (3-69) becomes

$$\gamma_f N_e W_\alpha^2 \triangleq \sigma_\alpha^2$$

$$= \sigma_\beta^2 \quad . \tag{3-70}$$

This limiting process was already implicit in the application of the Central Limit Theorem. The coefficient in Eq. (3-67) becomes

$$\lim_{\substack{N \to \infty \\ \ell_o \to 0}} \frac{K_{ha}^{N+1}}{2\pi\sigma_\alpha\sigma_\beta} = \lim_{\substack{N \to \infty \\ \ell_o \to 0}} \frac{(1 - \ell_o d_v \overline{C_\ell})^{N+1}}{2\pi\sigma_\alpha\sigma_\beta}$$

$$\cong \frac{\exp[-N_e(1 - \gamma_f)]}{2\pi\sigma_\alpha\sigma_\beta} \quad . \tag{3-71}$$

Finally, then, we can write down the angular impulse response of the entire cloud. We have

$$h_1(\alpha, \beta; \alpha_o, \beta_o) = \lim_{\substack{N \to \infty \\ \ell_o \to 0}} h_N(\alpha, \beta; \alpha_o, \beta_o)$$

$$= \frac{\exp[-N_e(1 - \gamma_f)]}{2\pi\sigma_\alpha\sigma_\beta} \exp\left[-\frac{(\alpha - \alpha_o)^2}{2\sigma_\alpha^2} - \frac{(\beta - \beta_o)^2}{2\sigma_\beta^2} \right] \quad . \tag{3-72}$$

Since the single-layer response (3-62) contains an impulsive term, it is clear that Eq. (3-72) should actually contain an impulse as well. This term corresponds to the unscattered residue of the incident wave. It is easily shown that the coefficient of the impulse is $\exp[-N_e]$, however, and we assume N_e to be large enough that this term is negligible compared to Eq. (3-71).

We observe two interesting and intuitively satisfying features of Eq. (3-72). First, the variances (3-70) are proportional to the quantity $\gamma_f N_e$, which is precisely the optical thickness the

cloud would have if its particles were lossless, in the sense that $\overline{C_\ell}$ were zero and $\overline{C_{ext}}$ were reduced to $\overline{C_f}$. Second, the integral of Eq. (3-72) on α and β is $\exp[-N_e(1 - \gamma_f)]$, roughly the grand total of all scattered light which penetrates to the bottom of the cloud. This is precisely equal to the extinction attenuation which would be suffered by a plane wave traversing the cloud if the particles were completely lossy, in the sense that $\overline{C_f}$ were zero and $\overline{C_{ext}}$ were reduced to $\overline{C_\ell}$.

Having derived the angular impulse response (3-72) of the cloud, we can immediately write down its response $R(\alpha, \beta)$ to an arbitrary incident distribution $I(\alpha, \beta)$. Repeating the superposition arguments used in connection with Eq. (3-55), we have

$$R(\alpha, \beta) = \iint I(\alpha_o, \beta_o) \, h_I(\alpha, \beta; \; \alpha_o, \beta_o) \, d\alpha_o \, d\beta_o \quad . \tag{3-73}$$

We can now obtain explicit numerical criteria for the rather vague condition stated earlier that our results should be concentrated about $\Theta = 0$, in order that use of the coordinates α and β be permissible. After all intermediate calculations have been carried out, and we have arrived at a final answer [such as Eq. (3-73), for example], it will generally be appropriate to transform the result back to the conventional polar coordinates Θ and φ. As we explain in Appendix B, this is accomplished by using the transformations

$$\alpha = \Theta \cos \varphi \quad ,$$

$$\beta = \Theta \sin \varphi \quad ,$$

multiplying the function by the metric coefficient $\Theta / \sin \Theta$, and setting the result to zero for $\Theta > \pi/2$. The metric coefficient can be important in physical situations, as we shall see in Appendix G, because the parameters of actual clouds can often be such that the angular intensity distributions below them are nearly flat over most of the range of Θ from 0 to $\pi/2$.

A numerical criterion for the maximum permissible values of σ_α and σ_β in Eq. (3-72) follows when we impose the condition that the value of the (Θ, φ) transformation of Eq. (3-72) at $\Theta = \pi/2$ shall not exceed its value at $\Theta = 0$. In particular, let us suppose that $\alpha_o = \beta_o = 0$ in Eq. (3-72), and let us transform $h_I(\alpha, \beta; 0, 0)$ into a function $g(\Theta, \varphi)$. Recalling that $\sigma_\alpha^2 = \sigma_\beta^2$, we have

$$g(\Theta, \varphi) = C_1 \frac{\Theta}{\sin \Theta} \, \exp\left[-\frac{\Theta^2}{2\sigma_\alpha^2}\right] \quad , \tag{3-74a}$$

where

$$C_1 = \frac{\exp[-N_e(1 - \gamma_f)]}{2\pi\sigma_\alpha^2} \quad . \tag{3-74b}$$

The requirement that

$$g(\tfrac{\pi}{2}, \varphi) \leqslant g(0, \varphi)$$

leads to the condition

$$\frac{\pi/2}{\sin \pi/2} \, \exp\left[-\frac{\pi^2}{8\sigma_\alpha^2}\right] \leqslant 1 \quad ,$$

which is satisfied by

$$\sigma_\alpha^2 = \gamma_f N_e W_\alpha^2 \leqslant \frac{\pi^2}{8 \ln \pi/2}$$

$$\cong 2.73 \quad , \tag{3-75a}$$

or

$$\sigma_\alpha \leqslant 1.68 \quad . \tag{3-75b}$$

Now, we indicate in Appendix G that W_α and γ_f are very nearly 0.3 and 0.96, respectively, for most cloud particles at visible wavelengths. For these values Eq. (3-75a) yields the result

$$N_e \leqslant 31.6 \quad . \tag{3-75c}$$

We therefore have confidence in our analytical results for optical thicknesses less than about 32. In Appendix G we use published meteorological data to show that Eq. (3-75c) is satisfied by a broad range of naturally occurring clouds. For clouds of greater optical thicknesses, we are inclined to stipulate that angular intensity distributions are practically flat for all $\Theta \leqslant \pi/2$.

Equation (3-75a-c) is subject to a reasonable physical interpretation. We recognize that about 0.9 of the volume under a symmetric two-dimensional Gaussian function is contained within a radius 2σ about the origin. In particular, 0.9 of the volume under the cloud impulse response $h_I(\ )$ of Eq. (3-72) is contained within the region

$$\Theta = \sqrt{\alpha^2 + \beta^2} \leqslant 2\sigma_\alpha \quad .$$

When σ_α satisfies Eq. (3-75b) with equality, this becomes very nearly

$$\sqrt{\alpha^2 + \beta^2} \lesssim \pi \quad .$$

3.5 JOINT IMPULSE RESPONSE $h_p(\alpha, \beta, x, y;\ \alpha_0, \beta_0, x_0, y_0)$

A narrow beam of light traversing a cloud becomes spread out in both angle of arrival and cross-sectional area. We shall model this behavior of the cloud as a four-dimensional linear system, which is a natural extension of the results of the preceding section.

The joint impulse response $h_p(\alpha, \beta, x, y;\ \alpha_0, \beta_0, x_0, y_0)$ is defined as the power distribution function at coordinates (α, β, x, y) on the underside of a cloud when a quadruple-impulse beam of the form of Eq. (3-33) is incident on the top of the cloud at coordinates $(\alpha_0, \beta_0, x_0, y_0)$. As we showed in Sec. 3.2, the impulsive distribution [Eq. (3-33)] is a unit-power beam with infinitesimal angular dispersion which has intensity

$$\sec \Theta_0 u_0(x - x_0) u_0(y - y_0)$$

$$= \sec\left(\sqrt{\alpha_0^2 + \beta_0^2}\right) u_0(x - x_0) u_0(y - y_0) \text{ watts-m}^{-2} \quad . \tag{3-76}$$

We use the same technique in deriving $h_p(\ )$ that we used in finding $h_I(\ )$ in the preceding section; that is, we obtain the single-layer impulse response, construct an $(N-1)$-fold linear superposition integral, and take a limit as N goes to infinity.

The geometry of the single-layer configuration is shown in Fig. 3-7. It is convenient to begin by writing down the response $s_1(\alpha_1, \beta_1, x_1, y_1;\ \alpha_0, \beta_0, x_0, y_0)$ to the hybrid incident distribution

$$P_i(\alpha, \beta, x, y) = u_0(\alpha - \alpha_0) u_0(\beta - \beta_0) u_{-1}(x - x_0) u_{-1}(y - y_0) \quad , \tag{3-77}$$

27
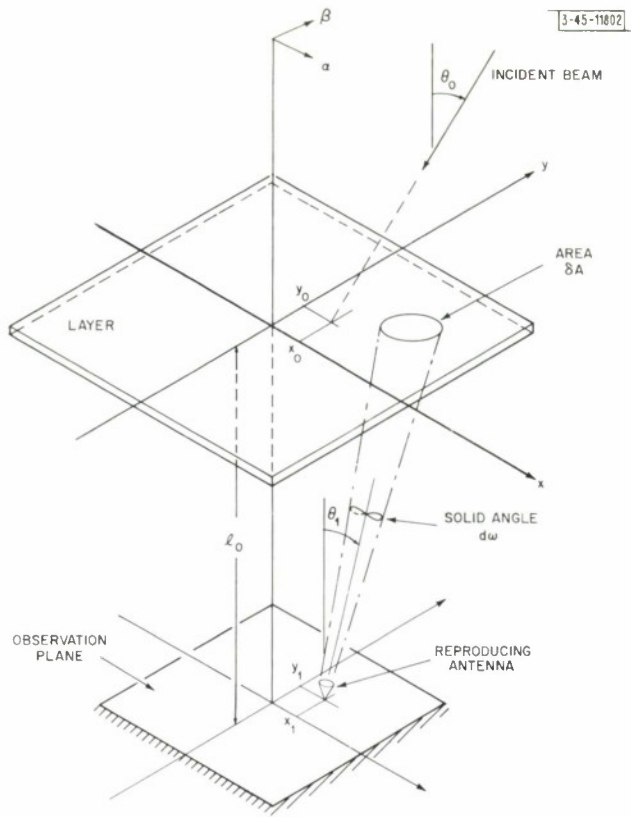
Fig. 3-7. Geometry for single-layer power function response.

in which $u_{-1}(\ )$ is the unit step function. Equation (3-77) corresponds to a plane wave with angle of arrival (α_0, β_0) whose intensity at the surface of the layer is

$$I_{pi}(x, y) = \begin{cases} \sec\left(\sqrt{\alpha_0^2 + \beta_0^2}\right) & , \quad \text{if } x \geqslant x_0 \quad \text{and} \quad y \geqslant y_0 \quad ; \\ 0 & , \quad \quad \text{elsewhere} \quad . \end{cases} \qquad (3\text{-}78)$$

The quadruple-impulse response $h_1(\ )$ of a single layer is obtained by differentiating $s_1(\ )$ with respect to x_1 and y_1. This step is permissible specifically because: (a) the scattering mechanism is linear, and (b), $s_1(\ )$ turns out to be a function of the differences $(x_1 - x_0)$ and $(y_1 - y_0)$.

The antenna in Fig. (3-7), which is the reproducing antenna defined in connection with Eq. (3-35) in Sec. 3.2, is pointed in the direction (α_1, β_1). Its effective aperture area in the plane perpendicular to its boresight axis is $dx\,dy \cos\Theta_1$. The coordinates (x_A, y_A) of the center of the region δA on the layer are given by

$$\begin{aligned} x_A &= \ell_0 \tan\Theta_1 \cos\varphi_1 + x_1 \\ &\simeq \ell_0 \Theta_1 \cos\varphi_1 + x_1 \\ &= \ell_0 \alpha_1 + x_1 \end{aligned} \qquad (3\text{-}79a)$$

and

$$\begin{aligned} y_A &= \ell_0 \tan\Theta_1 \sin\varphi_1 + y_1 \\ &\simeq \ell_0 \beta_1 + y_1 \quad , \end{aligned} \qquad (3\text{-}79b)$$

28

where φ_1 is the azimuth angle in spherical coordinates of the direction in which the antenna is pointed. It is clear that the antenna receives a signal only when δA lies in the region over which the incident illumination [Eq. (3-77)] is nonzero; that is, we must have

$$\ell_o \alpha_1 + x_1 > x_o \tag{3-80a}$$

and

$$\ell_o \beta_1 + y_1 > y_o \tag{3-80b}$$

simultaneously.

Given that the conditions of Eq. (3-80) obtain, and given that a particle is present in δA, we can write down the conditional average scattered power

$$\frac{\sec \Theta_o \overline{C}_f}{\ell_o^2 \sec^2 \Theta_1} f_1(\alpha_1 - \alpha_o, \ \beta_1 - \beta_o) \cos \Theta_1 \ dx \, dy \tag{3-81}$$

received by the antenna. Our reasoning is analogous to that associated with Eq. (3-47) in Sec. 3.4. The extra factor $\sec \Theta_o$ in (3-81) is the intensity of the incident plane wave, and the antenna aperture area $\cos \Theta_1 \, dx \, dy$ also appears as a factor. We express the conditions (3-80) by multiplying (3-81) by the function

$$u_{-1}(x_1 - x_o + \ell_o \alpha_1) \, u_{-1}(y_1 - y_o + \ell_o \beta_1) \quad . \tag{3-82}$$

The condition that a particle be present in δA is removed as before by multiplying (3-81) by the probability

$$\rho \delta A = \rho \ell_o^2 \sec^3 \Theta_1 \ d\omega \tag{[Eq. (3-48)]}$$

that a particle is there. The result is

$$\overline{p_{rec, \, sca}}(\alpha_1, \beta_1, x_1, y_1; \ \alpha_o, \beta_o, x_o, y_o) = \rho \overline{C}_f \sec \Theta_o f_1(\alpha_1 - \alpha_o, \beta_1 - \beta_o)$$

$$\cdot u_{-1}(x_1 - x_o + \ell_o \alpha_1) \, u_{-1}(y_1 - y_o + \ell_o \beta_1) \ d\omega \, dx \, dy \quad , \tag{3-83}$$

the average scattered power received by the reproducing antenna. By reasoning similar to that preceding Eq. (3-50), we write down the average unscattered power

$$\overline{p_{rec, \, unsc}}(\ ) = (1 - \rho \overline{C}_{ext} \sec \Theta_o) \sec \Theta_o \cos \Theta_1 \cdot u_o(\alpha_1 - \alpha_o) \, u_o(\beta_1 - \beta_o)$$

$$\cdot u_{-1}(x_1 - x_o + \ell_o \alpha_1) \, u_{-1}(y_1 - y_o + \ell_o \beta_1) \ d\omega \, dx \, dy \tag{3-84}$$

received by the antenna. Again, the factor $\sec \Theta_o \cos \Theta_1$ accounts for the incident intensity and the effective antenna aperture. But the impulses in α and β in Eq. (3-84) constrain Θ_o and Θ_1 to be equal; hence

$$\sec \Theta_o \cos \Theta_1 = \sec \Theta_o \cos \Theta_o = 1 \quad . \tag{3-85}$$

In view of Eq. (3-35), we see that the average power distribution function below the layer in response to the hybrid input [Eq. (3-77)] is

$$s_1(\ ) = [d\omega\,dx\,dy]^{-1}\,[\overline{p_{rec,unse}}(\ ) + \overline{p_{rec,sca}}(\ )]$$

$$= [(1 - \rho\overline{C_{ext}}\,\widehat{\sec\Theta})\,u_o(\alpha_1 - \alpha_o)\,u_o(\beta_1 - \beta_o) + \rho\overline{C_f}\,\widehat{\sec\Theta}_o f_1(\alpha_1 - \alpha_o,\ \beta_1 - \beta_o)]$$

$$\cdot u_{-1}(x_1 - x_o + \ell_o\alpha_1)\,u_{-1}(y_1 - y_o + \ell_o\beta_1) \quad . \tag{3-86}$$

The replacement of $\sec\Theta_o$ by $\widehat{\sec\Theta}_o$ follows from the same reasoning that we used in connection with Eq. (3-52). As we stated earlier, the hybrid response $s_1(\ )$ is a function of the differences $(x_1 - x_o)$ and $(y_1 - y_o)$. Now, the quadruple-impulse incident distribution (3-33) is the second partial derivative with respect to x and y of the incident wave [Eq. (3-77)] which gave rise to the output $s_1(\ )$. The impulse response $h_1(\ )$ is therefore the derivative of $s_1(\ )$; that is

$$h_1(\ ) = \frac{\partial^2}{\partial x_1\,\partial y_1}\,[s_1(\ )] \quad . \tag{3-87}$$

The result is a duplicate of the rightmost member of Eq. (3-86), except that the two unit-step functions $u_{-1}(\ )$ are replaced by unit impulses $u_o(\ )$.

As in Sec. 3.4, we exploit the linearity of the model to construct an $(N-1)$-fold superposition integral for the response $h_N(\ )$ below N layers ℓ_o meters apart. We have

$$h_N(\alpha_N, \beta_N, x_N, y_N;\ \alpha_o, \beta_o, x_o, y_o) = \iint\cdots\int d\alpha_{N-1}\cdots d\alpha_1$$

$$\cdot \iint\cdots\int d\beta_{N-1}\cdots d\beta_1 \iint\cdots\int dx_{N-1}\cdots dx_1 \iint\cdots\int dy_{N-1}\cdots dy_1$$

$$\cdot h_1(\alpha_N, \beta_N, x_N, y_N;\ \alpha_{N-1}, \beta_{N-1}, x_{N-1}, y_{N-1})\cdots$$

$$\cdot h_1(\alpha_1, \beta_1, x_1, y_1;\ \alpha_o, \beta_o, x_o, y_o) \quad . \tag{3-88}$$

The limits of integration on all the α and β variables are $\pm\pi/2$, and the x and y integrals have limits $\pm\infty$.

Equation (3-88) cannot be solved by application of the Central Limit Theorem, because $h_1(\ )$ is not a function of the differences of its arguments. Even though we can replace $\sec\Theta_i$ by unity as before, the two impulses $u_o(x_i - x_{i-1} + \ell_o\alpha_i)$ and $u_o(y_i - y_{i-1} + \ell_o\beta_i)$ cannot be written as functions of $(\alpha_i - \alpha_{i-1})$ and $(\beta_i - \beta_{i-1})$. The equation has been solved, however, by a method which is approximate in the same sense as the technique used in Sec. 3.4. Because the procedure is long and involved, only the final answer is presented here; the solution is carried out in detail in Appendix D. In the limit as N goes to infinity, the result is the four-dimensional jointly Gaussian function

$$h_p(\alpha, \beta, x, y;\ \alpha_o, \beta_o, x_o, y_o) = \exp[-N_e(1 - \gamma_f)]\left[4\pi^2\sigma_\alpha\sigma_\beta\sigma_x\sigma_y\sqrt{(1 - \rho_{\alpha x}^2)(1 - \rho_{\beta y}^2)}\right]^{-1}$$

$$\cdot\exp\left[-\frac{1}{2(1 - \rho_{\alpha x}^2)}\left(\frac{(\alpha - \alpha_o)^2}{\sigma_\alpha^2} - 2\rho_{\alpha x}\frac{(\alpha - \alpha_o)(x - x_o + \tau\alpha_o)}{\sigma_\alpha\sigma_x} + \frac{(x - x_o + \tau\alpha_o)^2}{\sigma_x^2}\right)\right]$$

$$\cdot\exp\left[-\frac{1}{2(1 - \rho_{\beta y}^2)}\left(\frac{(\beta - \beta_o)^2}{\sigma_\beta^2} - 2\rho_{\beta y}\frac{(\beta - \beta_o)(y - y_o + \tau\beta_o)}{\sigma_\beta\sigma_y} + \frac{(y - y_o + \tau\beta_o)^2}{\sigma_y^2}\right)\right] , \tag{3-89}$$

30

in which

$$\sigma_\alpha^2 = \gamma_f N_e W_\alpha^2 \quad , \qquad\qquad\qquad \sigma_y^2 = \frac{\tau^2}{3} \sigma_\beta^2 \quad ,$$

$$\sigma_\beta^2 = \gamma_f N_e W_\beta^2 \quad , \qquad\qquad\qquad \rho_{\alpha x} = \rho_{\beta y} = -\frac{\sqrt{3}}{2} \quad . \qquad (3\text{-}90)$$

$$\sigma_x^2 = \frac{\tau^2}{3} \sigma_\alpha^2 \quad ,$$

The quantities γ_f, W_α^2 and W_β^2 are the single-particle scattering pattern parameters defined previously. The quantity τ is the physical thickness of the cloud in meters, and N_e is its optical thickness.

Now, since $h_N(\ )$ was defined as the impulse response over a plane ℓ_o meters below the Nth cloud layer, Eq. (3-89) is a power distribution function over the lower boundary plane of the cloud. In many situations we will want to know the impulse response over the ground plane h meters below the underside of the cloud. One could calculate the necessary transformation geometrically, but it is easily obtained from the single-layer impulse response $h_1(\ )$ that we have already derived. Let us visualize adding a fictitious planar layer ℓ_o meters below the cloud, on which the average particle density ρ is equal to zero. The quadruple-impulse response $h_1'(\ )$ of this layer is obtained from $h_1(\ )$ by replacing ρ by zero and ℓ_o by h; that is,

$$h_1'(\alpha, \beta, x, y;\ \alpha_o, \beta_o, x_o, y_o) = u_o(\alpha - \alpha_o)\, u_o(\beta - \beta_o)\, u_o(x - x_o + h\alpha)\, u_o(y - y_o + h\beta) \quad . \quad (3\text{-}91)$$

The impulse response $h_G(\ )$ of the cloud, measured over the ground, is given by the superposition integral

$$h_G(\alpha, \beta, x, y;\ \alpha_o, \beta_o, x_o, y_o) = \iiiint d\alpha'\, d\beta'\, dx'\, dy'$$

$$\cdot\, h_1'(\alpha, \beta, x, y;\ \alpha', \beta', x', y') \cdot h_p(\alpha', \beta', x', y';\ \alpha_o, \beta_o, x_o, y_o) \quad . \qquad (3\text{-}92)$$

The solution of Eq. (3-92) is another four-dimensional Gaussian function,

$$h_G(\alpha, \beta, x, y;\ \alpha_o, \beta_o, x_o, y_o) = \exp[-N_e(1 - \gamma_f)]$$

$$\cdot \left[4\pi^2 \sigma_{\alpha G} \sigma_{\beta G} \sigma_{xG} \sigma_{yG}\ \sqrt{(1 - \rho_{\alpha xG}^2)(1 - \rho_{\beta yG}^2)} \right]^{-1}$$

$$\cdot \exp\left[-\frac{1}{2(1 - \rho_{\alpha xG}^2)} \left(\frac{(\alpha - \alpha_o)^2}{\sigma_{\alpha G}^2} - 2\rho_{\alpha xG} \frac{(\alpha - \alpha_o)(x - x_o + (\tau + h)\,\alpha_o)}{\sigma_{\alpha G}\sigma_{xG}} \right.\right.$$

$$\left.\left. + \frac{(x - x_o + (\tau + h)\,\alpha_o)^2}{\sigma_{xG}^2} \right) \right]$$

$$\cdot \exp\left[-\frac{1}{2(1 - \rho_{\beta yG}^2)} \left(\frac{(\beta - \beta_o)^2}{\sigma_{\beta G}^2} - 2\rho_{\beta yG} \frac{(\beta - \beta_o)(y - y_o + (\tau + h)\,\beta_o)}{\sigma_{\beta G}\sigma_{yG}} \right.\right.$$

$$\left.\left. + \frac{(y - y_o + (\tau + h)\,\beta_o)^2}{\sigma_{yG}^2} \right) \right] \quad , \qquad (3\text{-}93)$$

31

in which

$$\sigma_{\alpha G}^2 = \sigma_\alpha^2 \quad ,$$

$$\sigma_{\beta G}^2 = \sigma_\beta^2 \quad ,$$

$$\sigma_{xG}^2 = \sigma_x^2 - 2\rho_{\alpha x} h \sigma_x \sigma_\alpha + h^2 \sigma_\alpha^2 \quad ,$$

$$\sigma_{yG}^2 = \sigma_y^2 - 2\rho_{\beta y} h \sigma_y \sigma_\beta + h^2 \sigma_\beta^2 \quad ,$$

$$\rho_{\alpha xG} = \frac{\rho_{\alpha x}\sigma_x - h\sigma_\alpha}{\sigma_{xG}} \quad ,$$

$$\rho_{\beta yG} = \frac{\rho_{\beta y}\sigma_y - h\sigma_\beta}{\sigma_{yG}} \quad . \tag{3-94}$$

We notice that the coefficient in front of the Gaussian exponentials in $h_G(\ )$ is identical to the coefficient in $h_p(\ )$, as it must be. In both cases, it is

$$3 \exp[-N_e(1 - \gamma_f)]\,[\pi\tau\gamma_f N_e W_\alpha W_\beta]^{-2} \quad . \tag{3-95}$$

We notice also that the integral of either $h_G(\ )$ or $h_p(\ )$ over all α, β, x and y is equal to $\exp[-N_e(1 - \gamma_f)]$, which is approximately equal to the total _power_ penetrating to the bottom of the cloud when the unit-power quadruple-impulse beam is incident on the top of it.

We can immediately write a superposition integral specifying the response $P_G(\alpha, \beta, x, y)$ over the ground beneath a cloud illuminated by an arbitrary incident power distribution function $P_i(\alpha_0, \beta_0, x_0, y_0)$. Specifically,

$$P_G(\alpha, \beta, x, y) = \iiiint d\alpha_0\, d\beta_0\, dx_0\, dy_0$$

$$\cdot P_i(\alpha_0, \beta_0, x_0, y_0)\, h_G(\alpha, \beta, x, y;\ \alpha_0, \beta_0, x_0, y_0) \quad . \tag{3-96}$$

The intensity variation across a laser beam is frequently approximated by a Gaussian function. Suppose such a beam were incident on the top of the cloud at an angle of arrival (α_i, β_i), and that it had negligible angular dispersion. Further, assume that the center of the beam intersects the upper surface of the cloud at the coordinates (x_i, y_i). An appropriate power distribution representation for this beam is

$$P_i(\alpha_0, \beta_0, x_0, y_0) = \frac{P_0}{2\pi\sigma_{xi}\sigma_{yi}} u_0(\alpha_0 - \alpha_i)\, u_0(\beta_0 - \beta_i)$$

$$\cdot \exp\left[-\frac{(x_0 - x_i)^2}{2\sigma_{xi}^2} - \frac{(y_0 - y_i)^2}{2\sigma_{yi}^2} \right] \quad , \tag{3-97}$$

where P_0 is the total power borne by the beam, provided that α_i and β_i are small. (In general, the beam intensity variation would be modeled as a Gaussian function over a plane perpendicular to the direction of propagation. One would transform it into a function of x_0 and y_0 over the horizontal plane, which would not necessarily be Gaussian, and use the result in Eq. (3-97).

32

The assumption of small α_i and β_i simplifies the mathematies for this example.) Inserting this expression into Eq. (3-96) and carrying out the integrations, we find that the resulting power distribution function $P_G(\alpha, \beta, x, y)$ over the ground has precisely the form (3-93), with the following modifieations:

    (a)   multiply (3-93) by P_o;

    (b)   replace α_o, β_o, x_o and y_o by α_i, β_i, x_i, and y_i; and

    (e)   replace σ_{xG}^2 by $(\sigma_{xG}^2 + \sigma_{xi}^2)$, and σ_{yG}^2 by $(\sigma_{yG}^2 + \sigma_{yi}^2)$.

The incident beam [Eq. (3-97) is particularly well suited for demonstrating the consistent relationship between the angular impulse response $h_I(\alpha, \beta; \alpha_o, \beta_o)$ of Eq. (3-72) and the joint impulse response $h_G(\alpha, \beta, x, y; \alpha_o, \beta_o, x_o, y_o)$. In the limit as σ_{xi} and σ_{yi} go to infinity, the ineident beam [Eq. (3-97)] looks like a uniform plane wave with angle of arrival (α_i, β_i), whose intensity is

$$I_p = \frac{P_o}{2\pi\sigma_{xi}\sigma_{yi}} \quad . \tag{3-98}$$

Meanwhile, the eorresponding response $P_G( )$ of the preeeding paragraph assumes the form

$$I_p \exp[-N_e(1-\gamma_f)] \, [2\pi\sigma_\alpha\sigma_\beta]^{-1} \cdot \exp\left[-\frac{(\alpha - \alpha_i)2}{2\sigma_\alpha^2} - \frac{(\beta - \beta_i)2}{2\sigma_\beta^2}\right] \quad , \tag{3-99}$$

whieh is preeisely the angular intensity distrihution that Eq. (3-72) gives in response to the same ineident plane wave.

33

CHAPTER 4
GENERALIZED SCATTERING FUNCTION

In Appendix A we consider the statistics of the scattered field on the ground beneath a cloud illuminated by a signal of the form

$$e_i(t, \vec{\rho}) = \text{Re} \left\{ s(t) \, E(\vec{\rho}) \, \exp(-j2\pi f_o t) \right\} \quad . \tag{4-1}$$

The function $s(t)$ is a narrow-band unit-energy complex envelope. The function $E(\vec{\rho})$ describes the variation of the field amplitude with position $\vec{\rho}$ over the top of the cloud. It is equal to a constant for all $\vec{\rho}$ when the incident illumination is uniform over the top of the cloud (e.g., a plane wave), but has the appropriate functional form when the illumination is nonuniform (e.g., a beam). It is shown in Appendix A that the resulting field at a point on the ground can be represented in terms of a complex Gaussian random process. Because of the spatial variation $E(\vec{\rho})$ in Eq. (4-1), the parameters of the received process depend upon the point of observation $\vec{r}$ on the ground plane.

Since it is a Gaussian process, the received field is completely characterized statistically by its mean (which is zero) and its correlation function. We shall write this function in terms of a generalized scattering function $\sigma(\tau, f, \vec{v}')$, which also depends upon the point of observation $\vec{r}$. These ideas are developed in Sec. 4.1. In the remaining four sections of the chapter, we examine and interpret both the correlation and scattering functions from several points of view.

4.1 SCATTERING FUNCTION $\sigma(\tau, f, \vec{v}')$

Some of the ideas exploited in this section are similar to those developed in detail in Appendix A. The reader may find it helpful to read the appendix before proceeding further with this analysis.

When the cloud is illuminated by the signal [Eq. (4-1)], the scattered field $y(t, \vec{r}, \vec{r}')$ in the vicinity of the point $\vec{r}$ on the ground plane is adequately approximated, as we show in Appendix A, by the expression

$$y(t, \vec{r}, \vec{r}') = \text{Re} \left\{ \sum_{n=1}^{M} \eta_n s(t - \tau_n) \right.$$

$$\left. \cdot \exp\left[-j2\pi t(f_o - f_n) - j\Theta_n - j\frac{2\pi}{\lambda_o} (\vec{r}' \cdot \vec{v}_n') \right] \right\} \quad , \tag{4-2}$$

in which both $\vec{r}'$ and $\vec{v}_n'$ are vectors drawn from the origin of a coordinate system S' centered at $\vec{r}$. The vector $\vec{r}'$ lies in the ground plane, and is small in magnitude compared to the distance of the cloud particles from $\vec{r}$. The unit vector $\vec{v}_n'$ points toward the last particle encountered by the nth signal component before it reached the ground. The number M is enormous, being the total of all possible single- and multiple-scattering paths from the top of the cloud to the ground. The amplitude factor η_n is very small; it is a random variable, and is statistically independent of all the other amplitudes. The quantities τ_n and f_n are the total path delay (often called the "range delay") and Doppler shift, respectively, associated with the nth path. In general, η_n, τ_n and f_n are implicitly dependent upon $\vec{r}$. The phase Θ_n is random, uniformly

35

distributed over $(-\pi, \pi)$, and is statistically independent of the phases on all the other paths. The last term in the exponent of Eq. (4-1) expresses the phase variation of the nth signal component with $\vec{r}'$.

Because of the uniformly distributed random phases, the mean $\overline{y(t, \vec{r}, \vec{r}')}$ of Eq. (4-2) is zero. Thus a complete statistical description of the process is provided by its correlation function $K(t_1, t_2, \vec{r}'_1, \vec{r}'_2)$. Like all the other functions considered in this chapter, $K(\ )$ is functionally dependent upon $\vec{r}$. Rather than carrying $\vec{r}$ along as an argument everywhere, we simply adopt the convention that the $\vec{r}$-variation is implicitly present in every case. The details of this dependence will be discussed explicitly where appropriate. In particular, we will find that the $\vec{r}$-dependence is important when the incident illumination is a beam, but absent under plane-wave illumination.

In deriving $K(\ )$ we adhere closely to an analysis carried out by Kennedy.[32] We have

$$K(t_1, t_2, \vec{r}'_1, \vec{r}'_2) = \overline{y(t_1, \vec{r}'_1)\, y(t_2, \vec{r}'_2)}$$

$$= \frac{1}{4} \overline{\sum_i \left[A_i(t_1, \vec{r}'_1)\, e^{-j\Theta_i} + A_i^*(t_1, \vec{r}'_1)\, e^{+j\Theta_i} \right]}$$

$$\cdot \overline{\sum_k \left[A_k(t_2, \vec{r}'_2)\, e^{-j\Theta_k} + A_k^*(t_2, \vec{r}'_2)\, e^{+j\Theta_k} \right]} \quad , \tag{4-3}$$

in which

$$A_i(t, \vec{r}') = \eta_i s(t - \tau_i) \exp\left[-j2\pi t(f_o - f_i) - j\frac{2\pi}{\lambda_o}(\vec{r}' \cdot \vec{v}'_i) \right] \quad .$$

Let us first average Eq. (4-3) over the phases Θ_i, conditioned on the random amplitudes η_i. Because of our assumptions about the phases, Eq. (4-3) becomes

$$K(t_1, t_2, \vec{r}'_1, \vec{r}'_2) = \frac{1}{2} \, \text{Re} \left[\sum_i \overline{A_i(t_1, \vec{r}'_1)\, A_i^*(t_2, \vec{r}'_2)}^{\eta_i} \right]$$

$$= \frac{1}{2} \, \text{Re} \left\{ \exp\left[-j2\pi f_o(t_1 - t_2) \right] \cdot \sum_i \left[\overline{|\eta_i|^2}\, s(t_1 - \tau_i)\, s^*(t_2 - \tau_i) \right. \right.$$

$$\left. \left. \cdot \exp\left(j2\pi f_i(t_1 - t_2) - j\frac{2\pi}{\lambda_o}(\vec{r}'_1 - \vec{r}'_2) \cdot \vec{v}'_i \right) \right] \right\} \quad . \tag{4-4}$$

Let us collect all the terms in the summand of Eq. (4-4) which have path delays τ_i in the range $(\tau, \tau + \Delta\tau)$, Doppler shifts f_i in the range $(f, f + \Delta f)$, and $\vec{v}'_i$ in the range $(\vec{v}', \vec{v}' + \Delta\vec{v}')$. It is convenient to defer the precise interpretation of the quantity $\Delta\vec{v}'$ to the following section; for the present, we simply assume that it is a well-defined quantity. We now add all these terms, writing their sum in the form

$$\frac{1}{2} \text{ Re} \left\{ \exp\left[-j2\pi f_o(t_1 - t_2)\right] \sum_m \left[\overline{|\eta_m|^2} \, s(t_1 - \tau_m) \, s^*(t_2 - \tau_m) \right. \right.$$

$$\left. \cdot \exp\left(j2\pi f_m(t_1 - t_2) - j\frac{2\pi}{\lambda_o}(\vec{r_1'} - \vec{r_2'}) \cdot \vec{v_m'}\right)\right] \right\}$$

$$\cong \frac{1}{2} \text{ Re} \left\{ \exp\left[-j2\pi f_o(t_1 - t_2)\right] W(\tau, f, \vec{v'}) \, \Delta\tau \, \Delta f \, \Delta\vec{v'} \right.$$

$$\left. \cdot s(t_1 - \tau) \, s^*(t_2 - \tau) \exp\left(j2\pi f(t_1 - t_2) - j\frac{2\pi}{\lambda_o}(\vec{r_1'} - \vec{r_2'}) \cdot \vec{v'}\right)\right\} \quad , \qquad (4\text{-}5)$$

in which the index m ranges over only those field components having τ_m, f_m and $\vec{v_m'}$ in the prescribed ranges. The weighting function $W(\ )$ is defined by the relation

$$W(\tau, f, \vec{v'}) \, \Delta\tau \, \Delta f \, \Delta\vec{v'} = \sum_m \overline{|\eta_m|^2} \quad , \qquad (4\text{-}6)$$

with m ranging over the values it assumed in Eq. (4-5). The approximate equality in Eq. (4-5) approaches equality as $\Delta\tau$, Δf and $\Delta\vec{v'}$ approach zero.

We visualize grouping all the terms in Eq. (4-4) into partial sums of the form given in Eq. (4-5) and adding them. In the limit, as $\Delta\tau$, Δf and $\Delta\vec{v'}$ approach the increments $d\tau$, df and $d\vec{v'}$, this sum approaches the multiple integral

$$K(t_1, t_2, \vec{r_1'}, \vec{r_2'}) = \frac{1}{2} \text{ Re} \left\{ \exp\left[-j2\pi f_o(t_1 - t_2)\right] \right.$$

$$\cdot \int d\tau \, df \, d\vec{v'} \, W(\tau, f, \vec{v'}) \, s(t_1 - \tau) \, s^*(t_2 - \tau)$$

$$\left. \cdot \exp\left[j2\pi f(t_1 - t_2) - j\frac{2\pi}{\lambda_o}(\vec{r_1'} - \vec{r_2'}) \cdot \vec{v'}\right]\right\} \quad , \qquad (4\text{-}7)$$

where the range of integration includes all τ, f and $\vec{v'}$ for which $W(\ )$ is nonzero. From an engineering point of view, the function $W(\ )$ and the integral in Eq. (4-7) make sense when the weighting coefficients $|\eta_i|^2$ in Eq. (4-4) are small, the number of field components is very large, and the parameters of the field components are distributed over the applicable ranges of τ, f and $\vec{v'}$ in a reasonably smooth manner. We claim that these conditions are satisfied by our cloud model, under the assumptions we have made, and hence mathematical convergence questions need not be considered.

We now introduce the generalized channel scattering function

$$\sigma(\tau, f, \vec{v'}) \triangleq W(\tau, f, \vec{v'}) \left[\int d\tau \, df \, d\vec{v'} \, W(\tau, f, \vec{v'}) \right]^{-1} \quad , \qquad (4\text{-}8)$$

in which the integration range includes all τ, f, and $\vec{v'}$. We recognize that $\sigma(\ )$ depends in general upon $\vec{r}$ as well. Let us assume that the complex envelope $s(t)$ of the transmitted signal is so normalized that

$$\frac{1}{2} \int |s(t)|^2 \, dt = 1 \quad . \tag{4-9}$$

Without concerning ourselves at this time with the value of the signal energy incident on the cloud, we simply observe that the energy E_r per unit area borne by the received signal $y(t, \vec{r}, \vec{r}')$ is given by the relation

$$E_r = \int K(t, t, \vec{r}', \vec{r}') \, dt \quad . \tag{4-10}$$

It follows that Eq. (4-7) can be written in the form

$$
\begin{aligned}
K(t_1, t_2, \vec{r}_1', \vec{r}_2') = \frac{E_r}{2} \, \mathrm{Re} &\left\{ \exp[-j2\pi f_0(t_1 - t_2)] \right. \\
&\cdot \int d\tau \, df \, d\vec{v}' \, \sigma(\tau, f, \vec{v}') \, s(t_1 - \tau) \, s^*(t_2 - \tau) \\
&\left. \cdot \exp\left[j2\pi f(t_1 - t_2) - j\frac{2\pi}{\lambda_0} (\vec{r}_1' - \vec{r}_2') \cdot \vec{v}' \right] \right\} \quad .
\end{aligned}
\tag{4-11}
$$

Equation (4-11) is the result that we seek. If we knew the scattering function at every $\vec{r}$, and the transmitted signal envelope $s(t)$, the relation (4-11) would give us a complete statistical description of the field everywhere on the ground plane. Of course, the determination of the scattering function in any specific case can be a major undertaking. We have obtained only a partial description of the function for the cloud communication problem, as we explain in succeeding sections of this chapter.

Nevertheless, assuming we have complete knowledge of $\sigma(\tau, f, \vec{v}')$ and $s(t)$, the formulation of Eq. (4-11) leads to a description of the optimum receiver for the case in which the total received process

$$r(t, \vec{r}) = Y(t, \vec{r}) + N(t, \vec{r}) \quad , \tag{4-12}$$

where the noise $N(\ )$ is a Gaussian random process, statistically independent of the signal $Y(\ )$. Kennedy[32] has outlined the processing such a receiver must perform, over an aperture which is small compared with the distance to the scattering medium, as a logical extension of known techniques[33] for the detection of Gaussian signals in Gaussian noise. He obtains a set of observables by expanding the received process on a complete set of orthonormal time-space functions $\varphi_i(t, \vec{r})$, and proceeds to a likelihood function. While the analysis is quite straightforward on an abstract level, the actual receiver processing in specific cases involves the solution of complicated integral equations in time and space.

We choose not to dwell upon the design of such an optimum receiver. Instead, we shall propose a scheme in Chapter 5 which is subject to a straightforward performance analysis. It is not clear how closely this scheme approaches the optimum performance, but it will give us a feeling for a lower bound on the performance one might expect to achieve. In designing this receiver, we shall use certain special cases and rough approximations of the correlation function and scattering function developed in this section. The remainder of this chapter is devoted to discussions of these specialized functions.

4.2 SPATIAL CORRELATION FUNCTION $K(\vec{r}_1, \vec{r}_2)$

A special case of Eq. (4-11) is the time-dependent spatial correlation function

$$K(t, t, \vec{r}_1', \vec{r}_2') = \frac{E_r}{2} \, \text{Re} \, \left\{ \int d\tau \, df \, d\vec{v}' \, \sigma(\tau, f, \vec{v}') \right.$$

$$\left. \cdot \, s(t-\tau) \, s^*(t-\tau) \, \exp\left[-j \frac{2\pi}{\lambda_0} (\vec{r}_1' - \vec{r}_2') \cdot \vec{v}'\right] \right\} \tag{4-13}$$

in the vicinity of a point $\vec{r}$ on the ground. Now, suppose that the complex transmitted-signal envelope $s(t)$ is extremely narrow band; that is, let it equal $\sqrt{2/T}$ over a time interval $-T/2 \leqslant t \leqslant +T/2$ which is very long compared with the interval along the τ-axis over which $\sigma(\tau, f, \vec{v}')$ is nonzero. We can then talk about a function

$$K(0, 0, \vec{r}_1', \vec{r}_2') = \frac{E_r}{T} \, \text{Re} \, \left\{ \int d\vec{v}' \, \sigma(\vec{v}') \, \exp\left[-j \frac{2\pi}{\lambda_0} (\vec{r}_1' - \vec{r}_2') \cdot \vec{v}'\right] \right\} \quad , \tag{4-14}$$

in which

$$\sigma(\vec{v}') = \int d\tau \, df \, \sigma(\tau, f, \vec{v}') \quad . \tag{4-15}$$

We can extend Eq. (4-14) to the case of CW illumination simply by setting

$$E_r = P_r T \tag{4-16}$$

and letting T go to infinity. P_r is the average received power, understood to be defined (like E_r) on a per-unit-area basis. Equation (4-14) is now a time-independent spatial correlation function, which we redesignate $K(\vec{r}_1', \vec{r}_2')$.

The quantity $\sigma(\vec{v}')$ in Eq. (4-14) has a natural interpretation in terms of the cloud impulse responses derived in Chapter 3. Suppose we regard $\vec{v}'$ as the radial unit vector

$$\vec{i}_r = \sin\Theta \, \cos\varphi \, \vec{i}_x + \sin\Theta \, \sin\varphi \, \vec{i}_y + \cos\Theta \, \vec{i}_z \tag{4-17}$$

in a spherical coordinate system centered at the point of observation $\vec{r}$ on the ground plane. The situation is illustrated in Fig. 4-1, for the case in which $\vec{r} = 0$. The indicated region $d\vec{v}'$ about $\vec{v}'$ is merely symbolic, since $d\vec{v}'$ has not yet been defined. From the defining Eqs. (4-6) and (4-8), we conclude for the CW case that $\sigma(\vec{v}') \, d\vec{v}'$ is proportional to the average total power scattered toward the origin of coordinates by all the cloud particles in the region $d\vec{v}'$ about $\vec{v}'$. We recognize that it is entirely consistent with this definition to let $d\vec{v}'$ be the incremental solid angle

$$d\omega = \sin\Theta \, d\Theta \, d\varphi \tag{4-18}$$

about $\vec{v}'$. Thus we can replace $\sigma(\vec{v}') \, d\vec{v}'$ by

$$\sigma(\Theta, \varphi) \, d\omega = \sigma(\Theta, \varphi) \, \sin\Theta \, d\Theta \, d\varphi \quad . \tag{4-19}$$

We remark in passing that a similar interpretation applies to the complete scattering function $\sigma(\tau, f, \vec{v}')$ for general $s(t)$; that is, we can replace $\sigma(\tau, f, \vec{v}') \, d\tau \, df \, d\vec{v}'$ by $\sigma(\tau, f, \Theta, \varphi) \, d\tau \, df \, d\omega$.

In terms of the orthogonal angular coordinates

$$\alpha = \Theta \, \cos\varphi \quad ,$$

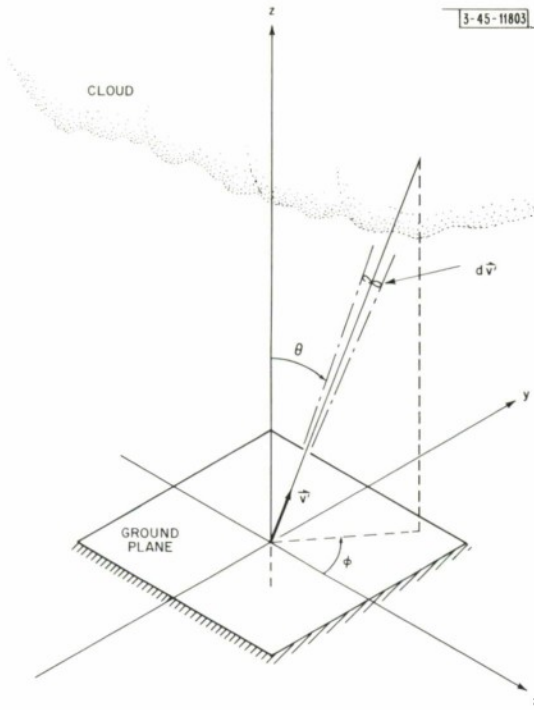$$\beta = \Theta \, \sin\varphi \quad , \tag{4-20}$$

Fig. 4-1. Spherical coordinates for $\sigma(\vec{v}')$.

defined in Appendix B, we have

$$\sigma(\Theta, \varphi)\, d\omega \cong \sigma(\alpha, \beta)\, d\alpha\, d\beta \quad . \tag{4-21}$$

Here α and β are measured, like Θ and φ, in a coordinate frame with its origin at the point of observation $\vec{r}$. Viewed in this manner, $\sigma(\alpha, \beta)$ embodies precisely the information provided by the impulse responses of Chapter 3. Thus it is appropriate to call $\sigma(\alpha, \beta)$ the angle-of-arrival scattering function. When the incident illumination is a superposition $I_{inc}(\alpha_o, \beta_o)$ of uniform plane waves over the top of the cloud we have, by Eq. (3-73) of Sec. 3.4,

$$\sigma(\alpha, \beta) = K_p \iint I_{inc}(\alpha_o, \beta_o)\, h_I(\alpha, \beta;\ \alpha_o, \beta_o)\, d\alpha_o\, d\beta_o \quad , \tag{4-22}$$

in which $h_I(\ )$ is the angular impulse response [Eq. (3-72)]. The proportionality constant K_p is included to satisfy the requirement that

$$\iint \sigma(\alpha, \beta)\, d\alpha\, d\beta = 1 \quad . \tag{4-23}$$

Because the incident radiation $I_{inc}(\ )$ is uniform over the horizontal plane, nothing on the right side of Eq. (4-22) depends upon position $\vec{r}$ (i.e., the Cartesian coordinates x and y) over the ground plane. Thus $\sigma(\alpha, \beta)$ is independent of $\vec{r}$ in this instance.

When the spatial variation of the incident radiation is more complicated (e.g., a narrow beam), it must be represented as a power distribution function $P_{inc}(\alpha_o, \beta_o, x_o, y_o)$ over the top of the cloud, as explained in Sec. 3.2. In this event, $\sigma(\alpha, \beta)$ does depend upon the horizontal coordinates (x, y). In view of Eq. (3-96) of Sec. 3.5, we have

40

$$\sigma(\alpha, \beta) = K_p \iiiint d\alpha_o \, d\beta_o \, dx_o \, dy_o$$

$$\cdot \, P_{inc}(\alpha_o, \beta_o, x_o, y_o) \, h_G(\alpha, \beta, x, y; \, \alpha_o, \beta_o, x_o, y_o) \quad , \tag{4-24}$$

in which $h_G(\;)$ is the joint impulse response [Eq. (3-93)]. As we showed in Sec. 3.5, Eq. (4-22) is simply a special case of Eq. (4-24) in the limit as the cross-sectional area of the incident beam goes to infinity.

It is worthwhile to calculate some typical examples of $K(\vec{r}_1', \vec{r}_2')$. Suppose first that the incident radiation is a single CW uniform plane wave with angle of arrival (α_o, β_o). We shall find that $K(\;)$ is independent of the coordinates x and y over the ground (as it is in every case when the incident illumination is uniform over the horizontal plane). Equation (4-22) now reduces to

$$\sigma(\alpha, \beta) = h_1(\alpha, \beta; \, \alpha_o, \beta_o)$$

$$= \frac{1}{2\pi \sigma_\alpha \sigma_\beta} \exp\left[-\frac{(\alpha - \alpha_o)^2}{2\sigma_\alpha^2} - \frac{(\beta - \beta_o)^2}{2\sigma_\beta^2} \right] \quad , \tag{4-25}$$

in which

$$\sigma_\alpha^2 = \sigma_\beta^2 = \gamma_f N_e W_\alpha^2 \quad .$$

The normalization of Eq. (4-25) is not quite right, of course, because we agreed that $h_1(\;)$ should be set to zero outside the ranges

$$|\alpha| \leqslant \pi/2 \quad ,$$

$$|\beta| \leqslant \pi/2 \quad . \tag{4-26}$$

This detail may be ignored when we deal with situations in which σ_α and σ_β are small enough that most of the volume under Eq. (4-25) is inside the region of Eq. (4-26).

We recall that the arguments of $K(\vec{r}_1', \vec{r}_2')$ are vectors of small magnitude, measured in a coordinate system S' with its origin at the point $\vec{r}$ about which $K(\;)$ is defined. The calculation of $K(\;)$ is facilitated by shifting $\vec{r}$ (and hence S') slightly so that

$$\vec{r}_1' = \frac{x'}{2} \, \vec{i}_x + \frac{y'}{2} \, \vec{i}_y = -\vec{r}_2' \quad , \tag{4-27}$$

where x' and y' are also measured in S'. In view of Eq. (4-17), we have

$$(\vec{r}_1' - \vec{r}_2') \cdot \vec{v}' = x' \sin\Theta \, \cos\varphi + y' \sin\Theta \, \sin\varphi$$

$$\cong x'\alpha + y'\beta \quad . \tag{4-28}$$

Equation (4-14) now becomes

$$K(\vec{r}_1', \vec{r}_2') = P_r \, Re\left\{ \iint d\alpha \, d\beta \cdot \sigma(\alpha, \beta) \exp\left[-j \frac{2\pi}{\lambda_o} (x'\alpha + y'\beta) \right] \right\} \quad , \tag{4-29}$$

with $\sigma(\alpha, \beta)$ given by Eq. (4-25). This is simply the two-dimensional Fourier transform of a joint Gaussian function. We have immediately

$$K(\vec{r}_1', \vec{r}_2') = P_r \cos\left[\frac{2\pi}{\lambda_o} (x'\alpha_o + y'\beta_o)\right] \exp\left[-\frac{R_{12}^2}{2\sigma_R^2}\right] \quad , \tag{4-30}$$

in which

$$R_{12}^2 = |\vec{r}_1' - \vec{r}_2'|^2 = x'^2 + y'^2 \tag{4-31a}$$

and

$$\sigma_R^2 = \left(\frac{\lambda_o}{2\pi\sigma_\alpha}\right)^2 \quad . \tag{4-31b}$$

As we show in Appendix G, typical values for σ_α^2 might be in the neighborhood of 0.5. Suppose we stipulate that the correlation distance associated with a Gaussian-shaped correlation function is about two standard deviations. For α_o and β_o near zero, then, the correlation distance associated with $K(\vec{r}_1', \vec{r}_2')$ is typically a few tenths of a wavelength.

Equation (4-29) does not change drastically when the incident illumination is a beam of finite cross section, except that K( ) becomes a function of the ground-plane coordinates (x, y) of the point $\vec{r}$ about which it is defined. As a specific example, let the incident beam have the Gaussian form [Eq. (3-97)],

$$P_{inc}(\alpha_o, \beta_o, x_o, y_o) = \frac{P_o}{2\pi\sigma_i^2} u_o(\alpha_o) u_o(\beta_o) \cdot \exp\left[-\frac{x_o^2 + y_o^2}{2\sigma_i^2}\right] \quad ,$$

which might correspond to a CW laser beam of negligible angular dispersion at vertical incidence, centered at coordinates $x_o = y_o = 0$ on the top of the cloud. In accordance with Eq. (4-24), we see that the angle-of-arrival scattering function $\sigma(\alpha, \beta)$ in this situation is proportional to the four-dimensional joint Gaussian function $P_G(\alpha, \beta, x, y)$ described immediately below Eq. (3-97). Let us suppose again that the coordinate system has been shifted slightly, so that the vectors $\vec{r}_1'$ and $\vec{r}_2'$ are given by Eq. (4-27). Let us further suppose that the variation of $\sigma(\alpha, \beta)$ with $\vec{r}$ is slow enough, and the magnitude of $\vec{r}_1' - \vec{r}_2'$ is small enough, that $\sigma(\alpha, \beta)$ is identical at $\vec{r}_1'$ and $\vec{r}_2'$ with its value at $x' = y' = 0$. (This is nearly always true, even when the incident beam is extremely tight, because of the x and y dispersion effected by the cloud.) Without going through the algebra in detail, we write the answer obtained from Eq. (4-29). We have

$$K(\vec{r}_1', \vec{r}_2') = P_r(x, y) \exp\left[-\frac{R_{12}^2}{2\sigma_{R1}^2}\right] \quad , \tag{4-32}$$

in which R_{12}^2 is the same as Eq. (4-31a) and

$$\sigma_{R1}^2 = \left(\frac{\lambda_o}{2\pi\sigma_\alpha}\right)^2 \frac{\sigma_i^2 + \sigma_\alpha^2\left(\frac{\tau^2}{3} + \tau h + h^2\right)}{\sigma_i^2 + \sigma_\alpha^2 \frac{\tau^2}{12}} \quad .$$

42

τ is the thickness of the cloud in meters, and h is the height of the bottom of the cloud above ground. The average power $P_r(x, y)$ in Eq. (4-32) is proportional to the joint Gaussian function

$$\exp\left[-\frac{x^2 + y^2}{2\sigma_{xG}^2}\right] \quad ,$$

with x and y measured in the fixed coordinate system on the ground plane, where

$$\sigma_{xG}^2 = \sigma_i^2 + \sigma_\alpha^2\left(\frac{\tau^2}{3} + \tau h + h^2\right) \quad .$$

If the beam $P_{inc}(\ )$ had been incident at some angle (α_i, β_i) slightly off the vertical, a cosine term similar to that in Eq. (4-30) would appear in Eq. (4-32), except that the argument of the cosine would involve algebraic functions of α_i, β_i, τ and h.

Notice that σ_{R1}^2 approaches the parameter σ_R^2 of Eq. (4-31b) in the limit as the width σ_i of the incident beam goes to infinity. Even for modest σ_i the correlation distance for Eq. (4-32) is comparable to the wavelength λ_o (except in the extreme case when h becomes very large, so that the cloud begins to look like a point source, and σ_{R1} becomes proportional to h). These small correlation distances, for both Eqs. (4-30) and (4-32), substantiate the assumption made in Appendix A and in this chapter that the vector $\vec{r}'$ in the expression (4-2) for the scattered field is small compared with the distance from the ground to the cloud particles.

4.3 SPATIAL CORRELATION FUNCTIONS FOR ANTENNAS

An interesting extension of the angle-of-arrival scattering function $\sigma(\alpha, \beta)$ allows us to calculate a spatial correlation function for signals observed with directive receiving antennas. We begin by establishing certain conventions for an adequate mathematical description of an antenna. As in Sec. 3.2, we shall characterize its power gain pattern by a function $g(\alpha', \beta')$ whose arguments are orthogonal angular coordinates measured from the antenna boresight axis. When it is aimed at angle (α_a, β_a) and illuminated by an intensity distribution $I(\alpha, \beta)$, the antenna receives

$$Ag(\alpha - \alpha_a, \beta - \beta_a)\, I(\alpha, \beta)\, d\alpha\, d\beta \tag{4-33}$$

watts of power from the solid angle $d\alpha\, d\beta$ at (α, β). The quantity A is the area of the antenna aperture. Under an illumination $P(\alpha, \beta, x, y)$ which varies over the horizontal plane, the aperture area A must be replaced by an appropriate aperture function $A(\alpha, \beta, x, y)$, as we explain in connection with Eq. (3-36) of Sec. 3.2. When the antenna is located at coordinates (x_a, y_a) and aimed in direction (α_a, β_a), then, it receives

$$A(\alpha - \alpha_a, \beta - \beta_a, x - x_a, y - y_a)\, g(\alpha - \alpha_a, \beta - \beta_a)$$

$$\cdot P(\alpha, \beta, x, y)\, d\alpha\, d\beta\, dx\, dy \tag{4-34}$$

watts of power over the area $dx\, dy$ at (x, y), from the solid angle $d\alpha\, d\beta$ at (α, β). We shall obtain explicit results in this section under the assumption that the illumination on the top of the cloud is uniform over the horizontal plane, so that (4-33) applies. The extension of the results to nonuniform illumination, where (4-34) applies, is a straightforward exercise. It is outlined but not carried out.

Whenever it is necessary to assume a specific functional form for $g(\alpha, \beta)$ in this section, it will be convenient to use the symmetric Gaussian power gain pattern

$$g(\alpha', \beta') = \frac{1}{2\pi\sigma_{ant}^2} \exp\left[-\frac{\alpha'^2 + \beta'^2}{2\sigma_{ant}^2}\right] \quad . \tag{4-35}$$

This is neither essential to our model, nor (generally) realistic, although it is not unreasonable when σ_{ant} is small compared with $\pi/2$. We use Eq. (4-35) here simply because it permits us to work out meaningful examples with minimum labor.

The results we shall obtain are subject to an intuitively satisfying interpretation in terms of diffraction-limited antennas. For this purpose we stipulate that Eq. (4-35) represents the power gain pattern of a diffraction-limited antenna with a circular aperture of diameter D when

$$\sigma_{ant} = \frac{B}{\pi} \quad , \tag{4-36}$$

where

$$B \simeq \frac{\lambda_o}{D} \tag{4-37}$$

is the familiar rule-of-thumb approximation for the antenna beamwidth. The proportionality factor $1/\pi$ in Eq. (4-36) is chosen for convenience, as we shall see. We do not claim that it gives the "best" fit in any sense, but only that it is roughly correct. The accuracy of this analysis is such that factors of two are unimportant.

Consider two identical antennas, both having a power gain pattern $g(\alpha', \beta')$. Let them be centered about the points $\vec{r}_1'$ and $\vec{r}_2'$, respectively, measured from some point $\vec{r}$ on the ground plane. Their apertures are assumed to be small and nonoverlapping (the meaning of the term "small" in this context will be clarified below). Let the antenna at $\vec{r}_1'$ be aimed in the direction (α_1, β_1), while that at $\vec{r}_2'$ is aimed toward (α_2, β_2). The correlation function of the signals received by the two antennas is readily obtained by appropriately modifying the analysis in Sec. 4.1. Our starting point is Eq. (4-3),

$$K(t_1, t_2, \vec{r}_1', \vec{r}_2') = \overline{y(t_1, \vec{r}_1') \, y(t_2, \vec{r}_2')} \quad ,$$

in which we interpret the functions $y(t_1, \vec{r}_1')$ and $y(t_2, \vec{r}_2')$ as the signals measured by the first and second antennas, respectively. Now, we have seen that all the field components arriving at a point on the ground beneath a cloud add incoherently; that is, because of their independent random phases, their intensities add. Therefore, if the component intensities entering an antenna aperture from the direction (α, β) are weighted by the function $g(\ )$, it is reasonable to treat the component amplitudes as though they had the angular weighting $g(\ )^{1/2}$. Thus the signal $y(t_1, \vec{r}_1')$ measured by the first antenna includes the factor $g(\alpha - \alpha_1, \beta - \beta_1)^{1/2}$, while $y(t_2, \vec{r}_2')$ contains the factor $g(\alpha - \alpha_2, \beta - \beta_2)^{1/2}$. Carrying these factors along through the analysis in Sec. 4.1, one finds that they can simply be lumped with the scattering function $\sigma(\tau, f, \vec{v}')$ of Eq. (4-8), to form the <u>directive-antenna scattering function</u>

$$\sigma_a(\tau, f, \alpha, \beta; \; \alpha_1, \beta_1, \alpha_2, \beta_2)$$

$$= [g(\alpha - \alpha_1, \beta - \beta_1) \, g(\alpha - \alpha_2, \beta - \beta_2)]^{1/2} \, \sigma(\tau, f, \vec{v}') \quad . \tag{4-38}$$

This equation incorporates the interpretation of $\vec{v}'$ in terms of the angular coordinates α and β, as we explained in Sec. 4.2. In this section we are concerned only with CW illumination;

hence, by analogy with the ideas expressed in Eqs. (4-13) through (4-15), Eq. (4-38) reduces to the directive-antenna angle-of-arrival scattering function

$$\sigma_a(\alpha, \beta;\ \alpha_1, \beta_1, \alpha_2, \beta_2)$$

$$= [g(\alpha - \alpha_1,\ \beta - \beta_1)\ g(\alpha - \alpha_2,\ \beta - \beta_2)]^{1/2}\ \sigma(\alpha, \beta) \quad . \tag{4-39}$$

The function $\sigma(\alpha, \beta)$ on the right side is the angle-of-arrival scattering function of the field at the point $\vec{r}$ in the absence of the antennas. Let us denote the correlation function of the signals measured by the two antennas as $K_a(\vec{r}_1', \vec{r}_2', \alpha_1, \beta_1, \alpha_2, \beta_2)$, with the extra arguments indicating the explicit dependence of the function upon the antenna pointing angles. Assuming that the co-ordinate system has been shifted slightly, so that Eq. (4-27) holds, we obtain $K_a(\ )$ simply by inserting Eq. (4-39) in place of $\sigma(\alpha, \beta)$ in Eq. (4-29). Thus we have

$$K_a(\vec{r}_1', \vec{r}_2', \alpha_1, \beta_1, \alpha_2, \beta_2) = P_r\ \text{Re}\ \left\{ \iint d\alpha\ d\beta \right.$$

$$\left. \cdot\ \sigma_a(\alpha, \beta;\ \alpha_1, \beta_1, \alpha_2, \beta_2)\ \exp\left[-j\ \frac{2\pi}{\lambda_o}\ (x'\alpha + y'\beta)\right] \right\} \quad . \tag{4-40}$$

We recall that this equation is valid under the assumption that the magnitudes of $\vec{r}_1'$ and $\vec{r}_2'$ are small compared with the distance from the point $\vec{r}$ to the cloud. Also, we recall that the scattering function and the correlation function both depend, in general, upon $\vec{r}$. As we stated earlier, we shall restrict our attention for the present to situations in which the light illuminating the top of the cloud is uniform over the horizontal plane, so that the $\vec{r}$-dependence vanishes. In particular, let the illumination be a single uniform plane wave, vertically incident on the top of the cloud. In the absence of the antennas, the resulting angle-of-arrival scattering function would be given by Eq. (4-25) with $\alpha_o = \beta_o = 0$,

$$\sigma(\alpha, \beta) = \frac{1}{2\pi\sigma_\alpha^2}\ \exp\left[-\frac{\alpha^2 + \beta^2}{2\sigma_\alpha^2}\right] \quad . \tag{4-41}$$

Assuming the Gaussian antenna beam pattern [Eq. (4-35)], we see that Eq. (4-39) becomes

$$\sigma_a(\alpha, \beta;\ \alpha_1, \beta_1, \alpha_2, \beta_2) = [4\pi^2\sigma_\alpha^2\sigma_{ant}^2]^{-1}$$

$$\cdot\ \exp\left[-\frac{\alpha^2}{2\sigma_\alpha^2} - \frac{(\alpha - \alpha_1)^2}{4\sigma_{ant}^2} - \frac{(\alpha - \alpha_2)^2}{4\sigma_{ant}^2}\right]$$

$$\cdot\ \exp\left[-\frac{\beta^2}{2\sigma_\alpha^2} - \frac{(\beta - \beta_1)^2}{4\sigma_{ant}^2} - \frac{(\beta - \beta_2)^2}{4\sigma_{ant}^2}\right] \quad . \tag{4-42}$$

Notice that Eq. (4-42) is not normalized to unit volume, as a scattering function ought to be. We are not concerned about this detail at present, since we are interested only in the functional form of the results. Substituting Eq. (4-42) into Eq. (4-40) and carrying out the integrations, we obtain

45

$$K_a(\vec{r}_1', \vec{r}_2', \alpha_1, \beta_1, \alpha_2, \beta_2)$$

$$= C_1 \cos \left\{ \frac{\pi \sigma_\alpha^2}{\lambda_o(\sigma_\alpha^2 + \sigma_{ant}^2)} \left[x'(\alpha_1 + \alpha_2) + y'(\beta_1 + \beta_2) \right] \right\}$$

$$\cdot \exp\left[-\frac{R_{12}^2}{2\sigma_{Ra}^2} \right] \exp\left[-\frac{\psi_{12}^2}{2\sigma_\psi^2} \right] \cdot \exp\left[-\frac{\alpha_1^2 + \beta_1^2 + \alpha_2^2 + \beta_2^2}{4(\sigma_\alpha^2 + \sigma_{ant}^2)} \right] \quad , \quad (4\text{-}43)$$

in which

$$R_{12}^2 = |\vec{r}_1' - \vec{r}_2'|^2 = x'^2 + y'^2 \quad , \quad (4\text{-}44a)$$

$$\sigma_{Ra}^2 = \frac{\lambda_o^2(\sigma_\alpha^2 + \sigma_{ant}^2)}{(2\pi \sigma_\alpha \sigma_{ant})^2} \quad , \quad (4\text{-}44b)$$

$$\psi_{12}^2 = (\alpha_1 - \alpha_2)^2 + (\beta_1 - \beta_2)^2 \quad , \quad (4\text{-}44c)$$

and

$$\sigma_\psi^2 = \frac{4\sigma_{ant}^2(\sigma_\alpha^2 + \sigma_{ant}^2)}{\sigma_\alpha^2} \quad . \quad (4\text{-}44d)$$

The calculation of C_1 is straightforward but uninteresting. The cosine term in Eq. (4-43), which fluctuates very rapidly with x' and y', is also of secondary importance; it is tantamount to a high-frequency "carrier" in the correlation function. The first exponential in Eq. (4-43) expresses the dependence of $K_a(\ )$ upon the horizontal separation R_{12} of the centers of the two apertures, and the second exponential expresses the behavior of $K_a(\ )$ as a function of the angular separation ψ_{12} of the axes of the two beams. The third exponential in Eq. (4-43) simply expresses the decrease in received power when the antenna axes point in some direction other than the angle of arrival (in this case, $\alpha_o = \beta_o = 0$) of the plane wave illuminating the top of the cloud.

Now, we agreed in Sec. 4.2 that a reasonable estimate of the correlation distance for a Gaussian-shaped correlation function was two standard deviations. Equivalently, we regard the signals as being uncorrelated when their correlation function is down by at least $\exp[-2]$ from its maximum value. We see that this is always the case in Eq. (4-43) under either of the conditions

$$R_{12} \geqslant 2\sigma_{Ra} \quad (4\text{-}45)$$

or

$$\psi_{12} \geqslant 2\sigma_\psi \quad , \quad (4\text{-}46)$$

regardless of the behavior of the cosine term or the third exponential in Eq. (4-43). Thus the two antennas receive uncorrelated signals when the centers of their apertures are separated horizontally by a distance R_{12} obeying (4-45), regardless of the antenna pointing angles. On the other hand, if we form two beams with the same aperture (by making field measurements over two different Airy disks on the focal plane of an objective lens), the two signals are uncorrelated with each other whenever the angular separation of the two beams obeys Eq. (4-46). This result may be extended immediately to an array of many multibeam apertures distributed over the ground. We see that the signal received on each beam in the array is uncorrelated with the signal received on every other beam when (4-45) and/or (4-46) is satisfied for every pair of beams. Moreover, since all the signals are Gaussian, each of them is statistically independent of all the others.

Let us consider the magnitudes of the correlation distances $2\sigma_{Ra}$ and $2\sigma_\psi$. In the limit as the antenna beamwidth parameter σ_{ant} becomes large compared with σ_α, we see that Eq. (4-44b) becomes

$$\sigma_{Ra}^2 \cong \left(\frac{\lambda_o}{2\pi\sigma_\alpha}\right)^2 \quad , \tag{4-47}$$

which is precisely equal to the parameter σ_R^2 of the spatial correlation function $K(\vec{r}_1', \vec{r}_2')$ of the scattered field over the ground in the absence of antennas, given by Eq. (4-30). This is just as it should be, since Eq. (4-30) is equivalent to a spatial correlation function for signals measured by omnidirectional antennas. When σ_{ant} is small compared with σ_α, however, we have

$$\sigma_{Ra}^2 \cong \left(\frac{\lambda_o}{2\pi\sigma_{ant}}\right)^2 \quad . \tag{4-48}$$

Notice that the horizontal correlation distance

$$2\sigma_{Ra} \cong \frac{\lambda_o}{\pi\sigma_{ant}} \tag{4-49}$$

is then precisely equal to the aperture diameter D of a diffraction-limited antenna having an approximately Gaussian beam representation with parameter σ_{ant}, in accordance with the conventions (4-36) and (4-37). Thus two identical narrow-beam diffraction-limited antennas on the ground beneath the cloud receive uncorrelated signals if their apertures do not overlap, regardless of their beam pointing angles.

The nature of the parameter σ_ψ also depends upon the relative magnitudes of σ_α and σ_{ant}. Equation (4-44d) becomes

$$\sigma_\psi^2 \cong \frac{4\sigma_{ant}^4}{\sigma_\alpha^2} \tag{4-50}$$

when $\sigma_{ant} \gg \sigma_\alpha$, which simply implies that the concept of angular correlation distance becomes meaningless for very broad-beam antennas. When σ_{ant} is small compared with σ_α, Eq. (4-44d) reduces to

$$\sigma_\psi^2 \cong 4\sigma_{ant}^2 \quad . \tag{4-51}$$

47

For narrow-beam antennas, then, the angular correlation distance is approximately equal to $4\sigma_{ant}$. In view of Eq. (4-36), we see that two narrow diffraction-limited beams formed with the same aperture on the ground beneath the cloud receive uncorrelated signals when the angular separation between the beams is greater than about 1.27 B, where B is the conventional estimate (4-37) of the width of a single beam.

These results are readily extended to situations in which the illumination on the top of the cloud is more complicated (a group of plane waves, or a narrow beam). We know how to calculate the resulting intensity distribution $I(\alpha, \beta)$ or $\vec{r}$-dependent power distribution $P(\alpha, \beta, x, y)$ beneath the cloud, either of which can then be inserted into Eq. (4-39) in place of $\sigma(\alpha, \beta)$. When the $\vec{r}$-dependence is present, Eq. (4-40) is valid under the assumption that $\sigma_a(\ )$ varies slowly enough with $\vec{r}$, and $|\vec{r}_1'|$ and $|\vec{r}_2'|$ are small enough, that $\sigma_a(\ )$ is the same at both antennas. This is nearly always the case, even when the beam illuminating the top of the cloud is extremely tight, because of the spatial dispersion effected by the cloud. Carrying out the integrations in Eq. (4-40) when $\sigma(\alpha, \beta)$ is the joint impulse response $h_G(\alpha, \beta, x, y;\ \alpha_o, \beta_o, x_o, y_o)$ of Eq. (3-39), for example, one finds that $K_a(\ )$ depends upon the last six arguments of $h_G(\ )$ but the correlation distances (4-45) and (4-46) are practically unchanged. The algebra is straightforward but very tedious. When we apply the results of this section to the spatial diversity issue in Chapter 5, we shall be dealing with narrow-beam incident illumination. Thus the correlation function $K_a(\ )$ will, in fact, depend upon the coordinates of the point of observation $\vec{r}$ on the ground. We shall simplify the problem considerably by assuming that the scattered intensity over the ground is constant (independent of $\vec{r}$) over a suitably delineated region, and zero outside that region.

4.4 ANGLE-DEPENDENT RANGE SCATTERING FUNCTION $\sigma(\tau, \vec{v}_F')$

We shall show how to obtain the range scattering function

$$\sigma(\tau, \vec{v}_F') = \int \sigma(\tau, f, \vec{v}_F')\ df \tag{4-52}$$

over a small range $\Delta\vec{v}'$ about some fixed vector $\vec{v}_F'$. Interpreting $\vec{v}'$ in terms of α and β, as in Sec. 4.2, we see that Eq. (4-52) corresponds to the classical range scattering function

$$\sigma(\tau) = \int \sigma(\tau, f)\ df \tag{4-53}$$

for the signal measured by an antenna of beam solid angle

$$\Delta\omega = \Delta\alpha\ \Delta\beta \tag{4-54}$$

pointed in some fixed direction (α_F, β_F). In Sec. 4.5 we shall extend the results of this section to yield the function $\sigma(\tau, f, \vec{v}_F')$ over a range $\Delta\vec{v}'$ about $\vec{v}_F'$. For the case in which the incident illumination is uniform over the horizontal plane, so that nothing depends upon $\vec{r}$, knowledge of $\sigma(\tau, f, \vec{v}_F')$ for each of a suitable set of vectors $\vec{v}_F'$ would give us an estimate of $\sigma(\tau, f, \vec{v}')$ for all $\vec{r}$ and $\vec{v}'$. For beam illumination, with $\sigma(\ )$ depending upon $\vec{r}$, one could obtain adequate knowledge of the generalized scattering function over the entire ground plane by calculating $\sigma(\tau, f, \vec{v}_F')$ for a set of vectors $\vec{v}_F'$, for each of a suitable set of positions $\vec{r}$ on the ground.

As a first step in determining $\sigma(\tau, \vec{v}_F')$, consider the angular impulse response $h_I(\alpha, \beta;\ \alpha_o, \beta_o)$ given by Eq. (3-72) in Sec. 3.4. This function is defined in such a way that the quantity

$$I_\Delta(\alpha, \beta;\ \alpha_o, \beta_o) = h_I(\alpha, \beta;\ \alpha_o, \beta_o)\ \Delta\omega \tag{4-55}$$

is the average total intensity arriving at the ground through the small solid angle $\Delta\omega = \Delta\alpha\,\Delta\beta$ about the direction (α, β), when the top of the cloud is illuminated by a constant unit-intensity uniform plane wave with angle of arrival (α_o, β_o). Now, suppose we regard the field components making up $I_\Delta(\ )$ as a bundle of rays, with one ray corresponding to each scattering path through the cloud which contributes to $I_\Delta(\ )$. The nth ray in this bundle has a path length ℓ_n and an intensity weight w_n associated with it. The path length is measured from the point at which the nth ray, while still a part of the incident wave, enters the top of the cloud.

In a more general situation, the plane wave illuminating the top of the cloud has a complex amplitude envelope $s(t)$. The time origin is referred to a specific point (say $x = y = 0$) on the top of the cloud. The intensity weight of the nth ray in the bundle $\Delta\omega$ now becomes the time function

$$\frac{1}{2}\,w_n\,\left|s\!\left(t - T_{no} - \frac{\ell_n}{c}\right)\right|^2 \quad , \tag{4-56}$$

where T_{no} is a constant which depends upon the location of the point at which the ray enters the top of the cloud, and upon the angle of arrival of the plane wave. The total intensity of the bundle of rays in $\Delta\omega$ is then given by the time function

$$I_\Delta(t, \alpha, \beta;\ \alpha_o, \beta_o) = \sum \frac{1}{2}\,w_n\,\left|s\!\left(t - T_{no} - \frac{\ell_n}{c}\right)\right|^2 \tag{4-57}$$

Now, the correlation function $K(t_1, t_2, \vec{r}_1', \vec{r}_2')$ of Eq. (4-11), evaluated at $t_1 = t_2 = t$ and $\vec{r}_1' = \vec{r}_2' = \vec{r}'$, is the average intensity at time t of the radiation incident at the point $\vec{r}'$ on the ground. The vector $\vec{r}'$ is measured from some point $\vec{r}$. We recall that both $K(\ )$ and the scattering function $\sigma(\tau, f, \vec{v}')$ depend upon $\vec{r}$, in general. By virtue of Eq. (4-11) we have

$$K(t, t, \vec{r}', \vec{r}') = \frac{E_r}{2}\,\mathrm{Re}\left\{\int d\tau\,df\,d\vec{v}' \cdot \sigma(\tau, f, \vec{v}')\,\left|s(t - \tau)\right|^2\right\} \quad . \tag{4-58}$$

Let us select a transmitted signal envelope $s(t)$ such that

$$\left|s(t)\right|^2 = 2\delta(t) \quad , \tag{4-59}$$

where $\delta(t)$ is a unit-area pulse which is very short compared with the length of an interval in τ over which $\sigma(\tau, f, \vec{v}')$ varies appreciably. Equation (4-58) then becomes

$$K(t, t, \vec{r}', \vec{r}') = E_r \int d\vec{v}'\,\sigma(t, \vec{v}') \quad . \tag{4-60}$$

We shall interpret $\vec{v}'$ and $d\vec{v}'$ in terms of α and β as before. Suppose now that we observe the field at $\vec{r}$ with an antenna of unit aperture area, pointed in the direction (α, β). Let the power gain of the antenna be unity over a very small solid angle $\Delta\omega$, and zero elsewhere. By Eq. (4-60), we see that the average power measured by the antenna at time t is

$$p_a(t, \alpha, \beta) = E_r\,\Delta\omega\,\sigma(t, \alpha, \beta) \quad . \tag{4-61}$$

Again, this quantity is a function of the point of observation r. But let us choose the incident illumination on top of the cloud to be a uniform plane wave, arriving from $(\alpha_o\beta_o)$. Both sides of Eq. (4-61) are then independent of $\vec{r}$, and both are functions of α_o and β_o. Let us rewrite

Eq. (4-61) to indicate this dependence; that is, the average power received by the antenna at time t is

$$p_a(t, \alpha, \beta; \alpha_o, \beta_o) = E_r \Delta\omega \sigma(t, \alpha, \beta; \alpha_o, \beta_o) \quad . \tag{4-62}$$

We now observe that Eq. (4-62) may be interpreted as being precisely the function $I_\Delta(\ )$ of Eq. (4-57), when the signal envelope s(t) in Eq. (4-57) obeys Eq. (4-59). Thus

$$\sigma(t, \alpha, \beta; \alpha_o, \beta_o) = \frac{1}{E_r \Delta\omega} \sum w_n \, \delta\left(t - T_{no} - \frac{\ell_n}{c}\right) \quad , \tag{4-63}$$

in which n ranges over all the rays in the solid angle $\Delta\omega$. Because $\delta(\ )$ is very short compared with the rate at which $\sigma(\ )$ changes with time, it is clear that

$$\sigma(t, \alpha, \beta; \alpha_o, \beta_o) \, \Delta t \cong \frac{1}{E_r \Delta\omega} \sum w_i \quad , \tag{4-64}$$

where i ranges over all rays in $\Delta\omega$ such that

$$t \leqslant T_{io} + \frac{\ell_i}{c} \leqslant t + \Delta t \quad . \tag{4-65}$$

Except for certain special cases, the evaluation of the sum on the right side of Eq. (4-64) will require numerical computation. In Appendix E we consider one of these special cases, with α, β, α_o and β_o all equal to zero. By making a series of approximations we find that the range scattering function for this situation, denoted for brevity by $\sigma_o(t)$, is given by

$$\sigma_o(t) \cong C_3 \left(\frac{4\gamma_f N_e(t - \frac{h}{c})}{D_e/c}\right)^{-3/4} \exp\left[-\frac{(t - \frac{h}{c})}{D_e/c} + 2\left(\frac{\gamma_f N_e(t - \frac{h}{c})}{D_e/c}\right)^{1/2}\right] \tag{4-66}$$

when $t \geqslant (\tau + h)/c$, and zero elsewhere. Here τ is the cloud thickness in meters, h is the height of the bottom of the cloud above the ground, and c is the velocity of light. The factor C_3 in Eq. (4-66) is a normalizing constant. A typical $\sigma_o(t)$ is illustrated in Fig. E-1 in Appendix E. The multipath spread L of $\sigma_o(t)$, its approximate width, is given by

$$L \cong \frac{D_e}{c} [1 + 2\sqrt{N_e}] \quad . \tag{4-67}$$

In Appendix E we also outline procedures for obtaining $\sigma(t, \alpha, \beta; \alpha_o, \beta_o)$ numerically, in more general situations. For illumination other than a vertically incident plane wave, some form of Monte Carlo simulation must be used.

4.5 RANGE-DOPPLER SCATTERING FUNCTION $\sigma(\tau, f, \vec{v}_F')$

We assume that each cloud particle has a random velocity component, superimposed upon a slowly varying mean. The mean velocity, which has no effect upon the scattering function $\sigma(\tau, f, \vec{v}')$, is presumed to be equal for all particles to the average wind velocity. The random velocity component $\vec{V}_r$ is caused by local phenomena such as turbulence and thermal mixing. It is assumed to be identically distributed for all particles, with a probability density function which is uniform over any solid angle. By this we mean that its magnitude V_r is random, nonnegative, and independent of the spherical coordinates Θ_r and φ_r of its direction, while Θ_r and φ_r are so distributed that the direction of $\vec{V}_r$ lies in any solid angle Ω with probability $\Omega/4\pi$. Thus the

joint probability that Θ_r is in the range $(\Theta, \Theta + d\Theta)$ and φ_r is in the range $(\varphi, \varphi + d\varphi)$ is given by

$$\frac{1}{4\pi} \sin\Theta \, d\Theta \, d\varphi \quad . \tag{4-68}$$

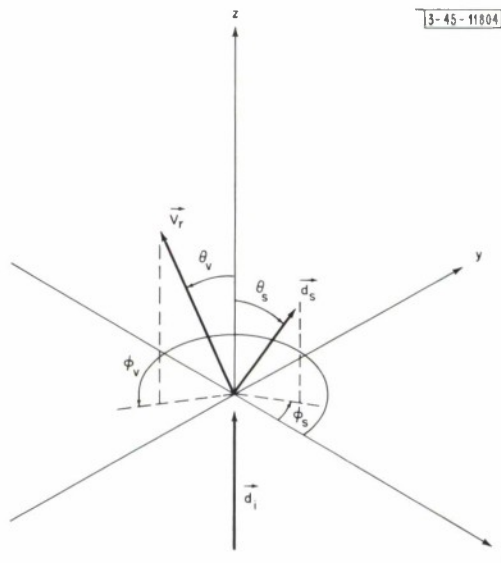We may regard Θ_r and φ_r as having the joint probability density

$$P_{\Theta_r, \varphi_r}(\Theta, \varphi) = \frac{\sin\Theta}{4\pi} \quad , \quad \begin{cases} 0 \leqslant \Theta \leqslant \pi \quad , \\ 0 \leqslant \varphi \leqslant 2\pi \quad . \end{cases} \tag{4-69}$$

The Doppler shift associated with a single scattering event is given by

$$f_{d1} = \frac{f_o}{c} [\vec{V}_r \cdot \vec{d}_s - \vec{V}_r \cdot \vec{d}_i] \quad , \tag{4-70}$$

where f_o is the carrier frequency and c is the velocity of light. The vectors $\vec{d}_s$ and $\vec{d}_i$ are unit

Fig. 4-2. Doppler shift geometry.

vectors in the directions of the scattered ray and the incident ray, respectively. The geometry of the situation is illustrated in Fig. 4-2. The coordinate system is so oriented that

$$\vec{d}_i = \vec{i}_z \quad , \tag{4-71}$$

and the scattering particle is at the origin. The coordinates Θ_s and φ_s of the direction of the scattered ray are assumed to be randomly distributed in accordance with the average single-particle forward-scattering pattern $f(\Theta)$, as explained in Appendix B. Thus Θ_s and φ_s obey the probability density function

$$P_{\Theta_s, \varphi_s}(\Theta, \varphi) = \sin\Theta \, f(\Theta) \quad , \quad \begin{cases} 0 \leqslant \Theta \leqslant \pi/2 \quad , \\ 0 \leqslant \varphi \leqslant 2\pi \quad , \end{cases} \tag{4-72}$$

with $f(\Theta)$ so normalized that

$$2\pi \int_o^{\pi/2} \sin\Theta \, f(\Theta) \, d\Theta = 1 \quad . \tag{4-73}$$

51

It is clear that

$$\vec{V}_r = V_r \{\sin\Theta_r \cos\varphi_r \, \vec{i}_x + \sin\Theta_r \sin\varphi_r \, \vec{i}_y + \cos\Theta_r \, \vec{i}_z\} \tag{4-74}$$

and

$$\vec{d}_s = \sin\Theta_s \cos\varphi_s \, \vec{i}_x + \sin\Theta_s \sin\varphi_s \, \vec{i}_y + \cos\Theta_s \, \vec{i}_z \quad , \tag{4-75}$$

so that Eq. (4-70) becomes

$$f_{d1} = \frac{f_o}{c} \, V_r \, [\sin\Theta_s \cos\varphi_s \sin\Theta_r \cos\varphi_r$$
$$+ \sin\Theta_s \sin\varphi_s \sin\Theta_r \sin\varphi_r + \cos\Theta_s \cos\Theta_r - \cos\Theta_r] \quad . \tag{4-76}$$

Although we shall not do so, it is possible in principle to calculate the probability density function of f_{d1} from Eq. (4-76). Although the algebra is rather tedious, it is a straightforward task to obtain the more limited results

$$\overline{f_{d1}} = 0 \tag{4-77}$$

and

$$\overline{f_{d1}^2} = \mathrm{var}\,(f_{d1}) \equiv \sigma_{f1}^2$$

$$= \frac{2f_o^2}{3c^2} \, \overline{V_r^2} \, \int_o^{\pi/2} 2\pi \sin\Theta \, f(\Theta) \, [1 - \cos\Theta] \, d\Theta \quad . \tag{4-78}$$

Provided that its magnitude is much less than the carrier frequency f_o, the Doppler shift f_{dk} of a kth-order scattered wave is approximately the sum of k first-order Doppler shifts. We assume that all the first-order Doppler shifts f_{d1} are statistically independent and identically distributed. Invoking the Central Limit Theorem, we write

$$p_{f_{dk}}(f) \cong \frac{1}{\sigma_{f1} \sqrt{2k\pi}} \, \exp\left[-\frac{f^2}{2k\sigma_{f1}^2}\right] \tag{4-79}$$

for large k. Now, we know that this approximation can be very good over the central region even for fairly small k, if the first-order density function is smooth, symmetric and unimodal. It is reasonable to assume that f_{d1} has such a density, as long as the velocity magnitude V_r is reasonably well behaved. Equation (4-79) will be seriously in error out in its tails for small values of k; for purposes of estimating the shape and width of the scattering function, however, we can ignore the tails. In any case, as we indicate in Appendix E, when $N_e \geqslant 5$, the rays of low scattering order contribute only weakly to the total received energy. On these grounds, then, we shall assume that Eq. (4-79) is valid for all $k \geqslant 1$.

In Appendix F we derive an approximate form for the angle-dependent range-Doppler scattering function $\sigma(\tau, f, \vec{v}_F')$ for the special case in which the incident illumination is a uniform plane wave, and α, β, α_o and β_o are all zero. The result is left in the form of an infinite sum, [Eq. (F-2)], which could be approximated numerically if desired. The Doppler spread B of the function is approximated by

$$B \cong \frac{2W_\alpha}{\lambda_o} \left[\frac{2\pi N_e}{3} \right]^{1/2} \left(\overline{V_r^2} \right)^{1/2} \quad , \tag{4-80}$$

in which $W_\alpha = W_\beta$ is the average single-particle scattering pattern width parameter, λ_o is the carrier wavelength, and $(\overline{V_r^2})^{1/2}$ is the RMS value of the random component of the velocity of the cloud particles.

Using the multipath spread

$$L \cong \frac{D_e}{c} \left[1 + 2 \sqrt{N_e} \right] \tag{4-81}$$

derived for this same special case in Appendix E, we find that the BL product is

$$BL \cong 2 \sqrt{\frac{2\pi}{3}} \frac{\tau W_\alpha}{\lambda_o} \frac{\left(\overline{V_r^2} \right)^{1/2}}{c} \left[2 + \frac{1}{\sqrt{N_e}} \right] \quad , \tag{4-82}$$

where τ is the cloud thickness. Notice that BL becomes independent of the cloud optical thickness N_e (and hence independent of the particle density d_v) as N_e becomes large.

Appendix F also indicates numerical techniques for calculating $\sigma(t, f, v_F')$ in more general cases. For the most part, Monte Carlo simulation appears to be the most attractive alternative.

CHAPTER 5
COMMUNICATION SYSTEMS FOR THE CLOUD CHANNEL

We have seen in Sec. 4.1 that the generalized scattering function $\sigma(\tau, f, \vec{v}')$ embodies a complete statistical description of the received field over the ground plane beneath a cloud. An extension of known techniques can be utilized to obtain a mathematical description of the optimum receiver for the cloud channel. The processing such a receiver must perform involves the solution of difficult integral equations in both time and space. In general, these operations cannot be readily interpreted in terms of components we know how to build. We consider a communication scheme in this chapter which we know how to interpret and to analyze. Although we do not know the degree to which the proposed system approaches the optimum, our analysis will provide a lower bound to the performance that the optimum system could achieve.

An important feature of the proposed receiver is spatial diversity, which we obtain by taking independent samples of the received field over the ground plane. In Sec. 5.1 we estimate the degree of spatial diversity which can be achieved. Section 5.2 deals with the sources and character of noise corrupting the received field. The proposed receiver is described in Sec. 5.3, and its performance is analyzed in Sec. 5.4.

5.1 SPATIAL DIVERSITY

It is clear from our results in Chapter 4 that one can obtain many statistically independent samples of the received field over the ground plane. The degree of spatial diversity K_s of the cloud channel is the largest possible number of such samples which contain significant signal energy. In this section we estimate the magnitude of K_s for an array of identical field-sensing devices, and we argue that it would not be appreciably greater for a composite array of nonidentical devices.

It is clear that our field-sensing devices should be located only where significant signal energy is incident on the ground. Moreover, they must be directive; that is, the solid angle over which a sensor has nonzero gain must not exceed the solid angle over which the signal energy is significant. A larger sensor field of view would only admit more noise, causing the signal-to-noise ratio to deteriorate. Having concluded that the sensors should have restricted angular beam patterns, we realize that each of them must have an aperture area associated with it. We are free to think of them as antennas. An antenna of a given beamwidth B must have an aperture area at least as great as

$$\frac{\pi D^2}{4} = \frac{\pi \lambda_o^2}{4B^2} \quad , \tag{5-1}$$

where λ_o is the carrier frequency and D is the diameter of the aperture of a diffraction-limited telescope with beamwidth B. We shall think of our sensors as completely general antennas, each having some beamwidth B and some aperture area A which is lower bounded by the relation (5-1). The maximum obtainable spatial diversity is achieved by packing as many sensors into the "active region" on the ground plane as possible. (By the term "active region" we mean the area on the ground plane over which significant signal energy is received.) Clearly, the maximum spatial diversity is infinite when the illumination incident on the cloud is uniform over the entire horizontal plane, because the resulting active region on the ground has infinite area.

This is not surprising, because the transmitted signal energy in such a case must also be infinite. Thus the spatial diversity is finite only when the incident illumination is a beam of finite cross-sectional area.

When this is the case, the analysis of Sec. 3.5 leads us to an expression for the power distribution function $P(\alpha, \beta, x, y)$ incident on the ground. To facilitate the mathematics of estimating the spatial diversity, let us assume that the incident illumination has the form of Eq. (3-97), a unit-power beam with negligible angular dispersion which has Gaussian intensity variation over its cross section. Let it be symmetric in x and y, with

$$\sigma_{xi}^2 = \sigma_{yi}^2 = \sigma_i^2 \quad . \tag{5-2}$$

The resulting average power distribution over the ground is

$$P_G(\alpha, \beta, x, y) = \exp[-N_e(1 - \gamma_f)]$$

$$\cdot \left[4\pi^2 \sigma_{\alpha s} \sigma_{\beta s} \sigma_{xs} \sigma_{ys} \sqrt{(1 - \rho_{\alpha xs}^2)(1 - \rho_{\beta ys}^2)} \right]^{-1}$$

$$\cdot \exp\left[\frac{-1}{2(1 - \rho_{\alpha xs}^2)} \left(\frac{(\alpha - m_\alpha)^2}{\sigma_{\alpha s}^2} - 2\rho_{\alpha xs} \frac{(\alpha - m_\alpha)(x - m_x)}{\sigma_{\alpha s}\sigma_{xs}} + \frac{(x - m_x)^2}{\sigma_{xs}^2} \right) \right]$$

$$\cdot \exp\left[\frac{-1}{2(1 - \rho_{\beta ys}^2)} \left(\frac{(\beta - m_\beta)^2}{\sigma_{\beta s}^2} - 2\rho_{\beta ys} \frac{(\beta - m_\beta)(y - m_y)}{\sigma_{\beta s}\sigma_{ys}} + \frac{(y - m_y)^2}{\sigma_{ys}^2} \right) \right] \quad . \tag{5-3}$$

The parameters in this equation are

$$\sigma_{\alpha s}^2 = \sigma_{\beta s}^2 = \gamma_f N_e W_\alpha^2$$

$$\sigma_{xs}^2 = \sigma_{ys}^2 = \sigma_i^2 + \gamma_f N_e W_\alpha^2 \left(\frac{\tau^2}{3} + \tau h + h^2 \right)$$

$$\rho_{\alpha xs} = \rho_{\beta ys} = - \frac{\gamma_f N_e W_\alpha^2 \left(\frac{\tau}{2} + h \right)}{\left[\sigma_{\alpha s}^2 \left(\frac{\tau^2}{3} + \tau h + h^2 \right) + \sigma_i^2 \right]^{1/2}} \quad . \tag{5-4}$$

We recall that γ_f is the average single-particle forward-scattering efficiency, N_e is the optical thickness of the cloud, τ is its physical thickness, and h is the height of the bottom of the cloud above the ground. The quantity W_α is the width parameter of the average single-particle scattering pattern, which is symmetric in α and β. The mean values m_α, m_β, m_x and m_y, which are functions of the coordinates α_i, β_i, x_i and y_i of the incident beam, will not enter into our results.

Let us assume that the aperture area A_s of a single antenna at coordinates (x_1, y_1) on the ground plane is small enough that the x- and y-dependent portion of Eq. (5-3) is virtually constant over it. The angular intensity distribution incident upon the antenna is therefore proportional to

$$[2\pi\sigma_{\alpha s}^2(1 - \rho_{\alpha xs}^2)]^{-1} \exp\left[-\frac{(\alpha - m_\alpha')^2 + (\beta - m_\beta')^2}{2\sigma_{\alpha s}^2(1 - \rho_{\alpha xs}^2)} \right] \quad , \tag{5-5}$$

with m'_α and m'_β dependent upon x_1 and y_1. Suppose that the antenna has multiple receiving beams, each adequately represented by the symmetric Gaussian power gain pattern [Eq. (4-35)],

$$g(\alpha', \beta') = \frac{1}{2\pi\sigma_{ant}^2} \exp\left[-\frac{\alpha'^2 + \beta'^2}{2\sigma_{ant}^2}\right] \quad ,$$

and each having the same (fixed) beamwidth parameter σ_{ant}. We wish to estimate how many such beams to use in order to obtain the maximum number N_b of statistically independent "looks" at the distribution (5-5) incident on the aperture A_s. By Eq. (4-51), we know that multiple beams from the same aperture receive statistically independent signals when their boresight axes are separated from each other by at least $4\sigma_{ant}$ radians. This is equivalent to stating that each beam occupies an effective solid angle

$$\omega_b = 4\pi\sigma_{ant}^2 \quad . \tag{5-6}$$

Thus we have

$$N_b = \frac{\Omega_{inc}}{\omega_b} \quad , \tag{5-7}$$

where Ω_{inc} is the effective solid angle over which the intensity distribution (5-5) has significant magnitude. We estimate Ω_{inc} by again invoking the approximation that most of the volume under a symmetric two-dimensional Gaussian function is contained within a circle of radius 2σ about the mean. Thus we shall approximate (5-5) by a distribution which is uniform over a solid angle

$$\Omega_{inc} = 4\pi\sigma_{\alpha s}^2(1 - \rho_{\alpha xs}^2) \quad , \tag{5-8}$$

and zero elsewhere. [Note the consistent relationship between Eqs. (5-8) and (5-6).] Equation (5-7) now becomes

$$N_b \cong \frac{\sigma_{\alpha s}^2(1 - \rho_{\alpha xs}^2)}{\sigma_{ant}^2} \quad . \tag{5-9}$$

By referring to Eq. (5-3), we realize that (5-5) depends upon the coordinates (x_1, y_1) of the center of the aperture A_s only through the mean (m'_α, m'_β). Thus Eq. (5-9) is valid for any aperture similar to A_s located anywhere in the active region on the ground plane. Let us now estimate the maximum number of such apertures which one could pack into the active region, subject to the requirement that statistical independence holds among all beams in the entire array. We showed in Sec. 4.3 that each beam from one aperture receives a signal which is independent of every beam from an adjacent aperture when the centers of the two apertures are separated by at least the distance [Eq. (4-48)],

$$\Delta x = \frac{\lambda_o}{\pi\sigma_{ant}} \quad .$$

Roughly speaking, then, we can place one aperture on the ground plane for every

$$\pi\left(\frac{\Delta x}{2}\right)^2 = \frac{\lambda_o^2}{4\pi\sigma_{ant}^2} \tag{5-10}$$

57

square meters of area in the active region. But let us note that a diffraction-limited antenna whose beam pattern is approximated by a symmetric Gaussian function with parameter σ_{ant} has aperture area

$$A_{d\ell} = \pi \frac{D^2}{4} = \frac{\lambda_o^2}{4\pi\sigma_{ant}^2} \quad , \tag{5-11}$$

in accordance with our convention [Eq. (4-36)]. Observe that

$$A_s > A_{d\ell} \quad , \tag{5-12}$$

as we pointed out in connection with Eq. (5-1), and that $A_{d\ell}$ is equal to Eq. (5-10). If our antennas are not diffraction limited, we cannot pack the maximum number N_a of apertures into the active region unless we are willing to allow them to overlap each other to some extent. If we do not permit overlapping apertures, then we must use diffraction-limited antennas to achieve the maximum spatial diversity. We see that

$$N_a = \frac{A_{active}}{A_{d\ell}} \quad , \tag{5-13}$$

where A_{active} is the area of the active region. We estimate A_{active} by again using the approximation that led to Eq. (5-8). Thus we integrate the received power distribution function [Eq. (5-3)] on α and β to obtain

$$\iint P_G(\alpha, \beta, x, y) \, d\alpha \, d\beta = [2\pi\sigma_{xs}^2]^{-1} \exp\left[-\frac{(x - m_x)^2 + (y - m_y)^2}{2\sigma_{xs}^2}\right] \quad , \tag{5-14}$$

and approximate this result by a uniform distribution over a circle of radius $2\sigma_{xs}$ in the (x, y) plane, centered about (m_x, m_y). The area of the circle is

$$A_{active} = 4\pi\sigma_{xs}^2 \quad . \tag{5-15}$$

Equation (5-13) now becomes

$$N_a = \frac{16\pi^2\sigma_{xs}^2\sigma_{ant}^2}{\lambda_o^2} \quad . \tag{5-16}$$

Using the assumed receiving apparatus (i.e., an array of identical multibeam antennas with beamwidth parameter σ_{ant}), we see that the maximum achievable spatial diversity is

$$K_s = N_a N_b = \frac{16\pi^2\sigma_{xs}^2\sigma_{\alpha s}^2(1 - \rho_{\alpha xs}^2)}{\lambda_o^2} \quad . \tag{5-17}$$

But we observe that Eq. (5-17) is independent of σ_{ant}. Thus any set of identical diffraction-limited multibeam antennas (or nondiffraction-limited antennas with suitably overlapping apertures) could be used to achieve the maximum diversity [Eq. (5-17)], regardless of the value of σ_{ant}. This statement is subject, of course, to the condition that the effective solid angle ω_b of an individual beam must not exceed the effective solid angle Ω_{ine} of the angular intensity distribution (5-5) incident on the aperture associated with the beam. If ω_b were, in fact, equal to Ω_{ine}, we

see that each aperture would observe all the signal energy incident on it with a single beam ($N_b = 1$), and we would have

$$\sigma_{ant} = \sigma_{\alpha s} \sqrt{(1 - \rho_{\alpha xs}^2)} \quad .$$

Inserting this value in Eq. (5-16), we find that

$$K_s = N_a N_b = N_a$$

would still be given by the right side of Eq. (5-17).

We imagine that it might be possible to achieve slightly greater spatial diversity by using some composite of various aperture sizes and beamwidths. It is reasonable to assume, however, that the increase would only be comparable to the errors inherent in the approximations made in deriving Eq. (5-17). Thus it is fair to say that the value of K_s obtained here is a reasonable approximation to the maximum spatial diversity achievable by any scheme.

Suppose that we were only willing to process over some limited area $A_{\ell im}$ on the ground plane, which is within but smaller than the active region. The maximum spatial diversity $K_{s\ell}$ obtainable under these circumstances is found by multiplying Eq. (5-17) by $(A_{\ell im}/4\pi\sigma_{xs}^2)$, which gives the result

$$K_{s\ell} = \frac{4\pi A_{\ell im}\sigma_{\alpha s}^2(1 - \rho_{\alpha xs}^2)}{\lambda_o^2} \quad . \tag{5-18}$$

We see that the maximum spatial diversity in either case is equal to the product of the solid angle subtended by the incident radiation, times the ground-plane area over which we process, times the factor λ_o^{-2}.

It is interesting to calculate the value of K_s for a typical set of cloud parameters. From Appendix G, we see that a reasonable set of numbers is

$$\tau = h = 1000 \text{ meters}$$

$$\lambda_o = 5 \times 10^{-7} \text{ meter}$$

$$W_\alpha = 0.3 \text{ radian}$$

$$N_e = 10$$

$$\gamma_f = 0.96 \quad . \tag{5-19}$$

Let us assume that the incident beam on top of the cloud is small enough that σ_i^2 is negligible compared with σ_{xs}^2. By using (5-19) in Eq. (5-4), we find that

$$\sigma_{\alpha s}^2 = 0.9$$

$$\sigma_{xs}^2 = 2.1 \times 10^6$$

$$(1 - \rho_{\alpha xs}^2) = 0.035 \quad . \tag{5-20}$$

Equation (5-21) then becomes

$$K_s = 4.25 \times 10^{19} \quad . \tag{5-21}$$

If we process over a total aperture area of only one square meter, Eq. (5-18) yields

$$K_{s\ell} = 1.6 \times 10^{12} \quad . \tag{5-22}$$

5.2 NOISE MODELS

There are five types of noise to consider in communicating over the cloud channel: quantum noise, diffuse sky noise, sunlight, light from the stars and the moon, and backscattered light from terrestrial sources. The quantum noise, which is always present, assumes major importance when the number of signal photons received per second is small. This issue will be discussed quantitatively in the following section. The communication system we shall propose will be operated in such a way that the quantum noise can be lumped with the additive Gaussian noise, in order that the system design and performance analysis may be carried out using conventional techniques. This issue is discussed in detail in Sec. 5.4.

The diffuse sky noise, which is present only in the daytime, is the result of atmospheric scattering of sunlight. Its spectral density has been reported[34] as about 1.33×10^{-14} watts per (meter^2-steradian-Hertz). It is not clear whether this noise model is meaningful when clouds are occupying much of the atmosphere where it is "generated." For present purposes, we shall assume that the diffuse sky noise is absent.

The sun's radiation is approximately white over the band of visible-light frequencies, with spectral density[35]

$$N_{sun} = 1.67 \times 10^{-12} \text{ watts/(meter}^2\text{-Hz)} \tag{5-23}$$

just outside the earth's atmosphere. We can regard it as an incoherent superposition of uniform plane waves. The angular dispersion of the arriving plane waves is small compared to the spreading in angle that the light experiences in traversing a cloud. In the presence of the idealized cloud of Sec. 3.1, the angular impulse response $h_I(\alpha, \beta; \alpha_o, \beta_o)$ of Eq. (3-72) immediately gives us an estimate of the angular intensity distribution $I_{Ns}(\alpha, \beta; \alpha_{sun}, \beta_{sun})$ of scattered sunlight incident on the ground. We have

$$I_{Ns}(\alpha, \beta; \alpha_{sun}, \beta_{sun}) = \frac{N_{sun} \exp[-N_e(1 - \gamma_f)]}{2\pi\sigma_\alpha\sigma_\beta}$$

$$\cdot \exp\left[-\frac{(\alpha - \alpha_{sun})^2}{2\sigma_\alpha^2} - \frac{(\beta - \beta_{sun})^2}{2\sigma_\beta^2}\right] \quad , \tag{5-24}$$

which has the dimensions of watts per (meter^2-steradian-Hz). The quantities α_{sun} and β_{sun} are the angular coordinates of the center of the sun. Knowing Eq. (5-24), we can immediately calculate the noise spectral density due to sunlight which is received by an antenna of given beam pattern and aperture area.

At night the chief sources of noise (aside from quantum noise) are moonlight, starlight, and backscattered light from terrestrial sources. Given a model for the angular and spectral distribution of light from the moon and stars arriving at the earth, the angular impulse response

analysis of Sec. 3.4 would easily lead to an expression similar to Eq. (5-24). The effects of back-scattered light from nearby sources on the earth would have to be estimated by some other means. One could probably obtain sufficiently good results with a crude analytical approach based on single or double scattering. Another alternative is Monte Carlo simulation. We choose not to dwell upon nighttime optical noise here. The communication system we analyze in this chapter will be assumed to be operating during the day, in the presence of scattered sunlight described by Eq. (5-24).

5.3 PROPOSED COMMUNICATION SYSTEM

As we indicated in Sec. 4.1, it is possible in principle to proceed from the generalized scattering function $\sigma(\tau, f, \vec{v}')$ and the transmitted signal envelope s(t) to a mathematical description of the optimum receiver for the cloud channel, in the presence of an additive Gaussian noise $N(t, \vec{r})$. We shall not attempt to do so here. Instead we propose an ad hoc scheme that is easy to analyze, allowing us to obtain a lower bound for the performance achievable with the optimum system. We make no claims about the practicality or optimality of the system considered here; indeed, it is possible that the performance bound we obtain is quite pessimistic. To facilitate the analysis, we make several simplifying assumptions, which will be enumerated below. The system can then be regarded as a classical fading dispersive channel with a high degree of explicit (spatial) diversity. The analysis of its error probability is a straightforward application of known results.

The receiver that we shall consider is shown diagrammatically in Fig. 5-1. Each of the K_A channels receives a statistically independent sample of the received field, obtained in the
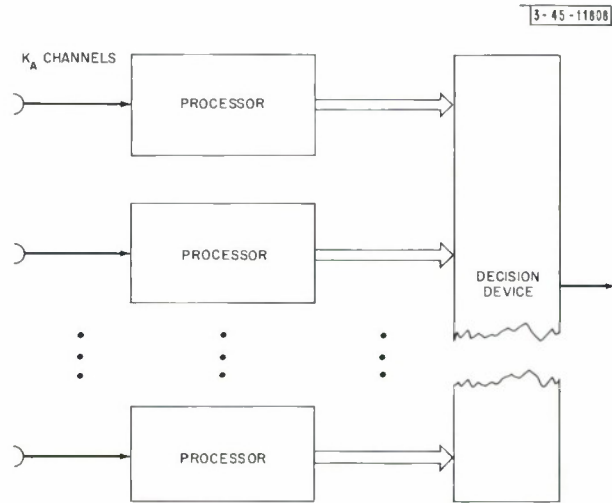
Fig. 5-1. Proposed receiver structure.

manner described in the preceding section. Thus each channel could correspond to a single wide-angle antenna, or several channels could be obtained with each of a number of multibeam antennas. We imagine that the latter might be the more practical alternative. Such an antenna could be realized by making observations at a number of points on the focal plane of a telescope. We shall assume that the receiver measures the incident field, rather than the intensity. Physically, this implies the use of heterodyning, with the local oscillator signal appropriately

introduced in the focal plane. We assume that K_A is less than the maximum achievable spatial diversity K_S of Eq. (5-17), so that it will be meaningful to analyze the behavior of the system error probability as a function of K_A.

The absence of nonuniform weighting at the processor outputs in Fig. 5-1 embodies the assumption that all spatial diversity paths have equal gain. Moreover, we shall assume that the range-Doppler scattering function $\sigma(\tau, f)$ and the statistics of the received process are identical on all spatial paths (and on all channels we might later add, to increase K_A). We justify this assumption on the grounds that the available spatial diversity per square meter is so enormous [cf. Eq. (5-22)] that we can obtain all the independent channels we are willing to deal with by using only a modest area on the ground plane, and a modest total solid angle. A final simplifying assumption we shall make is that the correlation function of the noise-free received process on each diversity path has K_1 equal-eigenvalue orthonormal eigenfunctions $\varphi_i(t)$ (which, of course, depend in general upon the transmitted signal). Note that the assumptions described in this paragraph are not essential; we use them because they will simplify our performance analysis considerably. For a thorough discussion of these issues, and of more general fading dispersive channels, the reader is referred to Kennedy.[36]

Each box labeled PROCESSOR in Fig. 5-1 contains all the components of a conventional receiver for a fading dispersive channel, except the decision device. We assume that the noise is additive, white and Gaussian. One of the possible realizations of the processor is illustrated in Fig. 5-2, for the simple transmission strategy of binary on-off signaling. The envelopes of the impulse responses of the bandpass matched filters (which depend upon our choice of a transmitted signal) are the time-reversed and delayed eigenfunctions $\varphi_i(T - t)$, $i = 1, 2, \ldots, K_1$. Each
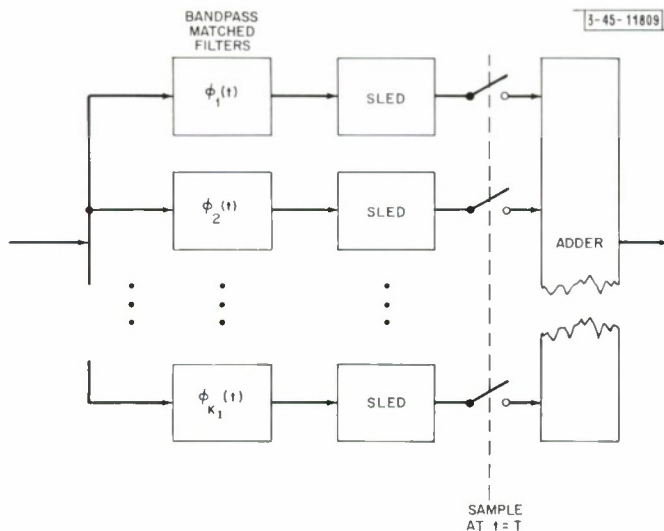
Fig. 5-2. Processor.

box labeled SLED contains an envelope detector followed by a square-law device. In the receiver of Fig. 5-1, the outputs of all the processors are added and (in the binary case) compared with a threshold.

The extension of the receiver structure to M-ary signaling alphabets is straightforward. Each processor would then contain a set of M banks of apparatus similar to Fig. 5-2. The matched filters would differ from one bank to the next, of course, since the eigenfunctions depend

upon the transmitted signal. A vector of M numbers would be computed by each of the K_A processors. The decision device would add corresponding components of all the vectors and would pick the largest of the results. Again, we refer to Kennedy[36] for a complete discussion of the details. Particular attention is directed to the remarks in his Chapters 4 and 6 concerning explicit diversity.

5.4 SYSTEM PERFORMANCE

We begin the analysis by calculating the signal power and noise spectral density measured by an antenna on the ground beneath a cloud. The signal-to-noise ratio is obtained, taking proper account of quantum noise. We summarize known methods for calculating bounds to the error probability of fading dispersive channels, and apply them to the proposed cloud-channel communication system of Sec. 5.3. The channel capacity is calculated, and it is shown that the error probability decreases exponentially with the spatial diversity K_A. These results are illustrated with typical numerical examples.

The calculation of the signal power received by an antenna is a straightforward application of the results of Chapter 3. As in Sec. 5.1, let us suppose that the top of the cloud is illuminated by a narrow CW beam with symmetric Gaussian intensity variation over its cross section. The resulting power distribution function $P_G(\alpha, \beta, x, y)$ over the ground is given by Eqs. (5-3) and (5-4) when the illumination carries unit power. Assuming the total power in the incident beam to be P_0 watts, we simply multiply Eq. (5-3) by P_0. As we showed in Sec. 3.5, the average power P_s received by an antenna with this illumination is determined by integrating Eq. (5-3) over the beam pattern and the aperture of the antenna. When the beam solid angle ω_s and the aperture area A_s of the antenna are small compared with the total solid angle and total ground-plane area of Eq. (5-3), respectively, we can approximate the integral by the product

$$P_s = A_s \omega_s P_0 P_G(\alpha, \beta, x, y) \quad , \tag{5-25}$$

where the quantities in the argument of $P_G(\ )$ are the antenna coordinates. Now, we recall that the averaging process utilized in Chapter 3 was, in fact, an ensemble averaging. Thus Eq. (5-25) represents the statistical average of the power received by the antenna at an instant of time. By assuming ergodicity, we can interpret Eq. (5-25) as a time average, when the illumination on the top of the cloud is CW. This interpretation is approximately valid for a time-limited transmitted signal, also, if the duration T_{tr} of the signal is long compared with the multipath spread L of the channel. The total signal energy received by the antenna is then

$$E_s = P_s T_{tr} \quad . \tag{5-26}$$

We observe that the material in Chapter 3 [and hence Eq. (5-25)] does not apply for transmitted pulses which are short compared with L. The analysis in this section assumes that $T_{tr} \gg L$, and we do not attempt to determine the receiver performance for short signals. This issue will be discussed further in Chapter 6.

The calculation of the spectral density of background noise measured by the antenna follows easily from the results of Sec. 5.3. Equations (5-23) and (5-24) give us the angular intensity distribution $I_{Ns}(\ )$ of scattered sunlight, which we assume to be the dominant background noise. As we stated immediately above Eq. (5-23), its spectrum is essentially flat at optical frequencies, and the arguments in Appendix A cause us to conclude that it is Gaussian. By the same reasoning that led to Eq. (5-25), we see that the sun noise spectral density received by an antenna of

small solid angle ω_s and aperture area A_s is given by

$$N_o = A_s \omega_s I_{Ns}(\ )$$

$$= \frac{1.67 \times 10^{-12} \exp[-N_e(1 - \gamma_f)]}{2\pi\sigma_{\alpha s}^2} \exp\left[-\frac{\psi_s^2}{2\sigma_{\alpha s}^2}\right] A_s \omega_s \quad , \tag{5-27}$$

where ψ_s is the angular separation between the antenna boresight axis and the geometric line of sight to the sun. The units of Eq. (5-27) are watts per Hertz; the conventional two-sided noise spectral density $N_o/2$ is equal to Eq. (5-27) divided by 2.

The received signal is corrupted by photon noise, in addition to the background noise. Assuming heterodyne detection, with a strong local oscillator signal (as we do here), it has been shown[37,38] that the effect of photon noise is equivalent to that of an additive white Gaussian process with (two-sided) spectral density $hf_o/4\eta$, statistically independent of the signal and the background noise. The constant h is Planck's constant, f_o is the optical carrier frequency, and $\eta \leqslant 1$ is the quantum efficiency of the detector. Thus one accounts for the quantum noise (really local oscillator shot noise, in this case) by replacing the classical white noise spectral density $N_o/2$ by

$$\frac{N_o}{2} + \frac{hf_o}{4\eta} \quad . \tag{5-28}$$

We now see that the ratio of signal energy to noise spectral density for the antenna considered in this section is equal to

$$\frac{P_s T_{tr}}{(N_o/2) + (hf_o/4\eta)} \quad , \tag{5-29}$$

with P_s given by Eq. (5-25) and N_o given by Eq. (5-27). Let us examine this ratio quantitatively. Assume that the antenna is so oriented that P_s is maximized; that is, let its pointing angle (α, β) and its ground plane coordinates (x, y) be equal to the mean values $(m_\alpha, m_\beta, m_x, m_y)$ of the power distribution function [Eq. (5-3)] incident on the ground. Equation (5-25) becomes

$$P_s = A_s \omega_s P_o \exp[-N_e(1 - \gamma_f)] \cdot [4\pi^2 \sigma_{\alpha s}^2 \sigma_{xs}^2 (1 - \rho_{\alpha xs}^2)]^{-1} \quad , \tag{5-30}$$

with $\sigma_{\alpha s}$, σ_{xs} and $\rho_{\alpha xs}$ given by Eq. (5-4). Let the background noise N_o have its worst-case value, with the sun located directly behind the source. With ψ_s equal to zero, then, Eq. (5-27) gives us

$$\frac{N_o}{2} = A_s \omega_s \frac{8.4 \times 10^{-13} \exp[-N_e(1 - \gamma_f)]}{2\pi\sigma_{\alpha s}^2} \quad . \tag{5-31}$$

Assuming a detector quantum efficiency η equal to unity, the quantum noise term in (5-29) is

$$\frac{hf_o}{4} \cong 10^{-19} \text{ joules} \tag{5-32}$$

at visible-light frequencies. Observe that both P_s and $N_o/2$ are proportional to the quantity $A_s \omega_s$ while $hf_o/4$ is a constant. Thus the signal-to-noise ratio (5-29) increases monotonically with $A_s \omega_s$. As a numerical example, let us compute (5-29) for the set of cloud and signal

parameters [Eqs. (5-19) and (5-20)]. The result is

$$\frac{P_s T_{tr}}{(N_o/2) + (hf_o/4)} \simeq \frac{A_s \omega_s P_o T_{tr} \times 2.57 \times 10^{-7}}{A_s \omega_s \times 10^{-13} + 10^{-19}} \quad . \tag{5-33}$$

We recognize that the antenna must be diffraction-limited in this case, so that the received field is coherent across the entire aperture, in order that heterodyne detection can be performed. In accordance with our conventions [Eqs. (4-36) and (5-6)], we would then have

$$A_s \omega_s \simeq \left(\frac{\pi D^2}{4}\right)\left(\frac{4\lambda_o^2}{\pi D^2}\right) = \lambda_o^2 = 2.5 \times 10^{-13} \tag{5-34}$$

at 0.5-micron wavelength. The background noise term in the denominator of Eq. (5-33) would become

$$\frac{N_o}{2} = 2.5 \times 10^{-26} \quad , \tag{5-35}$$

which is far smaller than the photon noise term. In order to get some idea of the magnitude of the corresponding signal-to-noise ratio, let us assume that the average transmitted power P_o is 500 watts, and that T_{tr} is 1000 times the multipath spread L of the scattering function $\sigma(\tau, f)$. The particular scattering function obtained in Appendix E had

$$L = \frac{D_e}{c} (1 + 2\sqrt{N_e}) \tag{5-36}$$

[Eq. (E-36)]. For the assumed numerical values in this example, we have

$$L \simeq 2.44 \times 10^{-6} \text{ second,} \tag{5-37}$$

whence

$$T_{tr} \simeq 2.44 \times 10^{-3} \text{ second.} \tag{5-38}$$

Equation (5-33) then becomes

$$\text{SNR} \simeq 0.784 \quad . \tag{5-39}$$

It is clear that one could realize a far better signal-to-noise ratio (SNR) by using a nondiffraction-limited antenna, having a larger value of $A_s \omega_s$. We could no longer use hetero-dyne detection, however, because the aperture would now be larger than the coherence area of the field received from the solid angle ω_s. But one might be willing to consider a scheme such as optical filtering followed by square-law detection, followed by electrical filtering and processing. Although the nature of the necessary filtering and processing is not yet known, it is interesting to calculate the achievable SNR improvement. We notice that Eq. (5-33) would approach its largest possible value for any $A_s \omega_s$ greater than about 10^{-4}, which could correspond to, say, $\omega_s = 0.01$ steradian and $A_s = 0.01$ square meter. Using the above values for P_o and T_{tr}, we see that Eq. (5-33) would then become

$$\text{SNR} = 3.13 \times 10^6 \quad . \tag{5-40}$$

Obviously one could achieve an adequate SNR with this scheme by using far lower transmitted power and shorter signals. The tradeoff is reflected in the fact that the square-law detection

scheme combines a large number of spatial diversity paths to obtain one received signal. It appears that some form of direct detection would be much more attractive than the field measurement scheme proposed and analyzed here. As we have already noted, the receiver structure described in this chapter was chosen simply because it can be analyzed easily by means of known results.

We turn now to a brief summary of the error probability bounds for fading dispersive channels presented in detail by Kennedy[36] in his Chapters 4 and 5. Let us first discuss the quantities which appear in the bounds. One ordinarily assumes that the average total signal energy received by the entire system is a known quantity E_r. The noise is assumed to be additive, white and Gaussian, with spectral density $N_o/2$. An important parameter in the performance bounds is the ratio

$$\alpha \triangleq \frac{E_r}{N_o} \quad . \tag{5-41}$$

The received signal energy is assumed to be divided among some number K_E of explicit diversity paths, obtained in space, time or frequency. On each of these paths one can obtain a number of statistically independent samples by correlating the received process with each member of the set of orthonormal eigenfunctions $\{\varphi_i(t)\}$ of the correlation function $R(t, \tau)$ of the signal part of the process. Thus we can think of an explicit diversity path as having an implicit diversity K_I associated with it, where K_I is the number of eigenfunctions having nonzero eigenvalues. The so-called fractional path strengths of the implicit diversity paths are the eigenvalues λ_i, $i = 1, 2, \ldots, K_I$ of the $\{\varphi_i(t)\}$. The eigenfunctions depend upon the transmitted signal, along with K_I and the $\{\lambda_i\}$. It is known that a system with K_I equal eigenvalues has better performance than any other system with the same number of eigenvalues. It is convenient to analyze the performance of an unequal-eigenvalue system in terms of the performance of an equivalent equal-strength system. We shall simplify the analysis of the cloud-channel receiver by assuming at the outset that each explicit diversity path has equal eigenvalues. Moreover, we shall assume that each explicit diversity path has the same number K_I of eigenvalues. Thus we may regard the entire system as having a total diversity

$$D = K_E K_I \quad . \tag{5-42}$$

One associates a time constraint length τ_t with each signal transmission. It is necessary for the analysis that the received signals resulting from two successive transmissions do not overlap. We choose to insure this by setting

$$\tau_t = T_{tr} + L \cong T_{tr} \quad . \tag{5-43}$$

If the size of the signaling alphabet is M, the information rate R of the system is

$$R = \frac{\log_2 M}{\tau_t} \text{ bits/sec} \quad . \tag{5-44}$$

The capacity C of the channel is identical to that of a nondispersive Gaussian channel with the same value of the ratio P_r/N_o, where

$$P_r = \frac{E_r}{\tau_t} \tag{5-45}$$

is the average received signal power. Thus the capacity is

$$C = \frac{\alpha}{\tau_t \ln 2} \quad . \tag{5-46}$$

The bounds to the system error probability $P(\epsilon)$ have the form

$$K_L 2^{-\tau_t C E} \leqslant P(\epsilon) \leqslant K_U 2^{-\tau_t C E} \quad . \tag{5-47}$$

Since the coefficients K_L and K_U are slowly varying compared to the exponential, it is sufficient for our purposes to concentrate on the exponential part of Eq. (5-47),

$$P(\epsilon) \cong 2^{-\tau_t C E} \quad . \tag{5-48}$$
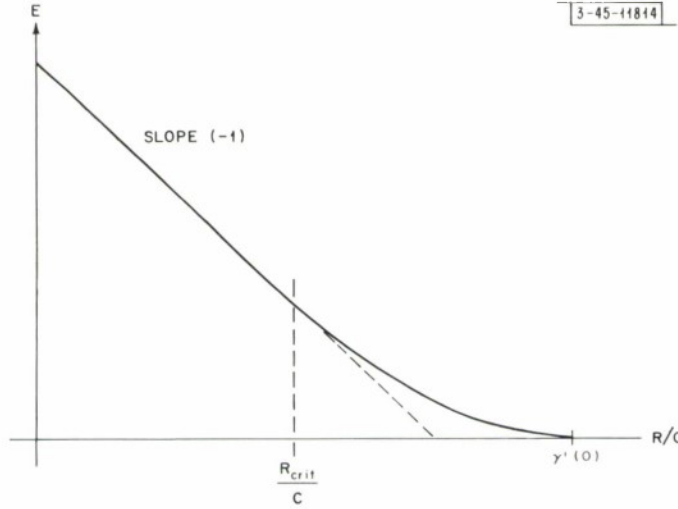
Fig. 5-3. System reliability function E.

The quantity E in the exponent, called the system reliability function, has the familiar shape shown in Fig. 5-3. It is defined by the parametric expression

$$E \triangleq \begin{cases} -2\gamma(-\frac{1}{2}) - R/C \quad , & 0 \leqslant \frac{R}{C} \leqslant \frac{R_{crit}}{C} \tag{5-49a} \\ \\ s\gamma'(s) - \gamma(s) \quad , & \frac{R_{crit}}{C} \leqslant \frac{R}{C} \leqslant \gamma'(0) \quad , \tag{5-49b} \end{cases}$$

in which

$$\gamma(s) = -\frac{K_E}{\alpha} \sum_{i=1}^{K_1} \left[\ln\left(1 - s\alpha \frac{\lambda_i}{K_E}\right) + s \ln\left(1 + \alpha \frac{\lambda_i}{K_E}\right) \right] \quad , \quad -\frac{1}{2} \leqslant s \leqslant 0 \tag{5-50}$$

and

$$\frac{R}{C} = (s + 1) \gamma'(s) - \gamma(s) \tag{5-51}$$

67

in Eq. (5-49b). The critical rate R_{crit} is given by

$$\frac{R_{crit}}{C} = \frac{1}{2} \gamma'(-\frac{1}{2}) - \gamma(-\frac{1}{2}) \quad . \tag{5-52}$$

The value of E can be maximized for given values of α and of R/C by optimizing the eigenvalues λ_i and the total diversity D. The eigenvalues λ_i are all equal in the optimum system. The total diversity D is adjusted so that α/D, the signal-to-noise ratio per diversity path, has an optimum value α_p^o determined for given R/C as the solution of a set of nonlinear equations. The quantity α_p^o increases monotonically from about three for very small R/C to extremely large values as R/C approaches unity. The optimum diversity is

$$D^o = \begin{cases} \dfrac{\alpha}{\alpha_p^o} & , \quad \alpha > \alpha_p^o \\[2ex] 1 & , \quad \alpha \leqslant \alpha_p^o \quad . \end{cases} \tag{5-53}$$

The corresponding optimized reliability E^o, which also depends only upon α and R/C, is qualitatively similar to Fig. 5-3, except that it intercepts the R/C axis at the point

$$R/C = 1 \quad . \tag{5-54}$$

The application of these results to the cloud channel is straightforward. The total average received signal energy E_r on the cloud channel is not fixed; as we have shown, it is proportional to the spatial diversity K_A. By Eq. (5-26), the received signal energy per antenna beam is

$$E_s = P_s T_{tr} \quad , \tag{5-55}$$

and the total received signal energy is

$$E_r = K_A E_s \quad , \tag{5-56}$$

where we assume that all K_A spatial paths are identical. Because of Eq. (5-43), the average total received signal power is

$$P_r = \frac{E_r}{\tau_t} = \frac{E_r}{T_{tr}} = K_A P_s \quad . \tag{5-57}$$

In view of (5-28), the quantity α of Eq. (5-41) becomes

$$\alpha \triangleq \frac{E_r}{N_o + (hf_o/2\eta)} = \frac{K_A E_s}{N_o + (hf_o/2\eta)} \tag{5-58}$$

for our ad hoc receiver. The capacity of the cloud channel is

$$C_{cl} = \frac{\alpha}{\tau_t \ln 2}$$

$$= K_A C_s \quad , \tag{5-59}$$

where

$$C_s = \frac{\alpha_s}{\tau_t \ln 2} \tag{5-60}$$

68

is the capacity per spatial diversity path. The quantity

$$\alpha_s = \frac{\alpha}{K_A} = \frac{E_s}{N_o + (hf_o/2\eta)} \qquad (5\text{-}61)$$

is the energy-to-noise ratio per spatial diversity path.

There are two cases of interest in applying the performance bounds to the cloud channel. In case I we assume that the ratio R/C_{cl} is held constant; that is, we let the rate R be proportional to the number K_A of telescope beams. In case II we investigate the error probability for communication at a fixed rate R_f.

Case I is equivalent to adopting the policy of increasing our communication rate by a fixed amount each time another spatial diversity path is added to the system. Let us identify the spatial diversity K_A with the explicit diversity K_E of Eq. (5-42). We see that Eq. (5-50) then becomes

$$\gamma(s) = -\frac{1}{\alpha_s} \sum_{i=1}^{K_I} [\ln(1 - s\alpha_s\lambda_i) + s \ln(1 + \alpha_s\lambda_i)] \quad , \qquad (5\text{-}62)$$

which is independent of K_A. By inspection of Eqs. (5-49), we find that the reliability E is also independent of K_A, and the error probability [Eq. (5-48)] becomes

$$P(\epsilon) \cong 2^{-\tau_t C_{cl} E}$$
$$= 2^{-\tau_t K_A C_s E} \quad , \qquad (5\text{-}63)$$

which decreases exponentially with increasing K_A.

In view of Eq. (5-62), we conclude that the optimized reliability E^o of the channel in case I is that of a single spatial path with energy-to-noise ratio α_s. We compute α_p^o for the given value of R/C_{cl} and determine the optimum implicit diversity per spatial path by the relation

$$K_I^o = \begin{cases} \dfrac{\alpha_s}{\alpha_p^o} \quad , & \alpha_s > \alpha_p^o \\[3mm] 1 \quad , & \alpha_s \leqslant \alpha_p^o \end{cases} \qquad (5\text{-}64)$$

independent of K_A. The optimum total diversity is simply

$$D^o = K_A K_I^o \quad , \qquad (5\text{-}65)$$

regardless of the value of K_A. The resulting optimized error probability is

$$P(\epsilon) = 2^{-\tau_t K_A C_s E^o} \quad , \qquad (5\text{-}66)$$

still exponentially decreasing with K_A.

Under case II, where we communicate at the fixed rate R_f, the system reliability E of Eqs. (5-49) depends upon K_A through the quantity

$$\frac{R}{C} = \frac{R_f}{C_{cl}} = \frac{R_f}{K_A C_s} \quad . \qquad (5\text{-}67)$$

69

We note that the function $\gamma(\ )$ is still given by Eq. (5-62), and is independent of K_A, as is the quantity R_{crit}/C of Eq. (5-52). In view of Eq. (5-67), Eqs. (5-49) may be rewritten as

$$
E = \begin{cases}
-2\gamma(-\frac{1}{2}) - \dfrac{R_f}{K_A C_s} \quad , & \dfrac{R_f/C_s}{R_{crit}/C} \leq K_A < \infty & \text{(5-68a)} \\[3ex]
s\gamma'(s) - \gamma(s) \quad , & \dfrac{R_f/C_s}{\gamma'(0)} \leq K_A \leq \dfrac{R_f/C_s}{R_{crit}/C} & \text{(5-68b)} \\[3ex]
0 \quad , & K_A \leq \dfrac{R_f/C_s}{\gamma'(0)} \quad , & \text{(5-68c)}
\end{cases}
$$

where

$$
\frac{R_f}{K_A C_s} = (s + 1)\gamma'(s) - \gamma(s) \tag{5-69}
$$

in Eq. (5-68b). For K_A in the interval in Eq. (5-68a), the error exponent

$$
\tau_t C_{cl} E = \tau_t K_A C_s E
$$
$$
= -2\tau_t K_A C_s \gamma(-\frac{1}{2}) - \tau_t R_f \tag{5-70}
$$

again increases linearly with K_A. For K_A in the interval in Eq. (5-68b), the situation is more complicated. The corresponding range of R/C lies between R_{crit}/C and $\gamma'(0)$. Now, the derivative of E with respect to R/C increases from -1 to 0 as R/C increases from R_{crit}/C to $\gamma'(0)$. In view of Eq. (5-67), we see that the derivative of E with respect to K_A increases from zero to $R_f/(K_A^2 C_s)$ as K_A increases over the interval in Eq. (5-68b). Therefore, the error exponent $\tau_t K_A C_s E$ increases faster than linearly with K_A over this interval. Finally, for K_A in the interval in Eq. (5-68c), the reliability E is zero because the system is attempting to operate at a rate above capacity.

The optimization of the diversity in case II is quite simple. For each value of

$$
\frac{R}{C} = \frac{R_f}{K_A C_s}
$$

we can calculate α_p^o, and

$$
D^o = K_A K_I = \frac{\alpha}{\alpha_p^o} = \frac{K_A \alpha_s}{\alpha_p^o} \tag{5-71}
$$

as before. For given R/C and α we calculate E^o. The error exponent $\tau_t K_A C_s E^o$ is zero for

$$
K_A \leq \frac{R_f}{C_s} \quad , \tag{5-72}
$$

increases faster than linearly with K_A when

$$
\frac{R_f}{C_s} \leq K_A \leq \frac{(R_f/C_s)}{(R_{crit}/C)} \tag{5-73}
$$

70

and goes up linearly with K_A for

$$\frac{(R_f/C_S)}{(R_{crit}/C)} \leqslant K_A < \infty \quad . \tag{5-74}$$

In the results of both cases I and II, we see the answer to the question of optimum spatial diversity K_A. Since the error probability decreases monotonically with increasing K_A, it is clear that the optimum value of K_A is simply the largest possible value, up to the maximum achievable spatial diversity K_S of Eq. (5-17) in Sec. 5.1. In a more realistic situation one would presumably assign a cost function to K_A, thereby allowing the optimum K_A to be determined by considerations external to the actual channel analysis.

As a numerical example, let us calculate some approximate figures for communication to the earth with a laser in a satellite in synchronous orbit, at a distance of about 20,000 miles. Let the laser have 500 watts of output power capability at 0.5-micron wavelength, and let it have 5-cm diffraction-limited optics. Using the conventions of Sec. 5.1, we model its intensity variation over the upper surface of a cloud layer on the earth as a symmetric Gaussian function of x and y, with

$$\sigma_i^2 \simeq 5 \times 10^3 \quad . \tag{5-75}$$

Let the cloud have the set of parameters of Eq. (5-19). We find that σ_i^2 is indeed negligible compared with the variance σ_{xs}^2, given by Eq. (5-20), of the resulting power distribution function $P_G(\alpha, \beta, x, y)$ [Eq. (5-3)] over the ground. Thus the three parameter values of Eq. (5-20) used in our earlier numerical examples are also correct in the present situation. Let us now make the same set of assumptions about the telescope and the signal that led to the signal-to-noise ratio [Eq. (5-39)] which we have already calculated. The telescope is located and aimed in such a way that the received signal power P_s is maximized; the sun is directly behind the satellite. The time duration of the transmitted signal is given by Eq. (5-38),

$$T_{tr} = 2.44 \times 10^{-3} \text{ second} \cong \tau_t \quad .$$

The resulting ratio of average received signal energy to (two-sided) noise spectral density for this single telescope beam is given by Eq. (5-39),

$$\frac{E_s}{(N_o/2) + (hf_o/4\eta)} \simeq 0.784 \quad . \tag{5-76}$$

Now, the signal-to-noise ratio α_s of Eq. (5-61) is the ratio of the received signal energy to the single-sided noise spectral density, for a single beam. Thus α_s is equal to one-half of Eq. (5-76) or

$$\alpha_s \simeq 0.392 \quad . \tag{5-77}$$

The received signal power per beam is

$$P_s = 3.21 \times 10^{-17} \text{ watt} \quad , \tag{5-78}$$

and the signal energy per beam is

$$E_s = P_s T_{tr} = 7.84 \times 10^{-20} \text{ joule} \quad . \tag{5-79}$$

Finally, let us assume that we form 10^3 beams, so that

$$K_A = 10^3 \quad , \tag{5-80}$$

and that we wish to communicate at a rate

$$R = 0.03 \, C_{cl} \quad , \tag{5-81}$$

which is just equal to R_{crit} for the given value [Eq. (5-77)] of α_s. We have

$$C_s = \frac{\alpha_s}{\tau_t \ln 2} \cong 2.32 \times 10^2 \text{ bits/sec} \tag{5-82}$$

and

$$C_{cl} = K_A C_s = 2.32 \times 10^5 \text{ bits/sec} \quad , \tag{5-83}$$

so that the desired rate is

$$R = 6.96 \times 10^3 \text{ bits/sec} \quad . \tag{5-84}$$

From Fig. 4a in Chapter 5 of Kennedy,[36] we find that $R/C = 0.03$ corresponds to the optimum signal-to-noise ratio

$$\alpha_p^o \cong 3.0 \tag{5-85}$$

per diversity path. The corresponding optimum implicit diversity is

$$K_I^o = \frac{\alpha_s}{\alpha_p^o} \to 1 \quad , \tag{5-86}$$

and the optimized total diversity (given that $K_A = 10^3$) is

$$D^o = K_A K_I^o = 10^3 \quad . \tag{5-87}$$

Exploiting the low-rate, small-α_s analysis in Kennedy's Chapter 5, we find that the error probability of the system is

$$P(\epsilon) = 10^{-6.63} \quad . \tag{5-88}$$

An unattractive feature of this example is the required size of the signaling alphabet, which is a consequence of the rather long constraint length τ_t we had to use. We require

$$M = 2^{R\tau_t} \cong 2^{17} \tag{5-89}$$

orthogonal waveforms. Equivalently, one could form the transmitted signals by coding 17 bits together. This high degree of complexity can be substantially ameliorated by exploiting known techniques[39,40] for efficient approximation of orthogonal signals. It is possible to generate a set of 2^K "almost orthogonal" waveforms with only about $K^{1/2}$ bits. In many applications, the resulting signal set will perform nearly as well as an orthogonal set.

CHAPTER 6
CONCLUSIONS AND SUGGESTIONS FOR FUTURE RESEARCH

The most significant results of this study are indications that communication through clouds at visible-light wavelengths is both feasible and capable of fairly impressive data rates. Even if one makes generous allowances for suboptimum signal and receiver design, the numerical examples of Sec. 5.4 indicate that a laser of modest power in a satellite, with a reasonably simple receiver on the ground beneath a cloud layer, could achieve kilobit rates with low error probability.

The primary objective of this research was the development of an adequate model for the cloud as an optical communication channel. The first step toward this end was a study of the spatial variation of the average intensity of light over the ground beneath a cloud, when the top of the cloud is subjected to CW illumination. This portion of the analysis (the material of Chapter 3) can be understood and applied without any background in communications theory. Using the ideas and techniques of linear systems analysis, we derived a linear superposition integral which describes the light on the ground as a function of the spatial character of the illumination on the top of the cloud (e.g., a uniform plane wave, a narrow beam, or any desired spatial variation). In general, the integral gives the average intensity of the light as a joint function of angle of arrival and horizontal coordinates (x, y) over the ground plane. It is shown that the received light has extremely small variance; that is, the instantaneous intensity is always very nearly equal to its average value. For the special case in which the illumination on the top of the cloud is uniform over the entire horizontal plane, the superposition integral simplifies considerably. The intensity of the light incident on the ground then depends only upon angle of arrival.

Light traversing a cloud suffers dispersion in time and frequency, as well as in space. Moreover, the received field at a point on the ground can be represented in terms of a complex Gaussian random process (the arguments leading to this conclusion are worked out in detail in Appendix A). Thus the received process at a point is equivalent to the signal received over a classical fading dispersive channel, such as a tropospheric-scatter microwave system. At visible-light frequencies, however, the spatial variation of the received field occurs on a scale which makes it both important and useful in receiver design. These ideas led to the characterization of the channel in terms of the generalized scattering function $\sigma(\tau, f, \vec{v}\,')$ of Sec. 4.1, which includes the dependence of the received field upon both angle of arrival and horizontal coordinates (x, y). If this function were known in detail for a particular physical situation, one would have a complete statistical description of the received process. On an abstract level this formulation is concise and efficient. It constitutes the most general form of our optical communication channel model for the cloud. We recognize, however, that the elegant function $\sigma(\tau, f, \vec{v}\,')$ is cumbersome and difficult to obtain in practical situations. In Secs. 4.2 through 4.5, we consider various specialized and easily calculable aspects of it. These include the spatial correlation function of the received field over the ground, the joint spatial and angular correlation function for directive receiving antennas, and the classical range-Doppler scattering function $\sigma(\tau, f)$ for a narrow-beam antenna of small aperture area. It is shown that the intensity distributions of Chapter 3 are simply special cases of the generalized scattering function.

The correlation functions are utilized in Chapter 5 to estimate the degree of spatial diversity achievable in a cloud communication system. An ad hoc receiver is proposed which exploits

the spatial diversity to obtain a number of statistically independent samples of the received field and processes the signal on each spatial diversity path in the manner of a classical fading dispersive channel receiver. The relationship between this receiver and the optimum communication system for the cloud channel is not known. The proposed receiver is easy to analyze, however, and the results provide a lower bound for communication rates and error performance that the optimum system could achieve.

Future theoretical investigations in the area of cloud communication could logically proceed along three fronts. These are refinement and extension of the present results, development and analysis of optimum and suboptimum receivers, and numerical computation of a variety of functions and parameters related to the problem. The first of these efforts should include a detailed study of the scattering function $\sigma(\tau, f, \vec{v}')$, which was discussed only briefly in this report. Our results also need clarification and interpretation for both small and large optical thicknesses N_e. The unscattered residue of the incident illumination, attenuated by the factor $\exp[-N_e]$, can be regarded as a specular component in the received signal. For optically thin clouds, one could perhaps realize a significant simplification in receiver structure by exploiting this specular signal appropriately. On another level, our Gaussian results for angular distributions of the scattered radiation can be in error even at substantial optical thicknesses when the single-particle scattering pattern is very strongly forward-directed. Evidence of this effect appears in certain of the Monte Carlo results of Kattawar and Plass[41] for nimbostratus clouds, in which the maximum of the particle radius distribution occurs at about 12 microns. At $\Theta = 0$, the average single-particle scattering pattern for such a cloud is greater by 10^6 than at $\Theta = \pi/2$. For $N_e = 10$, Kattawar and Plass found that the scattered light had an angular intensity distribution with about the same shape as our Gaussian predictions, except for a narrow peak at $\Theta = 0$ having a value about twice that at $\Theta = 1.5$ degrees. The reason for the erroneous behavior of our results in this case (which would predict a pure Gaussian) appears to be associated with the limiting processes carried out in Chapter 3. In a typical law of large numbers problem, one convolves some fixed unit-area probability density function $p(x)$ with itself $(N-1)$ times. It is easy to write down conditions on $p(x)$ such that the result converges to a Gaussian function in the limit as N goes to infinity. In Chapter 3, however, we carry out an $(N-1)$-fold convolution of a function of the form

$$ g(x) = (1 - \frac{b}{N}) u_o(x) + \frac{b}{N} p(x) \quad , \tag{6-1} $$

which is also a well-defined probability density function. The problem is that $g(x)$ varies with N, approaching a unit impulse as N approaches infinity. Our difficulty appears to be the fact that the result of the $(N-1)$ convolutions does not converge to a pure Gaussian curve as N becomes large, when $p(x)$ is too high and narrow. It would be interesting and worthwhile to derive the conditions on $p(x)$ such that the convergence does take place, and to study the behavior of the result when it does not converge properly.

At optical thicknesses greater than about 32, our Gaussian results become suspect. As we point out near the end of Sec. 3.4, in such cases we predict that the angular intensity distributions are practically flat for all $\Theta \leq \pi/2$. We do not yet know how nearly correct this is, nor precisely how other attributes of the received signal (such as time and frequency spreading) behave under these circumstances. These questions constitute another area of interest for further research.

74

The determination of the actual optimum receiver for the cloud channel is closely coupled with the study of the generalized scattering function $\sigma(\tau, f, \vec{v}')$. As we commented in Sec. 4.1, Kennedy[42] has outlined an extension of known techniques one might utilize to address this problem, if $\sigma(\ )$ were known. Among the useful results of a research program in this area would be an assessment of the "degree of optimality" of the proposed communication system of Chapter 5, and the ability to design other practical suboptimum systems. An unsolved problem of particular interest in this regard is the design and performance of both optimum and suboptimum receivers for very short transmitted pulses. The receiver of Chapter 5 assumed long pulses, in order that the CW results of Chapters 3 and 4 could be exploited. The author has done some preliminary work which indicates that the linear system approach of Chapter 3 could be successfully applied for an incident illumination which is impulsive in time as well as in α, β, x and y. Proceeding along these lines, one could presumably obtain an impulse response (and a superposition integral) which would describe the received process as a joint function of angle of arrival, x, y and time, for very short pulses.

Another interesting research area is the question of practical realization of receiving systems, both optimum and suboptimum. It is attractive to think of performing some of the signal processing optically, such as spatial or time-domain filtering. The extent to which such operations can be realized, using components which we know how to build, is an open question. One might also study the possibility of square-law detecting the received field (e.g., with a photomultiplier tube) and filtering the resulting intensity signal appropriately. Because all the phase information would be lost, it seems clear that one could not realize optimum performance with such a scheme, but it is possible that the performance would be good enough to be acceptable under some circumstances.

We remark that it is not always possible to regard the field incident on the ground as a time-continuous process. It is in fact a time-discrete sequence of light quanta, or photons, which can be treated as a continuous time function only when the number of photons arriving per second is very large. This was true in our receiver analysis of Chapter 5, and we have assumed it to be true throughout this report. A recent investigation[43] of pure quantum-mechanical communication systems has yielded results which appear to be applicable to communication over the cloud channel. In particular, the detection of the quantum-mechanical equivalent of Gaussian signals in Gaussian noise was considered. It would be worthwhile to undertake a study of the implications of these results in our problem, for both small and large signal levels.

It is clear that numerical simulation will be a valuable complement to analytical results in cloud channel communication system design. The work of Zaborowski, described in Appendix C, has considerably increased our confidence in the approximate methods used to solve the spatial impulse response equations. In addition to substantiating certain of our results, the Monte Carlo methods of Plass and Kattawar[41] can secure many results which we have not obtained analytically (e.g., backscattered intensity, polarization behavior, and the effects of reflection from the earth's surface). In Appendices E and F, we propose straightforward numerical methods for obtaining the range and range-Doppler scattering functions in simple cases, and we discuss the application of Monte Carlo methods to finding these functions in more general situations.

A fourth area of interest for future research is experimental investigation of some of our results. We suggest an equipment configuration similar to that used by Zaborowski, as described in Appendix G, which simulates the idealized cloud with a water suspension of scattering particles in a shallow transparent tank. The spatial intensity distributions could be measured

accurately with a carefully constructed narrow-beam detector, using a CW laser beam to illuminate the scatterers. It is conceivable that one could also obtain time-spreading information with this experimental model by square-wave modulating the incident beam and measuring the rise time of the output, if a modulator and a detector of sufficient bandwidth were obtainable. As we explain in Appendix G, one would expect rise times to be on the order of τ/c, where τ is the physical depth of the particle suspension. If the depth were a few centimeters, the rise time would be tenths of a nanosecond.

APPENDIX A
SCATTERED FIELD ON GROUND PLANE

The received field at a point $\vec{r}$ on the ground beneath a cloud is a superposition of an enormous number of scattered components. In general, a contribution arrives over every possible multiple-scattering path through the cloud. In this appendix we show, subject to certain reasonable assumptions, that the field on the ground plane can be represented in terms of a complex Gaussian random process.

Fig. A-1. Cloud configuration.
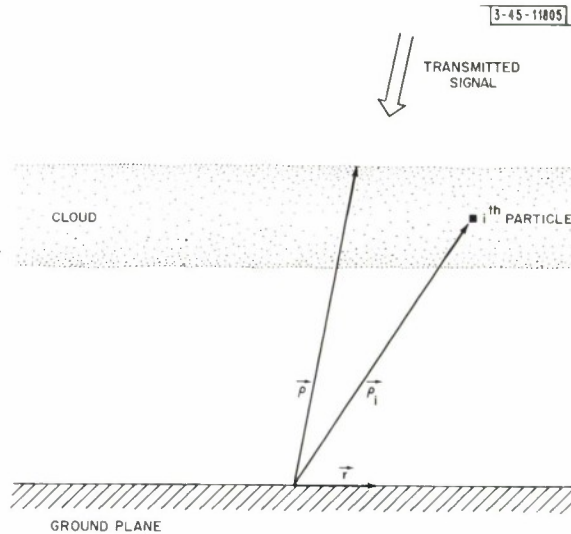
The configuration that we shall examine is illustrated in Fig. A-1. We visualize a transmitted signal of the form

$$e_i(t, \vec{\rho}) = \text{Re} \left[s(t) \, E(\vec{\rho}) \, \exp(-j2\pi f_o t) \right] \tag{A-1}$$

incident upon the top of the cloud, in which $s(t)$ is a narrow-band complex envelope. The term $E(\vec{\rho})$ allows us to treat infinite plane waves, narrow beams, or any other spatial variation in the same general formulation. It is clear that the received field varies with position $\vec{r}$ on the ground plane, depending in a complicated way upon $E(\vec{\rho})$. The spatial dependence is discussed in Chapter 4. For purposes of the analysis in this appendix, we take the point of view that the spatial dependence is implicitly included in all the field parameters that we use.

In studying the field in the vicinity of a point $\vec{r}$ on the ground plane, it is convenient to set up a new coordinate system S' with its origin at the point $\vec{r}$ in the fixed coordinate system S. We visualize a set of vectors $\{\vec{\rho}_i'\}$ from the origin of S' to all the particles in the cloud, and we specify positions on the ground in the vicinity of the point $\vec{r}$ by means of a vector $\vec{r}'$ from the origin of S'.

The signal scattered by the ith particle toward the point $\vec{r}$ on the ground consists of M_i components, where M_i is the number of wavelets incident upon the particle. These include the unscattered remnant of the incident signal (A-1) that penetrates to the particle, in addition to wavelets of all scattering orders arriving at the ith particle from all the other particles in the cloud. Many of these components, of course, will have been severely attenuated by multiple scattering or by scattering through large angles. If there are N_p particles in the cloud, the ith

particle is illuminated by $(N_p - 1)$ single-scattered components, $(N_p - 1)^2$ double-scattered components, and so on. There are $(N_p - 1)^{m-1}$ scattering paths of order m which encounter the ith particle and proceed directly to the point $\vec{r}$ on the ground. Although the total number M_i of all such scattering paths is infinite, in practice we shall regard it as a large but finite quantity, since we can ignore those components which have been scattered so many times that their amplitudes are negligible.

Let us assign an index k to each of the scattering paths which proceed to the point $\vec{r}$ via the ith particle, with k ranging from 1 to M_i. As it proceeds along the kth scattering path, a field component experiences a sequence of attenuations. Each time it is scattered through some angle Θ by a particle in the path, its amplitude suffers a loss proportional to $|F(\Theta)|^{1/2}$, where F( ) is the intensity scattering pattern of the particle, as discussed in Chapter 2. This loss can vary by order of magnitude, depending upon the size of Θ. Over the distance d between one particle and the next, the amplitude of the field component suffers both $1/d$ loss and an average extinction loss of $\exp[-d/2D_e]$ (the square root of the average extinction attenuation of its intensity). Finally, the component suffers scattering pattern loss and $1/d$ loss in proceeding from the ith particle to the point $\vec{r}$ on the ground. Let us lump all these losses on the kth path into a single amplitude factor η_{ki}, which is obviously very small in most cases. We shall use three additional parameters to characterize the kth path through the ith particle to the point $\vec{r}$. These are the total path length τ_{ki} (seconds), the total Doppler shift f_{ki}, and the phase Θ_{ki}. All three of these quantities include the effects of the final segment of the path, from the ith particle to the point $\vec{r}$.

Ignoring the effects of polarization (as we do throughout the report), we regard the total field component arriving at the ground from the ith particle as a sum of scalar quantities. We shall write down an expression for this component at a point $\vec{r}'$ in the vicinity of $\vec{r}$, where $\vec{r}'$ is measured in the coordinate system S' centered at $\vec{r}$. Let us denote this component as $y_i(t, \vec{r}, \vec{r}')$. We have

$$
y_i(t, \vec{r}, \vec{r}') = \mathrm{Re} \left\{ \sum_{k=1}^{M_i} \eta_{ki}\ s(t - \tau_{ki}) \right.
$$
$$
\left. \cdot \exp\left[-j2\pi t(f_o - f_{ki}) - j\Theta_{ki} - j\frac{2\pi}{\lambda_o}\frac{\vec{r}' \cdot \vec{\rho}_i'}{|\vec{\rho}_i'|} \right] \right\} \quad , \qquad (A-2)
$$

where $\vec{\rho}_i'$ is also measured in S'. This expression incorporates several assumptions which are frequently invoked in the study of scattering channels.[36,4] First, although we attribute the Doppler shift f_{ki} to the variation with time of the path delay τ_{ki}, only the nominal value of the path delay appears in the argument of the signal envelope s( ). This is consistent with the assumption that s( ) is a narrow-band waveform. Second, we have assumed that the magnitude of $\vec{r}'$ is small compared with that of $\vec{\rho}_i'$, so that the attenuation η_{ki} and the delay τ_{ki} (though implicitly dependent upon $\vec{r}$) are independent of $\vec{r}'$. The same assumption permits us to approximate the carrier phase variation with $\vec{r}'$ as indicated in Eq. (A-2). Specifically, the phase associated with propagation from $\vec{\rho}_i'$ to $\vec{r}'$ is given by

$$
\frac{2\pi}{\lambda_o} |\vec{\rho}_i' - \vec{r}'| = \frac{2\pi}{\lambda_o}(|\vec{\rho}_i'|^2 - 2\vec{r}' \cdot \vec{\rho}_i' + |\vec{r}'|^2)^{1/2}
$$

$$\frac{2\pi}{\lambda_o} |\vec{\rho_i}' - \vec{r}'| \cong \frac{2\pi}{\lambda_o} (|\vec{\rho_i}'|^2 - 2\vec{r}' \cdot \vec{\rho_i}')^{1/2}$$

$$\cong \frac{2\pi}{\lambda_o} \left(|\vec{\rho_i}'| - \frac{\vec{r}' \cdot \vec{\rho_i}'}{|\vec{\rho_i}'|} \right) \quad .$$

The first term is lumped with the overall path phase Θ_{ki} and the second term appears in the exponent of Eq. (A-2) by itself.

We justify the assumption that $|\vec{r}'| \gg |\vec{\rho_i}'|$ in terms of one of the results of Sec. 4.2, which states that the spatial correlation distance of the field over the ground is on the order of λ_o. When the field is being observed with a directive antenna of beamwidth B, the spatial correlation distance is roughly $\lambda_o B^{-1}$. In either case, it is not meaningful to describe the field at one point in terms of the field at another point, unless the fields at the two points are correlated. That is, $|\vec{r}'|$ should be less than the correlation distance, which, in turn, is much less than $|\vec{\rho_i}'|$ in any reasonable situation. Even when the plane of observation is within or at the lower boundary of the cloud, most of the particles contributing to the field at a point are far away from it, compared with the spatial correlation distance.

Another familiar assumption we shall make is that there is an uncertainty of many times the carrier period f_o^{-1} in our knowledge of the path delay τ_{ki}. We shall therefore take the path phase Θ_{ki} to be a random variable which is uniformly distributed between $-\pi$ and π. Moreover, it is reasonable to assume that similar uncertainties exist in our knowledge of the differences in delay between scattering paths; hence, we shall take each path phase Θ_{ki} to be statistically independent of all the others.

As we indicated earlier, the path attenuation η_{ki} can vary considerably with small changes in such details of the path as individual scattering angles. An additional element of uncertainty in η_{ki} results from the fact that the scattering pattern of any particle in the path depends upon the particle radius a, which we can regard as a random variable obeying a particle size distribution p(a). It is therefore reasonable to regard η_{ki} as a random variable. We have no reason to assume that η_{ki} is statistically dependent upon any other path attenuations, except possibly those of paths which are nearly identical to the kth. But suppose the mth path were everywhere identical with the kth except for one segment, where each of them contained one particle that was not in the other path. Even in this extreme case, that one different scattering angle could cause η_{ki} to differ from η_{mi} by orders of magnitude. But suppose one suspected that there was actually enough statistical coupling between the amplitudes (and perhaps the phases) on the kth path and those "nearly identical" to it to cause problems. In that case one could visualize dividing the M_i signals into M_i' groups, each containing a set of signals nearly identical to each other, and lumping the members of each group together into a single term, with a common delay, Doppler shift and phase. The only effect on Eq. (A-2) would be to reduce M_i to M_i', which is still an enormous number.

Thus we shall assume that the amplitude factors η_{ki} are statistically independent random variables, each described by a probability density function $p_{ki}(\ )$. Because of the spatial variation $E(\vec{\rho})$ of the incident signal, the density functions $p_{ki}(\ )$ will depend upon the locations of the paths and of the ith particle, in general, but knowledge of the density functions will not be necessary in our argument that the received process is Gaussian. In fact, the η_{ki} can even be nonrandom, so long as they are very numerous and very small.

The total received field $y(t, \vec{r}, \vec{r}')$ at points $\vec{r}'$ relative to $\vec{r}$ is simply the sum of contributions similar to Eq. (A-2) from every particle in the cloud. Thus

$$y(t, \vec{r}, \vec{r}') = \sum_{i=1}^{N_p} y_i(t, \vec{r}, \vec{r}')$$

$$= \mathrm{Re}\left\{ \sum_{i=1}^{N_p} \sum_{k=1}^{M_i} \eta_{ki} \, s(t - \tau_{ki}) \exp\left[-j2\pi t(f_o - f_{ki}) - j\Theta_{ki} - j\frac{2\pi}{\lambda_o} \frac{\vec{r}' \cdot \vec{\rho}_i'}{|\vec{\rho}_i'|} \right] \right\} \quad . \text{(A-3)}$$

The total received field $y(t, \vec{r}, \vec{r}')$ should include a specular component, the unscattered residue of the transmitted signal which penetrates the cloud to the ground. We shall simplify our problem somewhat by assuming that this component is so attenuated by the cloud that it is negligible compared with the scattered radiation.

By arguments similar to those used above, we immediately establish statistical independence between Θ_{ki} and Θ_{mn} for every value of m and n except $m = k$ and $n = i$. Similarly, η_{ki} is statistically independent of η_{mn}. Let us re-index all the terms in Eq. (A-3), replacing all the double subscripts ki by a single subscript n, which ranges from unity to

$$M = \sum_{i=1}^{N_p} M_i \quad . \tag{A-4}$$

The last term in the exponent in Eq. (A-3), which depends upon i, can be made to fit into this new formulation by defining new vectors

$$\vec{R}_n' \triangleq \begin{cases} \vec{\rho}_1' & , \quad n = 1, 2, \ldots, M_1 \\ \vec{\rho}_2' & , \quad n = M_1 + 1, M_1 + 2, \ldots M_1 + M_2 \\ \cdot & \quad \cdot \\ \cdot & \quad \cdot \\ \cdot & \quad \cdot \end{cases}$$

$$\text{(A-5)}$$

Equation (A-3) can then be rewritten as

$$y(t, \vec{r}, \vec{r}') = \mathrm{Re}\left\{ \sum_{n=1}^{M} \eta_n \, s(t - \tau_n) \cdot \exp\left[-j2\pi t(f_o - f_n) - j\Theta_n - j\frac{2\pi}{\lambda_o} \frac{\vec{r}' \cdot \vec{R}_n'}{|\vec{R}_n'|} \right] \right\} \quad . \text{(A-6)}$$

We have now put $y(t, \vec{r}, \vec{r}')$ into precisely the form obtained by Kennedy[36] for a signal transmitted through a single-scattering medium. The crucial assumptions are the same; that is, the number of components is very large, the amplitude factors η_n are small, and the phases Θ_n are statistically independent and uniformly distributed over $(-\pi, \pi)$. Under these conditions, we argue exactly as Kennedy did that the complex envelope of $y(t, \vec{r}, \vec{r}')$ is a complex Gaussian random process. The real and imaginary parts of the envelope are uncorrelated Gaussian random variables, having equal correlation functions and zero means. Knowledge of the correlation function is equivalent to knowledge of a complete statistical description of $y(t, \vec{r}, \vec{r}')$. These issues are discussed in Chapter 4.

APPENDIX B
ORTHOGONAL ANGULAR COORDINATES α AND β

Much of the analysis in this report uses orthogonal angular coordinates α and β to represent the positions of points in space. In this appendix we define the transformation to α and β from the spherical coordinates Θ and φ, and discuss the transformation of functions of Θ and φ into functions of α and β.

The most important advantage of the new coordinate system is that the orthogonality of α and β permits major simplifications in the calculation of convolutions of functions defined on the unit sphere. Another convenient feature is the ability to express the angular separation between two points in space in the (approximate) Cartesian form given by Eq. (B-3) below. The equivalent of Eq. (B-3) in spherical coordinates is a cumbersome expression obtained by solving a spherical triangle. Finally, the transformation maps the upper hemisphere into a finite region in a plane. As in the original problem, it is possible for a light ray to be scattered out to $\pi/2$ radians by means of a finite number of finite steps. This would not be the case under any transformation which mapped the upper hemisphere into the infinite plane.

The relationship of α and β with the zenith angle Θ and the azimuthal angle φ is closely analogous to the relationship of the Cartesian coordinates x and y with the polar coordinates r and φ in two dimensions. As illustrated in Fig. B-1, the transformation is accomplished by mapping the unit-radius sphere

Fig. B-1. Mapping of unit sphere onto (α, β) plane.

onto a plane tangent to the sphere at $\Theta = 0$. (The plane in the figure is drawn above the sphere for the sake of clarity.) The mapping is performed in such a way that azimuthal angles φ and polar arc lengths Θ are preserved. Thus the length of the radial line OP in the plane is equal to that of the arc OP on the unit sphere, which is Θ units long. The coordinates of the point P in the plane, measured along the orthogonal α and β axes, are

$$\alpha = \Theta \cos \varphi \text{ radians} \quad ,$$

$$\beta = \Theta \sin \varphi \text{ radians} \quad . \tag{B-1}$$

These equations define the transformation of coordinates. Although we can visualize mapping every point of the sphere onto the plane in this manner, we shall restrict our attention to the region $\Theta \leqslant \pi/2$. The corresponding region in the $\alpha - \beta$ plane is bounded by the circle

$$\alpha^2 + \beta^2 = (\pi/2)^2 \quad . \tag{B-2}$$

Although the transformation preserves distance along lines of constant φ, we observe that distance along circles of constant Θ is not preserved. The circle $\Theta = \Theta_0$ on the sphere has circumference $2\pi \sin \Theta_0$, while the corresponding circle in the $\alpha - \beta$ plane has circumference $2\pi \Theta_0$. In general, the distance between two arbitrary points in the plane differs from the great-circle
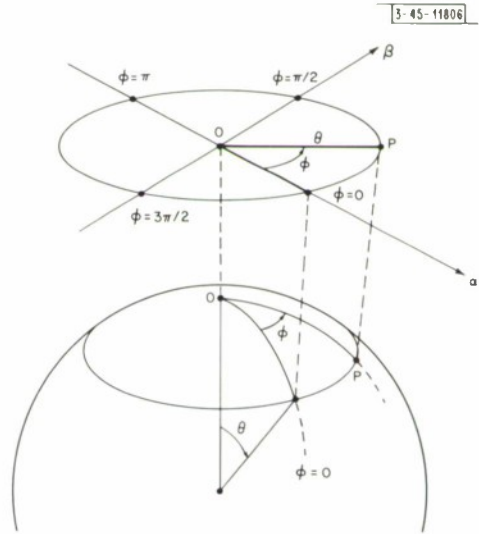
distance between the two corresponding points on the sphere. Let two points P_1 and P_2 be located at (α_1, β_1) and (α_2, β_2) on the $\alpha - \beta$ plane, while the corresponding points on the sphere are located at (Θ_1, φ_1) and (Θ_2, φ_2). The distance between the two points on the plane has the convenient Cartesian form

$$D_{12} = \sqrt{(\alpha_2 - \alpha_1)^2 + (\beta_2 - \beta_1)^2} \quad . \tag{B-3}$$

It is clear that D_{12} differs from the great-circle distance between the two points on the sphere by a factor which is upper-bounded by roughly $\Theta_m/\sin\Theta_m$, where

$$\Theta_m = \max[\Theta_1, \Theta_2] \quad . \tag{B-4}$$

We recall that Θ_m and $\sin\Theta_m$ are equal within 10 percent for

$$\Theta_m \leqslant 0.75 \text{ radian} \cong 43° \quad , \tag{B-5}$$

while the error does not exceed 20 percent for

$$\Theta_m \leqslant 1.03 \text{ radians} \cong 59° \quad . \tag{B-6}$$

Now, the great-circle arc length between P_1 and P_2 on the unit sphere is equal to their angular separation γ_{12} relative to the center of the sphere. Thus

$$D_{12} \cong \gamma_{12} \tag{B-7}$$

within 10 percent subject to condition (B-5), or within 20 percent under the condition (B-6).

The transformation of a function of Θ and φ defined over the surface of the unit sphere into a function of α and β is a straightforward matter. As a specific example, consider the normalized single-particle scattering pattern $f(\Theta)$ discussed in Chapter 3. This function is defined in such a way that $f(\Theta)\,d\omega$ is proportional to the intensity of the radiation scattered by the particle into the incremental solid angle (or area element)

$$d\omega = \sin\Theta\,d\Theta\,d\varphi \tag{B-8}$$

at coordinates (Θ, φ). The polar angle Θ is measured relative to the propagation vector of the plane wave incident on the particle. We wish to transform $f(\Theta)$ into a function $f_1(\alpha, \beta)$ subject to the condition that

$$\iint f(\Theta)\,\sin\Theta\,d\Theta\,d\varphi = \iint f_1(\alpha, \beta)\,d\alpha\,d\beta \quad , \tag{B-9}$$

where the domain of integration is the region $\Theta \leqslant \pi/2$. The transformation is a simple case of a general treatment summarized by Wozencraft and Jacobs,[44] in the context of reversible transformation of random vectors. The result is

$$f_1(\alpha, \beta) = J(\alpha, \beta)\,f[\Theta(\alpha, \beta)] \quad , \tag{B-10}$$

in which

$$J(\alpha, \beta) = \frac{\sin[\Theta(\alpha, \beta)]}{\Theta(\alpha, \beta)} \tag{B-11}$$

is the Jacobian of the transformation, often called the metric coefficient. The function $\Theta(\alpha, \beta)$ is the first member of the transformation which is the inverse of Eq. (B-1),

$$\Theta = (\alpha^2 + \beta^2)^{1/2} \quad ,$$

$$\varphi = \tan^{-1} \frac{\beta}{\alpha} \quad . \tag{B-12}$$

For the most part we shall ignore the metric coefficient [Eq. (B-11)], since we deal with functions which are concentrated in the region of small Θ, where Eq. (B-11) is nearly unity. Even when we perform a multiple convolution of a function like Eq. (B-10) with itself, we shall ignore Eq. (B-11) if the result of the convolution tails off to small values by the time $\sin\Theta/\Theta$ differs appreciably from unity. Somewhat more care is required, however, when we compute higher moments of a function such as Eq. (B-11). Suppose, for example, we want the variance $\overline{\alpha^2}$ of the function $f_1(\alpha, \beta)$, and that $f_1(\ )$ is quite large near $\Theta = 0$ but has tails which extend all the way out to $\Theta = \pi/2$. Regarding u and v as polar coordinates in the (α, β) plane, we have

$$\overline{\alpha^2} = \iint\limits_{\Theta \leqslant \pi/2} d\alpha \, d\beta \, \alpha^2 f_1(\alpha, \beta)$$

$$= \int_0^{2\pi} dv \int_0^{\pi/2} u \, du \, u^2 \cos^2 v \, \frac{\sin u}{u} \, f(u)$$

$$= \pi \int_0^{\pi/2} du \, u^2 \sin u \, f(u) \quad . \tag{B-13}$$

Because of the factor $u^2 \sin u$, the integrand in Eq. (B-13) might be small near the origin and fairly large as u approaches $\pi/2$. If we had not retained the metric coefficient $(\sin u)/u$, the factor $u^2 \sin u$ would have been replaced by u^3, and a substantial error in $\overline{\alpha^2}$ might have resulted.

All the analysis in this report is carried out in the (α, β) domain. When we arrive at a final answer, however, it will often be desirable to transform it back into spherical coordinates. The transformation of a function $I(\alpha, \beta)$ into a function $I_1(\Theta, \varphi)$ is simply the inverse of Eq. (B-10),

$$I_1(\Theta, \varphi) = \frac{\Theta}{\sin \Theta} \, I[\alpha(\Theta, \varphi), \, \beta(\Theta, \varphi)] \quad . \tag{B-14}$$

The arguments of $I[\ ]$ are given by the transformation (B-1).

APPENDIX C
TWO-DIMENSIONAL NUMERICAL SIMULATION

In the earlier stages of the research reported in this document, spatial impulse responses were derived for a two-dimensional model[45] of the idealized cloud presented in Chapter 3. The analog of the N-layer angular impulse response [Eq. (3-56)] in two dimensions was found to be

$$h_N(\alpha_N, \alpha_o) = \int\int_{-\pi/2}^{\pi/2} \cdots \int d\alpha_{N-1} \cdots d\alpha_1 \cdot h_1(\alpha_N, \alpha_{N-1}) \cdots h_1(\alpha_1, \alpha_o) \quad . \tag{C-1}$$

The single-layer impulse response was

$$h_1(\alpha, \alpha_o) = (1 - \rho a \,\widehat{\sec}\, \alpha) \, u_o(\alpha - \alpha_o) + \rho a \,\widehat{\sec}\, \alpha f(\alpha - \alpha_o) \quad , \tag{C-2}$$

in which

$$\widehat{\sec}\, \alpha \triangleq \begin{cases} \sec \alpha & , \quad \text{if } |\alpha| < \sec^{-1} \dfrac{1}{\rho a} \quad ; \\[2mm] \dfrac{1}{\rho a} & , \quad \text{otherwise} \quad . \end{cases} \tag{C-3}$$

Equation (C-2) was derived under the assumptions that all radiation incident on a particle was scattered forward, and that the two-dimensional particle cross section was equal to its diameter a. The function f( ) is the single-particle forward-scattering pattern. Observe that Eq. (C-2) would be practically identical to the three-dimensional single-layer impulse response [Eq. (3-54)] if the dependence upon β were deleted.

The application of the Central Limit Theorem to Eq. (C-1) was prevented, as was the case in Sec. 3.4, by the presence of the finite limits $\pm\pi/2$ and the terms $\widehat{\sec}\, \alpha$. Changing the limits to $\pm\infty$ and replacing $\widehat{\sec}\, \alpha$ by unity in Eq. (C-1) led to the result

$$h_N(\alpha_N, \alpha_o) = \frac{1}{\sigma_\alpha \sqrt{2\pi}} \exp\left[-\frac{(\alpha_N - \alpha_o)^2}{2\sigma_\alpha^2}\right] \tag{C-4}$$

in the limit as N goes to infinity, with

$$\sigma_\alpha^2 = N_c W_\alpha^2 \quad . \tag{C-5}$$

N_e is the optical thickness of the cloud and W_α^2 is the variance of f( ). Notice that this is nearly identical to the α-dependent factors in the solution (3-72) of Eq. (3-56).

Zaborowski[30] carried out numerical solutions of Eq. (C-1) and another equation to be described below, in order to test the validity of the approximations leading to Eq. (C-4). He programmed Eq. (C-1) just as it stands, retaining the integration limits $\pm\pi/2$ and retaining the terms $\widehat{\sec}\, \alpha$ in the kernels. Although the number $(N - 1)$ of integrations should ideally have been made very large, he found after extensive testing that the choice

$$N = 2\, N_e \tag{C-6}$$

led to results virtually indistinguishable from the results obtained by using much larger values of N. It is unfortunate that it was not yet clear that W_α^2 should be the variance of the rigorously correct Mie scattering pattern of the particles. Instead, the fact that the half-power beamwidth

of the scattering pattern goes roughly as λ/a, where a is the particle diameter, was used as justification for modeling the scattering pattern as

$$f(\alpha) \triangleq \begin{cases} \dfrac{1}{2\Theta_o} & , \quad |\alpha| \leqslant \Theta_o \quad ; \\ \\ 0 & , \quad \text{elsewhere} \quad . \end{cases} \tag{C-7}$$

The parameter Θ_o was so chosen that the standard deviation

$$W_\alpha = \left[\int \alpha^2 f(\alpha)\, d\alpha \right]^{1/2} = \frac{\Theta_o}{\sqrt{3}} \tag{C-8}$$

was equal to λ/a. Selecting $\lambda = 0.5$ micron and $a = 10$ microns as representative values led to the choice for Θ_o of 5 degrees. This figure was used in all of Zaborowski's work. The corresponding value of W_α was about 2.9 degrees, smaller by a factor of six than the correct value, which we show in Appendix G to be about 16.9 degrees, independent of particle size.

Nevertheless, his numerical solutions of Eq. (C-1) for large optical thicknesses give a rough indication of the behavior of the results that would be obtained at smaller optical thicknesses if the correct value of W_α were used. The largest value of N_e that he considered was 50. The result of this computation (for which the incident angle α_o was set equal to zero) is visually indistinguishable from a Gaussian curve, but its width is slightly greater than the predicted value. For $\Theta_o = 5$ degrees and $N_c = 50$, Eq. (C-5) predicts a standard deviation

$$\sigma_\alpha = 20.5 \text{ degrees} \quad . \tag{C-9}$$

The author has calculated the values of a Gaussian function with parameter (C-9) and compared it with Zaborowski's curve for $N_e = 50$ at various values of the argument. At $\alpha = \sigma_\alpha$ the simulated curve is larger by 3 percent than the true Gaussian. At $\alpha = 4.35$, $\sigma_\alpha \cong 89$ degrees, well out in the tail, the simulated curve is high by only a factor of ten; and it is down to 10^{-3} of its value at the origin.

The other equation which was solved numerically is the two-dimensional analog of the joint impulse response [Eq. (3-88)], having the form

$$h_p(\alpha_N, x_N; \ \alpha_o, x_o) = \int\limits_{-\pi/2}^{\pi/2}\!\!\int \cdots \int d\alpha_{N-1} \cdots d\alpha_1 \cdot \int\limits_{-\infty}^{\infty}\!\!\int \cdots \int dx_{N-1} \cdots dx_1$$

$$\cdot\ h_1(\alpha_N, x_N; \ \alpha_{N-1}, x_{N-1}) \cdots h_1(\alpha_1, x_1; \ \alpha_o, x_o) \quad . \tag{C-10}$$

The single-layer joint impulse response is

$$h_1(\alpha, x; \ \alpha_o, x_o) = [(1 - \rho a \ \widehat{\sec} \ \alpha)\, u_o(\alpha - \alpha_o)$$

$$+ \rho a \ \widehat{\sec} \ \alpha f(\alpha - \alpha_o)]\, u_o(x - x_o + \ell_o \tan \alpha) \quad . \tag{C-11}$$

Notice that Eq. (C-10) would be practically identical to the three-dimensional equation (3-88) if all functions of β and y were deleted. An approximate analytical solution for Eq. (C-10), obtained by a method analogous to that of Appendix D, looked like the α- and x-dependent factors of the solution (3-89) for Eq. (3-88). Zaborowski programmed a numerical solution for Eq. (C-10), again retaining the limits $\pm\pi/2$ on the α-variables and retaining the terms $\widehat{\sec} \ \alpha$ in the kernels.

He solved the equation in an efficient manner,[30] using a hybrid combination of Fourier transformation and convolution. Because the result is a function of two variables, comparing it with the theoretical curve is not quite so simple as in the preceding case. As he explains in detail, Zaborowski devised a way to calculate the standard deviations σ_α and σ_x and the correlation coefficient $\rho_{\alpha x}$ of each of his outputs. For $N_e = 50$, these quantities agreed with the theoretically predicted values within 1.4, 1.15, and 0.4 percent, respectively.

These results constitute a fairly strong argument that the approximations made in solving the multiple integral equations of Chapter 3 are valid. Since the value of W_α used in the numerical work was too small by a factor of six, the results that were obtained apply only for small optical thicknesses. Because the agreement between computed and theoretical results was so close, however, one imagines that the approximations are adequate for considerably greater optical thicknesses.

APPENDIX D
SOLUTION OF EQUATION (3-88)

An approximate solution has been obtained for Eq. (3-88), the N-layer four-dimensional impulse response $h_N(\alpha_N, \beta_N, x_N, y_N; \alpha_O, \beta_O, x_O, y_O)$. The keys to the solution are a series expansion and a limiting process which are carried out in the Fourier transform domain.

We begin by making the same two initial approximations that were used in Sec. 3.4 in solving the angular impulse response equation (3-56). Specifically, we increase the limits to $\pm\infty$ on the α and β integrals, and we assume that

$$\widehat{\sec} \Theta_i \cong 1 \quad , \quad \text{all } i \quad ,$$

over the angular ranges of interest. We then recast the single-layer impulse response in the form

$$h_1(\alpha_i, \beta_i, x_i, y_i; \alpha_{i-1}, \beta_{i-1}, x_{i-1}, y_{i-1}) \cong g(\alpha_i - \alpha_{i-1}, \beta_i - \beta_{i-1})$$

$$\cdot u_O(x_i - x_{i-1} + \ell_O\alpha_i) u_O(y_i - y_{i-1} + \ell_O\beta_i) \quad , \tag{D-1}$$

in which

$$g(\alpha_i - \alpha_{i-1}, \beta_i - \beta_{i-1}) \triangleq (1 - \rho\overline{C_{ext}}) u_O(\alpha_i - \alpha_{i-1}) u_O(\beta_i - \beta_{i-1})$$

$$+ \rho\overline{C_f} f_1(\alpha_i - \alpha_{i-1}, \beta_i - \beta_{i-1}) \quad . \tag{D-2}$$

Let us replace the two impulse functions in Eq. (D-1) by the inverses of their Fourier transforms. We then have

$$h_1( ) \cong g(\alpha_i - \alpha_{i-1}, \beta_i - \beta_{i-1})$$

$$\cdot \int_{-\infty}^{\infty} dX_i \, \exp\left[j2\pi X_i(x_i - x_{i-1} + \ell_O\alpha_i)\right]$$

$$\cdot \int_{-\infty}^{\infty} dY_i \, \exp\left[j2\pi Y_i(y_i - y_{i-1} + \ell_O\beta_i)\right] \quad . \tag{D-3}$$

Our next step is to make the substitution (D-3) everywhere in the superposition integral (3-88), and to carry out a sequence of operations exactly as one conventionally does in the solution of convolution integrals by Fourier transforms. Thus we rearrange orders of integration and carry out the integrals on all x_i and y_i to obtain a product of impulses in the "frequency" variables X and Y. A typical example of these integrals is

$$\int_{-\infty}^{\infty} dx_i \, \exp\left[j2\pi x_i(X_i - X_{i+1})\right] = u_O(X_i - X_{i+1}) \quad . \tag{D-4}$$

The superposition integral (3-88) now has the form

$$h_N(\ ) = \int\!\!\int_{-\infty}^{\infty}\ldots\int d\alpha_{N-1}\ldots d\alpha_1 \int\!\!\int_{-\infty}^{\infty}\ldots\int d\beta_{N-1}\ldots d\beta_1$$

$$\cdot\ g(\alpha_N - \alpha_{n-1},\ \beta_N - \beta_{N-1})\ \cdots\ g(\alpha_1 - \alpha_0,\ \beta_1 - \beta_0)$$

$$\cdot\ \int\!\!\int_{-\infty}^{\infty}\ldots\int dX_N\ldots dX_1 \int\!\!\int_{-\infty}^{\infty}\ldots\int dY_N\ldots dY_1$$

$$\cdot\ \exp[j2\pi(X_N x_N - X_1 x_0 + Y_N y_N - Y_1 y_0)]$$

$$\cdot\ \exp[j2\pi\ell_0(X_N\alpha_N + \ldots + X_1\alpha_1 + Y_N\beta_N + \ldots + Y_1\beta_1)]$$

$$\cdot\ u_0(X_{N-1} - X_N)\ \cdots\ u_0(X_1 - X_2)\,u_0(Y_{N-1} - Y_N)\ \cdots\ u_0(Y_1 - Y_2)$$

$$=\int\!\!\int_{-\infty}^{\infty}\ldots\int d\alpha_{N-1}\ldots d\alpha_1 \int\!\!\int_{-\infty}^{\infty}\ldots\int d\beta_{N-1}\ldots d\beta_1$$

$$\cdot\ g(\alpha_N - \alpha_{n-1},\ \beta_N - \beta_{N-1})\ \cdots\ g(\alpha_1 - \alpha_0,\ \beta_1 - \beta_0)$$

$$\cdot\ \int_{-\infty}^{\infty}dX_N\int_{-\infty}^{\infty}dY_N\ \exp[j2\pi X_N(x_N - x_0) + j2\pi Y_N(y_N - y_0)]$$

$$\cdot\ \exp[j2\pi\ell_0 X_N(\alpha_N + \ldots + \alpha_1) + j2\pi\ell_0 Y_N(\beta_N + \ldots + \beta_1)] \qquad . \tag{D-5}$$

Let us now replace each g( ) in Eq. (D-5) by the inverse Fourier transform

$$g(\alpha_i - \alpha_{i-1},\ \beta_i - \beta_{i-1}) = \int_{-\infty}^{\infty}dA_i\int_{-\infty}^{\infty}dB_i$$

$$\cdot\ \exp[j2\pi A_i(\alpha_i - \alpha_{i-1}) + j2\pi B_i(\beta_i - \beta_{i-1})]\,G(A_i,\,B_i) \qquad , \tag{D-6}$$

in which

$$G(A,\,B) = \int_{-\infty}^{\infty}d\alpha\int_{-\infty}^{\infty}d\beta\ \exp[j2\pi(\alpha A + \beta B)]\,g(\alpha,\beta) \qquad . \tag{D-7}$$

Rearranging orders of integration and carrying out all the α and β integrations, we obtain another product of impulses. A typical integral is

$$\int_{-\infty}^{\infty}d\alpha_i\ \exp[j2\pi\alpha_i(X_N\ell_0 + A_i - A_{i+1})] = u_0(X_N\ell_0 + A_i - A_{i+1}) \qquad . \tag{D-8}$$

Next, carrying out all the A and B integrations except those on A_N and B_N, we arrive at the equation

$$h_N(\ ) = \int_{-\infty}^{\infty} dX_N \int_{-\infty}^{\infty} dY_N \exp\left[j2\pi X_N(x_N - x_o + \ell_o \alpha_N + (N-1)\ell_o \alpha_o)\right]$$

$$\cdot \exp\left[j2\pi Y_N(y_N - y_o + \ell_o \beta_N + (N-1)\ell_o \beta_o)\right]$$

$$\cdot \int_{-\infty}^{\infty} dA_N \int_{-\infty}^{\infty} dB_N \exp\left[j2\pi A_N(\alpha_N - \alpha_o) + j2\pi B_N(\beta_N - \beta_o)\right]$$

$$\cdot \prod_{k=0}^{N-1} G(A_N - kX_N \ell_o,\ B_N - kY_N \ell_o) \quad . \tag{D-9}$$

The product on G( ) can be rewritten as

$$\exp\left[\sum_{k=0}^{N-1} \ln G(A_N - kX_N \ell_o,\ B_N - kY_N \ell_o)\right] \quad . \tag{D-10}$$

Recalling the definition in Eq. (D-2) of $g(\alpha, \beta)$, we see that

$$\ln G(A, B) = \ln\left[1 - \rho \overline{C_{ext}} + \rho \overline{C_f} F_1(A, B)\right] \quad , \tag{D-11}$$

in which $F_1(A, B)$ is the Fourier transform of the single-particle forward-scattering pattern $f_1(\alpha, \beta)$. Since $F_1(\ )$ may be interpreted as the conjugate of the characteristic function of a probability density $f_1(\ )$, we know that the magnitude of $F_1(\ )$ is upper-bounded by unity. Thus Eq. (D-11) becomes

$$\ln G(A, B) \cong -\rho \overline{C_{ext}} + \rho \overline{C_f} F_1(A, B)$$

$$= -\ell_o d_v \overline{C_{ext}} + \ell_o d_v \overline{C_f} F_1(A, B) \tag{D-12}$$

in the limit as ℓ_o becomes very small. Let us now replace $F_1(A, B)$ by the leading terms of its Taylor's series expansion,

$$F_1(A, B) \cong 1 - \frac{(2\pi W_\alpha)^2}{2} A^2 - \frac{(2\pi W_\beta)^2}{2} B^2 \quad , \tag{D-13}$$

where W_α and W_β are the single-particle scattering beamwidth parameters defined by Eq. (3-42) in Sec. 3.4. Equation (D-13) is actually valid to third order, since the coefficients of the third-order terms of the series turn out to be zero. For the time being, we shall assume that the series representation (D-13) is sufficiently accurate; later we shall justify the assumption. Incorporating Eqs. (D-12) and (D-13) into (D-10), we have

$$\prod_{k=0}^{N-1} G(\ ) = \exp\left[-N\ell_o d_v(\overline{C_{ext}} - \overline{C_f})\right]$$

$$\cdot \exp\left\{-\ell_o d_v \overline{C_f} \sum_{k=0}^{N-1} \left[\frac{(2\pi W_\alpha)^2}{2}(A_N - kX_N \ell_o)^2 + \frac{(2\pi W_\beta)^2}{2}(B_N - kY_N \ell_o)^2\right]\right\} \tag{D-14}$$

89

The first exponent in Eq. (D-14) is

$$-N\ell_o d_v (\overline{C_{ext}} - \overline{C_f}) = -N_e(1 - \gamma_f) \quad , \tag{D-15}$$

where N_e is the optical thickness of the cloud and γ_f is the single-particle forward-scattering efficiency. In the limit as ℓ_o goes to zero, the second exponent in Eq. (D-14) becomes an integral. Letting

$$k\ell_o \to u \quad ,$$

$$\ell_o \to du \quad ,$$

the exponent becomes

$$-d_v \overline{C}_f \int_o^\tau du \left[\frac{(2\pi W_\alpha)^2}{2} (A_N - X_N u)^2 + \frac{(2\pi W_\beta)^2}{2} (B_N - Y_N u)^2 \right]$$

$$= -\frac{\gamma_f N_e W_\alpha^2}{2} \left[(2\pi A_N)^2 - \tau(2\pi A_N)(2\pi X_N) + \frac{\tau^2 (2\pi X_N)^2}{3} \right]$$

$$-\frac{\gamma_f N_e W_\beta^2}{2} \left[(2\pi B_N)^2 - \tau(2\pi B_N)(2\pi Y_N) + \frac{\tau^2 (2\pi Y_N)^2}{3} \right] \quad . \tag{D-16}$$

Substituting Eqs. (D-16) and (D-15) into Eq. (D-14), and inserting (D-14) into Eq. (D-9), we find that $h_N(\ )$ is precisely the inverse of the Fourier transform of a four-dimensional jointly Gaussian function, multiplied by the factor $\exp[-N_e(1 - \gamma_f)]$. This joint Gaussian is considerably simpler than the general four-dimensional case, in that four of the six possible covariances are zero. Declining to write out all the algebra, we proceed directly to the answer. We have

$$h_N(\alpha_N, \beta_N, x_N, y_N; \ \alpha_o, \beta_o, x_o, y_o)$$

$$= \exp[-N_e(1 - \gamma_f)] \left[4\pi^2 \sigma_\alpha \sigma_\beta \sigma_x \sigma_y \sqrt{(1 - \rho_{\alpha x}^2)(1 - \rho_{\beta y}^2)} \right]^{-1}$$

$$\cdot \exp\left[\frac{-1}{2(1 - \rho_{\alpha x}^2)} \left(\frac{(\alpha_N - \alpha_o)^2}{\sigma_\alpha^2} - 2\rho_{\alpha x} \frac{(\alpha_N - \alpha_o)(x_N - x_o + \tau\alpha_o)}{\sigma_\alpha \sigma_x} \right.\right.$$

$$\left.\left. + \frac{(x_N - x_o + \tau\alpha_o)^2}{\sigma_x^2} \right) \right]$$

$$\cdot \exp\left[\frac{-1}{2(1 - \rho_{\beta y}^2)} \left(\frac{(\beta_N - \beta_o)^2}{\sigma_\beta^2} - 2\rho_{\beta y} \frac{(\beta_N - \beta_o)(y_N - y_o + \tau\beta_o)}{\sigma_\beta \sigma_y} \right.\right.$$

$$\left.\left. + \frac{(y_N - y_o + \tau\beta_o)^2}{\sigma_y^2} \right) \right] \quad , \tag{D-17}$$

in which

$$\sigma_\alpha^2 = \gamma_f N_e W_\alpha^2 \quad ,$$

$$\sigma_\beta^2 = \gamma_f N_e W_\beta^2 \quad ,$$

$$\sigma_x^2 = \frac{\tau^2}{3} \gamma_f N_e W_\alpha^2 \quad ,$$

$$\sigma_y^2 = \frac{\tau^2}{3} \gamma_f N_e W_\beta^2 \quad ,$$

$$\rho_{\alpha x} = \rho_{\beta y} = -\frac{\sqrt{3}}{2} \quad . \tag{D-18}$$

Observe that Eq. (D-17) incorporates the fact that the terms $\ell_o \alpha_N$ and $\ell_o \beta_N$ (D-9) go to zero with ℓ_o, while the terms $(N-1)\ell_o \alpha_o$ and $(N-1)\ell_o \beta_o$ become $\tau \alpha_o$ and $\tau \beta_o$ respectively.

As we stated in Sec. 3.5, the joint impulse response $h_P(\ )$ of the cloud is equal to the N-layer response $h_N(\ )$ in the limit as ℓ_o goes to zero. But we have already incorporated this limit in the derivation of Eq. (D-17); hence $h_P(\alpha, \beta, x, y; \alpha_o, \beta_o, x_o, y_o)$ is obtained from Eq. (D-17) by simply deleting the subscript N wherever it appears.

The relative simplicity of the result [Eq. (D-17)] was made possible by the assumption [Eq. (D-13)] that a third-order Taylor's series was an adequate approximation for the transform $F_1(A, B)$ of the single-particle scattering pattern. There are two indications that this assumption is consistent with the other approximations we have utilized. The first is a numerical solution of the two-dimensional analog of Eq. (3-88) for a joint distribution in α and x, which is discussed in detail in Appendix C. Over the region of interest, the numerical results agreed very well with an approximate analytic solution for the same equation, which was obtained by the same technique that we used here. The second indication is related to the joint distribution over the ground when the top of the cloud is illuminated by a beam of finite cross-sectional area, which is calculated by means of a convolution operation on Eq. (D-17). When the cross section of the incident beam becomes very large, the joint distribution over the ground reduces to precisely the angular intensity distribution [Eq. (3-72)] that is present below the cloud when the incident illumination is a uniform plane wave. The details of this issue are discussed in Sec. 3-5.

APPENDIX E
RANGE SCATTERING FUNCTION $\sigma_0(t)$

We shall calculate the range scattering function $\sigma(t, \alpha, \beta; \alpha_0, \beta_0)$ defined in Chapter 4, for the special case in which the illumination on the top of the cloud is a uniform plane wave, and α, β, α_0 and β_0 are all equal to zero. In addition, we outline procedures for obtaining $\sigma(\ )$ in more general cases (e.g., when the illumination is an obliquely incident plane wave or a narrow beam).

Equation (4-64) implies that

$$\sigma(t, \alpha, \beta; \alpha_0, \beta_0) \, dt = (E_r \Delta\omega)^{-1} \, p_a(t, \alpha, \beta; \alpha_0, \beta_0) \, dt$$

$$= (E_r \Delta\omega)^{-1} \sum_i w_i \quad , \tag{E-1}$$

where $p_a(\ )$ is the average value of the instantaneous power measured by a unit-area antenna of beam solid angle $\Delta\omega$ aimed in the direction (α, β). The quantities w_i are ray intensity weights, and i ranges over all rays such that

$$t \leqslant \left(T_{io} + \frac{\ell_i}{c} \right) \leqslant t + dt \quad . \tag{E-2}$$

The quantity ℓ_i is the length in meters of the path of the ith ray, and T_{io} is a geometry-dependent adjustment to the time origin for the signal borne by the ray. When $\alpha_0 = \beta_0 = 0$, the plane wave illumination is vertically incident on the top of the cloud, and the quantities T_{io} in (E-2) reduce to zero for all rays.

We shall calculate the sum $\Sigma \, w_i$ in Eq. (E-1) by subdividing the rays in $\Delta\omega$ by scattering order, computing the total intensity weight of all rays of each order which satisfy (E-2), and summing them over all scattering orders. Our first step is to calculate the terms in the time-independent sum

$$I_\Delta(\alpha, \beta; \, 0, 0) = \sum_{k=1}^{\infty} I_{k\Delta}(\alpha, \beta) \tag{E-3}$$

for a vertically-incident unit-intensity CW plane wave, with $I_{k\Delta}(\ )$ defined as the total intensity borne by all rays in $\Delta\omega$ which were scattered exactly k times. To this end, let us re-examine the $(N-1)$-fold integral equation (3-56) for the N-layer angular impulse response $h_N(\alpha_N, \beta_N; \alpha_0, \beta_0)$. Each of the N factors in the integrand is a single-layer impulse response, for which we use the approximate form (3-62),

$$h_1(\alpha_i - \alpha_{i-1}, \beta_i - \beta_{i-1}) \cong (1 - \rho\overline{C_{ext}}) \, u_0(\alpha_i - \alpha_{i-1}) \, u_0(\beta_i - \beta_{i-1})$$

$$+ \rho\overline{C_f} \, f_1(\alpha_i - \alpha_{i-1}, \beta_i - \beta_{i-1}) \quad .$$

The double-impulse term in $h_1(\ )$ corresponds to passing through the ith layer without scattering. The second term, involving the single-particle forward-scattering pattern $f_1(\ )$, corresponds to the occurrence of scattering at the ith layer. Let us multiply out all the N binomial terms $h_1(\ )$ in the integrand of Eq. (3-56). The result is a sum of 2^N $(N-1)$-fold double integrals, each having an integrand composed of the product of N monomial factors. Each of the monomials is

one of the two terms in $h_1(\ )$. There are precisely

$$\binom{N}{k} = \frac{N!}{k!(N-k)!} \tag{E-4}$$

of these integrals in which the first term of $h_1(\ )$ appears $(N-k)$ times and the second term of $h_1(\ )$ appears k times. We observe that each of these corresponds to one of the ways a light ray can undergo exactly k scatterings in traversing N layers, and that the $\binom{N}{k}$ integrals include all possible ways for this to occur. Now, these $\binom{N}{k}$ integrals are, in fact, identical to each other, because all the double impulses integrate out immediately. Thus each of the integrals reduces to the form

$$g_k(\alpha_N, \beta_N) = (1 - \rho\overline{C_{ext}})^{N-k} (\rho\overline{C_f})^k \cdot f_k(\alpha_N, \beta_N) \quad , \tag{E-5}$$

in which we have defined $f_k(\ )$ as the $(k-1)$-fold convolution of $f_1(\ )$ with itself,

$$f_k(\alpha_N, \beta_N) = \iint\ldots\int d\alpha_{k-1}\ldots d\alpha_1 \iint\ldots\int d\beta_{k-1}\ldots d\beta_1$$
$$\cdot f_1(\alpha_N - \alpha_{k-1}, \beta_N - \beta_{k-1})$$
$$\cdot f_1(\alpha_{k-1} - \alpha_{k-2}, \beta_{k-1} - \beta_{k-2})\ldots f_1(\alpha_1, \beta_1) \quad . \tag{E-6}$$

Note that both Eqs. (E-5) and (E-6) incorporate our present assumption that α_o and β_o are equal to zero. For $k = 0$, we have

$$g_o(\alpha_N, \beta_N) = (1 - \rho\overline{C_{ext}})^N u_o(\alpha_N) u_o(\beta_N) \quad , \tag{E-7}$$

corresponding to the rays which traverse the entire cloud without being scattered. Thus it is consistent to set $f_o(\alpha_N, \beta_N)$ equal to $u_o(\alpha_N) \cdot u_o(\beta_N)$. We can now write the expression

$$I_{k\Delta}(\alpha, \beta) = \binom{N}{k} g_k(\alpha, \beta) \Delta\omega$$
$$= \binom{N}{k} (1 - \rho\overline{C_{ext}})^{N-k} (\rho\overline{C_f})^k f_k(\alpha, \beta) \Delta\omega \tag{E-8}$$

for the average total intensity borne by all the kth-order scattered rays in the solid angle $\Delta\omega$ at (α, β). The coefficient on the right side of Eq. (E-8) may be rewritten as

$$\gamma_f^k \binom{N}{k} (1 - \rho\overline{C_{ext}})^{N-k} (\rho\overline{C_{ext}})^k \quad , \tag{E-9}$$

which has the form of a binomial probability multiplied by γ_f^k. Now, we obtained our results in Chapter 3 in the limit of infinite N. If N is very large and $\rho\overline{C_{ext}}$ is very small, while their product

$$N\rho\overline{C_{ext}} = N_e \tag{E-10}$$

is finite, the Poisson approximation[46] is valid; that is, (E-9) can be approximated as

$$\gamma_f^k \frac{N_e^k}{k!} \exp[-N_e] \quad . \tag{E-11}$$

Equation (E-8) is now

$$I_{k\Delta}(\alpha, \beta) = \gamma_f^k \frac{N_e^k}{k!} \exp[-N_e] \, f_k(\alpha, \beta) \, \Delta\omega \quad . \tag{E-12}$$

Observe that the integral of Eq. (E-12) over all α and β is given by

$$\frac{(\gamma_f N_e)^k}{k!} \exp[-N_e] \quad , \tag{E-13}$$

which we claim to be the total of all k^{th}-order scattered radiation emerging below the cloud. This is identical to a result obtained in Germany in 1941 by Hartel.[29] Observe also that the sum of the terms (E-13) over all k is $\exp[-N_e(1 - \gamma_f)]$, which is near unity. The integral of the un-scattered intensity [Eq. (E-7)] over α and β is $\exp[-N_e]$. We shall avoid the problems engen-dered by the presence of the impulses in Eq. (E-7) by assuming N_e to be large enough that the unscattered radiation is negligible compared with the scattered light. Thus we restrict our at-tention to $k \geqslant 1$ in the analysis below.

Let us interpret $I_{k\Delta}(\alpha, \beta)$ in accordance with the comments following Eq. (4-55). We see that

$$I_{k\Delta}(\alpha, \beta) = \sum w_m \quad , \tag{E-14}$$

a sum of intensity weights of rays in the solid angle $\Delta\omega$ at (α, β), where m ranges over the kth-order scattered rays only. Knowing the single-particle scattering pattern $f_1(\alpha, \beta)$, one could obtain each $I_{k\Delta}(\,)$ by calculating the functions $f_k(\alpha, \beta)$ numerically. A more attractive approach is to use the approximation

$$f_k(\alpha, \beta) \cong \frac{1}{2\pi k W_\alpha^2} \exp\left[-\frac{\alpha^2 + \beta^2}{2k W_\alpha^2}\right] \quad , \tag{E-15}$$

where $W_\alpha^2 = W_\beta^2$ is the width parameter of $f_1(\alpha, \beta)$. This approximation can be very good for reasonably small α and β, even for fairly small k, if $f_1(\,)$ is smooth, unimodal and symmetric. Furthermore, for large N_e the coefficients (E-11) are very small when k is small. Thus we shall use Eq. (E-15) in Eq. (E-12) for all $k \geqslant 1$, when N_e is large. In order to obtain results in a convenient analytic form, we shall specialize the present problem even further by setting

$$\alpha = \beta = 0 \quad . \tag{E-16}$$

Using Eq. (E-15), Eq. (E-12) then becomes

$$I_{k\Delta}(0, 0) = \frac{(\gamma_f N_e)^k}{2\pi W_\alpha^2 \, k \cdot k!} \Delta\omega \exp[-N_e] \quad . \tag{E-17}$$

Despite the extra factor k in the denominator, Eq. (E-17) behaves much like the Poisson prob-abilities. Thus the value of $I_{k\Delta}(0, 0)$ increases monotonically with k up to a maximum, beyond which it decreases monotonically with increasing k. To within a possible error of ±1, the value of k which maximizes $I_{k\Delta}(\,)$ is roughly N_e. This result may be restated as follows: the dom-inant scattering order k_d of the scattered light entering an upward-pointing narrow-beam antenna below a cloud is approximately equal to the cloud optical thickness N_e, rounded off to the nearest integer. For all N_e less than or equal to unity, k_d is equal to unity.

Our next step is to subdivide the rays in the bundle $I_{k\Delta}(\alpha, \beta)$ by path length. We begin by calculating the probability density $p_{\ell_k}(r)$ for the random path length ℓ_k of an arbitrary k^{th}-order scattered ray in the cloud. As we stated in Sec. 3.3, the extinction attenuation $\exp[-r/D_e]$ of a light wave in a cloud can be interpreted as the probability that a light ray traverses a distance r without being scattered. The path length ℓ_1 traversed by a light ray up to the first scattering event it experiences is therefore exponentially distributed, with probability density

$$p_{\ell_1}(r) = \frac{1}{D_e} \exp\left[-\frac{r}{D_e}\right] \quad , \qquad r \geqslant 0 \quad . \tag{E-18}$$

The same probability density applies to the length of the path segment between successive scattering events (which are assumed to be statistically independent of each other). Thus the length ℓ_k of the path from the starting point of the ray to the $(k + 1)^{th}$ scattering event is a gamma-distributed random variable, with

$$p_{\ell_k}(r) = \frac{r^k}{D_e^{k+1}\Gamma(k + 1)} \exp\left[-\frac{r}{D_e}\right] \quad , \qquad r \geqslant 0 \quad . \tag{E-19}$$

This applies, in particular, to a ray whose starting point happens to be at the top of the cloud. Now, suppose the ray emerges from the bottom of the cloud after the kth scattering event, having traversed a total distance ℓ'_k within the cloud. We show that ℓ'_k obeys the probability density [Eq. (E-19)] by the following simple argument. Observe that our assumptions imply that the occurrence of scattering events along the path of a ray, as a function of path length r, is a simple Poisson process with constant average frequency D_e^{-1}. Now, we know that the interval to the occurrence of an event in such a process, measured from an arbitrary point on the coordinate axis, obeys the same probability density whether one looks forward or backward from the point. Similarly, the length of path back to the kth scattering event from the point where the ray emerged from the cloud obeys the same probability density as the distance between any two successive scattering events on the path. Thus the length ℓ'_k of this k^{th}-order scattered path from the point of entrance into the top of the cloud to the point where it emerges from the bottom obeys the probability density [Eq. (E-19)], with one reservation: obviously ℓ'_k exceeds the cloud thickness τ in length. Applying Bayes' rule, we find that

$$p_{\ell'_k}(r \mid \ell'_k \geqslant \tau) = \begin{cases} \dfrac{A_k r^k}{D_e^{k+1}\Gamma(k + 1)} \exp\left[-\dfrac{r}{D_e}\right] & , \quad r \geqslant \tau \quad ; \\ \\ 0 & , \quad \text{elsewhere} \quad , \end{cases} \tag{E-20}$$

with

$$A_k^{-1} = \int_\tau^\infty \frac{r^k}{D_e^{k+1}\Gamma(k + 1)} \exp\left[-\frac{r}{D_e}\right] dr$$

$$= 1 - \sum_{m=k+1}^\infty \left(\frac{\tau}{D_e}\right)^m \frac{1}{m!} \exp\left[-\frac{\tau}{D_e}\right] \quad . \tag{E-21}$$

If we include the distance from the bottom of the cloud to the ground in ℓ'_k, the effect is to translate the probability density [Eq. (E-20)] along the r-axis by a deterministic amount. For

95

the particular case at hand in which the ray emerges traveling essentially vertically downward, the density is translated a distance h, the height of the bottom of the cloud above the ground. Thus Eq. (E-20) becomes

$$p_{\ell_k}(r | \ell_k \geqslant \tau + h) = \frac{A_k (r - h)^k}{D_c^{k+1} k!} \exp\left[-\frac{(r-h)}{D_e}\right] \quad , \quad r \geqslant (\tau + h) \quad . \tag{E-22}$$

A valid interpretation of Eq. (E-22) is the following: of a bundle of many k^{th}-order rays arriving at the ground in the solid angle $\Delta\omega$ about the vertical, a fraction

$$\frac{A_k (\ell - h)^k}{D_e^{k+1} k!} \exp\left[-\frac{(\ell-h)}{D_e}\right] d\ell \tag{E-23}$$

traversed paths of lengths between ℓ and $\ell + d\ell$ (where $\ell \geqslant \tau + h$). Alternately, we may say that a fraction

$$\frac{A_k c^{k+1} (t - \frac{h}{c})^k}{D_c^{k+1} k!} \exp\left[-\frac{(t - \frac{h}{c})}{D_e/c}\right] dt \tag{E-24}$$

experienced a time delay between t and t + dt, where $t \geqslant (\tau + h)/c$ and c is the velocity of light. Now, the total intensity weight of those k^{th}-order rays with time delays between t and t + dt is the product of $I_{k\Delta}(0, 0)$ and the expression (E-24). Adding these products for all $k \geqslant 1$, we find that

$$\frac{\exp[-N_e] c\Delta\omega}{2\pi W_\alpha^2 D_e} \exp\left[-\frac{(t - \frac{h}{c})}{D_e/c}\right] \left\{ \sum_{k=1}^{\infty} \frac{A_k}{k(k!)^2} \left(\frac{\gamma_f N_e (t - \frac{h}{c})}{D_e/c}\right)^k \right\} dt \tag{E-25}$$

is the total intensity weight of all scattered rays in $\Delta\omega$, of all orders, having time delays between t and t + dt [where, again, $t \geqslant (\tau + h)/c$].

Let us now assume that the envelope s(t) of the plane wave illuminating the cloud was such that

$$|s(t)|^2 = 2\delta(t) \quad , \tag{E-26}$$

where $\delta(t)$ is a very short unit-area pulse, as in Sec. 4.4. Recalling the definition of $\sigma(t, \alpha, \beta; \alpha_o, \beta_o) dt$ of Eq. (E-1), we now see that (E-25) is proportional to $\sigma(t, 0, 0; 0, 0) dt$, which we shall abbreviate as $\sigma_o(t) dt$. We have

$$\sigma_o(t) = C_1 \exp\left[-\frac{(t - \frac{h}{c})}{D_e/c}\right] \sum_{k=1}^{\infty} \frac{A_k}{k(k!)^2} \left(\frac{\gamma_f N_e (t - \frac{h}{c})}{D_e/c}\right)^k \tag{E-27}$$

for $t \geqslant (\tau + h)/c$, where C_1 includes everything in (E-25) which is not dependent upon k or t. We require C_1 to be such that

$$\int_0^\infty \sigma_o(t) dt = 1 \quad . \tag{E-28}$$

The term A_k, given by Eq. (E-21), complicates Eq. (E-27) to the extent that we do not know how to carry out the indicated summation. But we notice that A_k varies much more slowly with k than the other factors in the summand, such as $(k!)^2$. Without A_k, the terms in the sum peak up sharply for

$$k \cong \left[\frac{\gamma_f N_e (t - \frac{h}{c})}{D_e/c}\right]^{1/2} \gg N_e \sqrt{\gamma_f} \quad , \tag{E-29}$$

and a few terms with k near this value are much larger than the terms associated with higher or lower values of k. In the interest of obtaining a very rough closed-form approximation for Eq. (E-27), we replace A_k by a constant equal to its value when k is given by Eq. (E-29). This simply modifies the constant C_1. Now, since the important values of k are quite large, replacing the factor k by $(k + 1)$ in the denominator of the summand in Eq. (E-27) is also a reasonable approximation. Thus Eq. (E-27) becomes

$$\sigma_o(t) \cong C_2 \exp\left[-\frac{(t - \frac{h}{c})}{D_e/c}\right] \sum_{k=1}^{\infty} \frac{1}{k!(k+1)!} \left(\frac{\gamma_f N_e (t - \frac{h}{c})}{D_e/c}\right)^k \quad , \tag{E-30}$$

which is precisely equal to

$$C_2 \exp\left[-\frac{(t - \frac{h}{c})}{D_e/c}\right] \left[\frac{2 I_1(v)}{v} - 1\right] \quad , \tag{E-31}$$

where $I_1(\ )$ is the hyperbolic Bessel function of first order and first kind, and

$$v = \left[\frac{4\gamma_f N_e (t - \frac{h}{c})}{D_e/c}\right]^{1/2} \quad . \tag{E-32}$$

Since $t \geqslant (\tau + h)/c$, we have $v \geqslant 2 N_e \sqrt{\gamma_f}$. Letting our attention be restricted to values of N_e greater than about 5, we see that $v \gtrsim 10$. Under this condition the large-argument approximation[47]

$$I_1(v) \cong \frac{e^v}{\sqrt{2\pi v}} \tag{E-33}$$

is valid to better than one percent. Inserting Eq. (E-33) in (E-31), we have

$$\sigma_o(t) \cong \frac{C_2}{2\sqrt{\pi}} \left(\frac{4\gamma_f N_e (t - \frac{h}{c})}{D_e/c}\right)^{-3/4} \exp\left[-\frac{(t - \frac{h}{c})}{D_e/c} + 2\left(\frac{\gamma_f N_e (t - \frac{h}{c})}{D_e/c}\right)^{1/2}\right] \quad . \tag{E-34}$$

This function has a maximum at its left edge,

$$t = \frac{\tau + h}{c} \quad , \tag{E-35}$$

and decreases monotonically with increasing t. A plot of a typical $\sigma_o(t)$ is shown in Fig. E-1.

The most interesting feature of $\sigma_o(t)$ is its width, the multipath spread L. Like the bandwidth of a spectrum, the spread of $\sigma_o(t)$ can be defined in a number of ways. As Kennedy[36] points out, any reasonable definition of the spread parameters (in both time and frequency) is adequate, since they will be used only in an imprecise way in the channel analysis. In this particular case, it is convenient to use a measure which is akin to the $1/e$ width. Noticing that the exponential
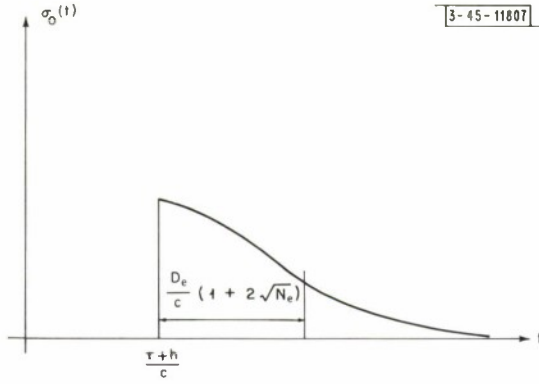
Fig. E-1. Typical scattering function $\sigma_o(t)$.

part of Eq. (E-34) dominates the function, we calculate the value of t for which the exponential is down by $1/e$ from its value at Eq. (E-35). The resulting estimate of the multipath spread is

$$L = \frac{D_e}{c} \left[1 + 2N_e(\gamma_f - \sqrt{\gamma_f}) + 2\sqrt{N_e^2(\sqrt{\gamma_f} - 1)^2 + N_e(2\gamma_f - \sqrt{\gamma_f})} \right] \quad , \qquad (E-36a)$$

which simplifies to

$$L \cong \frac{D_e}{c} [1 + 2\sqrt{N_e}] \qquad (E-36b)$$

when γ_f is very nearly unity, which is generally the case for nearly-lossless particles with the diameter-to-wavelength ratios typical for clouds at visible frequencies.

The determination of $\sigma(t, \alpha, \beta; \alpha_o, \beta_o)$ by means of the approach developed here, for more general illumination on the top of the cloud, will require numerical computation. The next level of generality above Eq. (E-34) is the case in which α_o and β_o are zero but α and β are arbitrary. For this situation we again want to know the quantity $\Sigma\, w_n$ of Eq. (E-1), hence we require knowledge of the terms $I_{k\Delta}(\alpha, \beta)$ in Eq. (E-3) for all scattering orders k. These functions, given by Eq. (E-12), can be computed for given α and β. If N_e is large enough (say, greater than about 5) and $f_1(\alpha, \beta)$ is sufficiently smooth, the Gaussian approximation of Eq. (E-15) for $f_k(\alpha, \beta)$ could be used in Eq. (E-12) when computing the functions $I_{k\Delta}(\alpha, \beta)$. The path lengths ℓ_k for the various values of k will still obey the density functions [Eq. (E-22)], except that we must make the substitution

$$h \rightarrow h \sec\left(\sqrt{\alpha^2 + \beta^2}\right) \quad . \qquad (E-37)$$

We make the same substitution in (E-24), multiply the result by $I_{k\Delta}(\alpha, \beta)$, and add these products numerically for all $k \geqslant 1$, for the desired set of values of t, to obtain a function proportional to $\sigma(t, \alpha, \beta; 0, 0)$. Finally, the proportionality constant must be adjusted so that

$$\int \sigma(t, \alpha, \beta; 0, 0)\, dt = 1 \quad .$$

This quasi-analytical approach becomes far too cumbersome for more general situations. When the cloud illumination is an obliquely incident plane wave, for example, or a narrow beam, one may resort to Monte Carlo simulation of light propagation through the cloud. By this means, it is possible[48] to keep track of the path lengths and intensities of all rays penetrating the cloud as a function of angle, thereby simulating the angle-dependent range scattering function.

98

APPENDIX F
RANGE-DOPPLER SCATTERING FUNCTION $\sigma_o(t, f)$

In this appendix, the range-Doppler scattering function $\sigma_o(t, f)$ is obtained by extension of the analysis leading to $\sigma_o(t)$ in Appendix E. The Doppler spread B is calculated, and the BL product is discussed. In addition, we outline numerical procedures for obtaining the complete scattering function $\sigma(t, f, \alpha, \beta)$ in more general situations.

Our point of departure is Eq. (E-27) in Appendix E, which gives an analytical expression for the range scattering function $\sigma_o(t)$. By assumption, the incident illumination was a vertically incident plane wave with some finite-energy complex envelope s(t). Equation (E-27) was based upon the assertion that, of all the energy arriving in the solid angle $\Delta\omega$ about the direction (0, 0), a fraction

$$C_1 \exp\left[-\frac{(t-h/c)}{D_e/c}\right] \frac{A_k}{k(k!)^2} \left(\frac{\gamma_f N_e(t-h/c)}{D_e/c}\right)^k dt \qquad (F-1)$$

was borne by k^{th}-order scattered rays having time delays between t and t + dt. Now, each of these rays has a random Doppler shift obeying the (approximate) probability density [Eq. (4-74)],

$$p_{f_{dk}}(f) = \frac{1}{\sigma_{f1} \sqrt{2k\pi}} \exp\left[-\frac{f^2}{2k\sigma_{f1}^2}\right] \quad .$$

The product of (F-1) and $p_{f_{dk}}(f)$ df is the fraction of received energy which is borne by k^{th}-order rays having time delays in the range (t, t + dt) and Doppler shifts in the range (f, f + df). The sum of these quantities for all $k \geqslant 1$ is equal to $\sigma_o(t, f)$ dt df. Thus

$$\sigma_o(t, f) = \sum_{k=1}^{\infty} \left\{ \frac{C_1 A_k}{\sigma_{f1} \sqrt{2k\pi} \, k(k!)^2} \left(\frac{\gamma_f N_e(t-h/c)}{D_e/c}\right)^k \cdot \exp\left[-\frac{(t-h/c)}{D_e/c} - \frac{f^2}{2k\sigma_{f1}^2}\right] \right\} \quad , \qquad (F-2)$$

where, again

$$t \geqslant \frac{\tau + h}{c} \quad . \qquad (F-3)$$

We know the shape of this function along the t-axis; it is simply $\sigma_o(t)$, Eq. (E-34). Each section of $\sigma_o(t, f)$ at fixed t is a weighted sum of Gaussian curves in f.

An estimate of the Doppler spread B of $\sigma_o(t, f)$ is reasonably easy to obtain. As we pointed out in Appendix E, any reasonable definition of B is adequate, since it will be used only in an approximate way in the channel analysis. In this case, it is mathematically convenient to calculate it from the definition

$$B = \left[\int_{-\infty}^{\infty} \sigma_o^2(f) \, df\right]^{-1} \qquad (F-4)$$

used by Kennedy,[36] in which

$$\sigma_o(f) = \int_{-\infty}^{\infty} \sigma_o(t, f) \, dt \qquad (F-5)$$

Integrating Eq. (F-2) over t, we have

$$\sigma_o(f) = \sum_{k=1}^{\infty} \frac{C_1(D_e/c)\,(\gamma_f N_e)^k}{k \cdot k!\, \sigma_{f1}\, \sqrt{2k\pi}} \exp\left[-\frac{f^2}{2k\sigma_{f1}^2}\right] \quad . \tag{F-6}$$

We determine the value of C_1 by noting that

$$\int_{-\infty}^{\infty} \sigma_o(f)\, df \equiv 1$$

$$= \sum_{k=1}^{\infty} \frac{C_1(D_e/c)\,(\gamma_f N_e)^k}{k \cdot k!}$$

$$\cong \sum_{k=1}^{\infty} \frac{C_1(D_e/c)\,(\gamma_f N_e)^k}{\gamma_f N_e (k+1)\,!}$$

$$\cong \frac{C_1(D_e/c)}{\gamma_f N_e} \exp[\gamma_f N_e] \quad . \tag{F-7}$$

Notice that two small terms were dropped in making the final step in Eq. (F-7). This approximation depends upon the assumption that $\gamma_f N_e$ is large (at least 5, and often much greater), so that $\exp[-\gamma_f N_e] \ll 1$. Equation (F-7) implies that

$$C_1 = \frac{c\gamma_f N_e}{D_e} \exp[-\gamma_f N_e] \quad . \tag{F-8}$$

Inserting Eq. (F-8) into Eq. (F-6), we find that

$$\int_{-\infty}^{\infty} \sigma_o^2(f)\, df = \exp[-2\gamma_f N_e] \cdot \sum_{m=1}^{\infty} \sum_{n=1}^{\infty} \frac{(\gamma_f N_e)^{m+n+2}}{m \cdot m! \cdot n \cdot n!\, \sigma_{f1}\, \sqrt{2\pi(m+n)}} \quad . \tag{F-9}$$

Again invoking the fact that the important terms in Eq. (F-9) are those for which m and n are near $\gamma_f N_e$, we make the approximation

$$\sqrt{m+n} \cong \sqrt{2\gamma_f N_e} \quad . \tag{F-10}$$

Equation (F-9) then becomes

$$\int_{-\infty}^{\infty} \sigma_o^2(f)\, df \cong \frac{\exp[-2\gamma_f N_e]}{\sigma_{f1}\, \sqrt{4\pi\gamma_f N_e}} \cdot \sum_{m=1}^{\infty} \sum_{n=1}^{\infty} \frac{(\gamma_f N_e)^{m+1}}{(m+1)!} \frac{(\gamma_f N_e)^{n+1}}{(n+1)!}$$

$$\cong (2\sigma_{f1}\, \sqrt{\pi\gamma_f N_e})^{-1} \quad , \tag{F-11}$$

whereupon Eq. (F-4) yields the result

$$B \cong 2\sigma_{f1}\, \sqrt{\pi\gamma_f N_e} \quad . \tag{F-12}$$

Let us make a rough estimate of σ_{f1}, so that we can examine the BL product of $\sigma_o(t,f)$. Equation (4-78) of Chapter 4 states that

$$\sigma_{f1} = \frac{2f_o^2}{3c^2} \overline{V_r^2} \int_o^{\pi/2} 2\pi \sin\Theta \, f(\Theta) \, [1 - \cos\Theta] \, d\Theta \quad , \tag{F-13}$$

where f_o is the carrier frequency and $\overline{V_r^2}$ is the mean-square value of the random particle velocity. If we assume that $\sin\Theta \, f(\Theta)$ becomes very small as Θ approaches $\pi/2$, it is reasonable to make the approximation

$$1 - \cos\Theta \cong \frac{\Theta^2}{2} \tag{F-14}$$

in Eq. (F-13). The integral then becomes

$$\pi \int_o^{\pi/2} \Theta^2 \sin\Theta \, f(\Theta) \, d\Theta \quad , \tag{F-15}$$

which is precisely the integral of Eq. (B-19) in Appendix B for the average single-particle scattering pattern width parameter

$$W_\alpha^2 = \overline{\alpha^2} \quad . \tag{F-16}$$

By making this substitution in Eq. (F-13), we find that

$$\sigma_{f_1} \cong W_\alpha \, \frac{f_o}{c} \, \sqrt{\frac{2}{3} \overline{V_r^2}} \quad , \tag{F-17}$$

whereupon Eq. (F-12) becomes

$$B \cong 2W_\alpha \, \frac{f_o}{c} \left[\frac{2\pi\gamma_f N_e \overline{V_r^2}}{3} \right]^{1/2} \quad . \tag{F-18}$$

Assuming that γ_f is very nearly unity, we multiply Eq. (F-18) by the multipath spread [Eq. (E-36b)] derived in Appendix E to obtain the channel time-bandwidth product

$$BL \cong 2 \sqrt{\frac{2\pi}{3}} \, \frac{\tau W_\alpha}{\lambda_o} \, \frac{(\overline{V_r^2})^{1/2}}{c} \left[2 + \frac{1}{\sqrt{N_e}} \right] \quad . \tag{F-19}$$

As we shall indicate in Appendix G, the channel is often overspread (BL >> 1) for typical sets of cloud parameters.

In more general situations, the determination of $\sigma(t, f, \alpha, \beta)$ for a small solid angle $\Delta\omega$ does not lend itself to analytical calculation. Numerical computation will generally be necessary. This is relatively easy when the incident illumination is a modulated uniform plane wave with $\alpha_o = \beta_o = 0$, but α and β are arbitrary. We carry out the steps detailed in the paragraph following Eq. (E-36) in Appendix E, up to the substitution (E-37). The product of (E-24) and $I_{k\Delta}(\alpha, \beta)$ is then multiplied by $p_{f_{dk}}(f)$, Eq. (4-79), and the result is summed over all $k \geqslant 1$ for the desired set of values of f and t. When the configuration is more complicated, one must again resort to a Monte Carlo simulation.
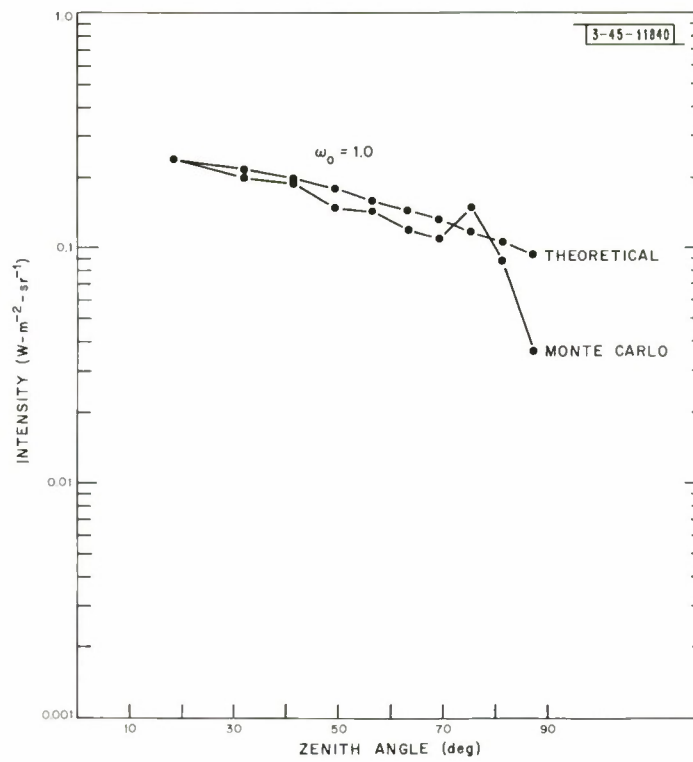
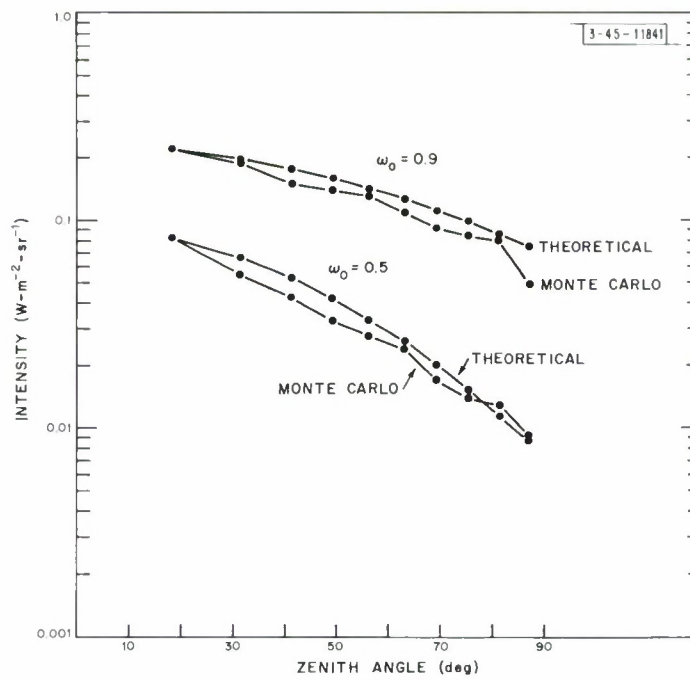Fig. G-1. Vertical incidence, $N_e = 10$, $\omega_o = 1.0$.

Fig. G-2. Vertical incidence, $N_e = 10$, $\omega_o = 0.9$ and 0.5.

APPENDIX G
COMPARISON OF RESULTS WITH PUBLISHED WORK

As we commented earlier, the recent literature contains a number of reports of both theoretical and experimental work on various specialized aspects of multiple scattering. In many instances it is not feasible to make explicit comparisons between the published work and the results of the present study, because the corresponding physical configurations differ drastically. For example, Reisman, et al.[2] have carried out measurements of light scattered by dense artificial fogs, but they observed the scattered light through a window in the side of the fog chamber.

An experimental study which is potentially well suited for comparison with our results was carried out by Smart, et al.[15] Their scattering chamber was a thin rectangular glass-walled cell containing a water suspension of polystyrene latex spheres that had an average diameter of 1.305 microns. They carried out measurements of scattered intensity vs angle of arrival for optical thicknesses ranging from 0.03 to 78.5. There are two obstacles to the convenient comparison of their data with our results. First, we need to know the average single-particle scattering-pattern width parameter W_α of the particles they used. Although the author of this report has not done so, one could presumably obtain an approximate value for this parameter by numerical integration of their measured intensity patterns for very small optical thicknesses. The other obstacle, which is considerably more troublesome, is an anomaly which appears in their measured curves for optical thicknesses greater than about 10. Although all these curves have a generally Gaussian shape, as we would predict, their widths are virtually independent of optical thickness. They are all down by a factor of 0.25 at the same angle, roughly 65 degrees. As the authors of the report point out, this may be due to the finite width of their receiving beam. At the larger angles of observation, it was presumably viewing unilluminated regions of the scattering cell, causing the measured power levels to be low. Indeed, the techniques evolved in the present study allow us to take account of this behavior, but the necessary computational labor would be odious.

Zaborowski[30] has carried out some experimental work of a preliminary nature, using equipment which closely resembled our assumed cloud model of Fig. 3-1 in Sec. 3.1. His scattering particles were suspended in water in a broad, shallow Plexiglas tank illuminated from above by a laser beam, with a narrow-beam measuring apparatus below it. He measured the scattered light intensity below the tank as a joint function of lateral displacement and angle of arrival. Using a scattering medium of dilute homogenized milk in one case, and polystyrene latex spheres in another, he obtained results which showed substantial qualitative similarity to the Gaussian joint impulse response $h_p(\alpha, \beta, x, y)$ we derived in Sec. 3.5.

The author has calculated a series of curves from the results of this study which show rather striking agreement with certain Monte Carlo results reported by Plass and Kattawar.[19-22] The specific curves that we consider are given in Figs. 12 and 13 of Ref. 19 and Fig. 4 of Ref. 21, all of which correspond to our angular impulse response $h_I(\ )$ of Chapter 3. Dr. Plass has kindly provided full-page copies of the figures to permit reading off the values with greater precision. The results are presented in Figs. G-1 through G-4. In each case, values were calculated only for those angles for which Monte Carlo data were given. The calculated results were all smaller by modest scale factors, as we explain below, but have been re-scaled as necessary for convenience in visual comparison of the curve shapes. Figure G-1 represents the intensity as a function of zenith angle below an idealized laminar cloud of optical thickness $N_e = 10$, illuminated
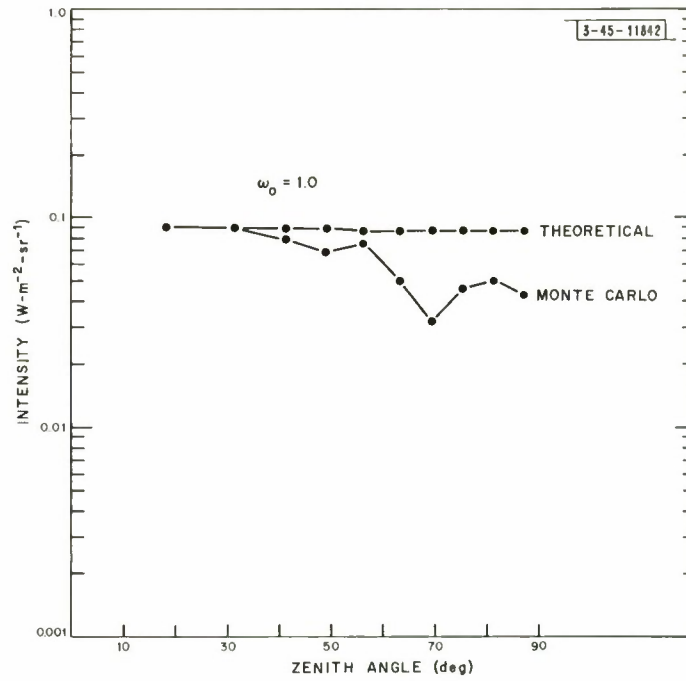
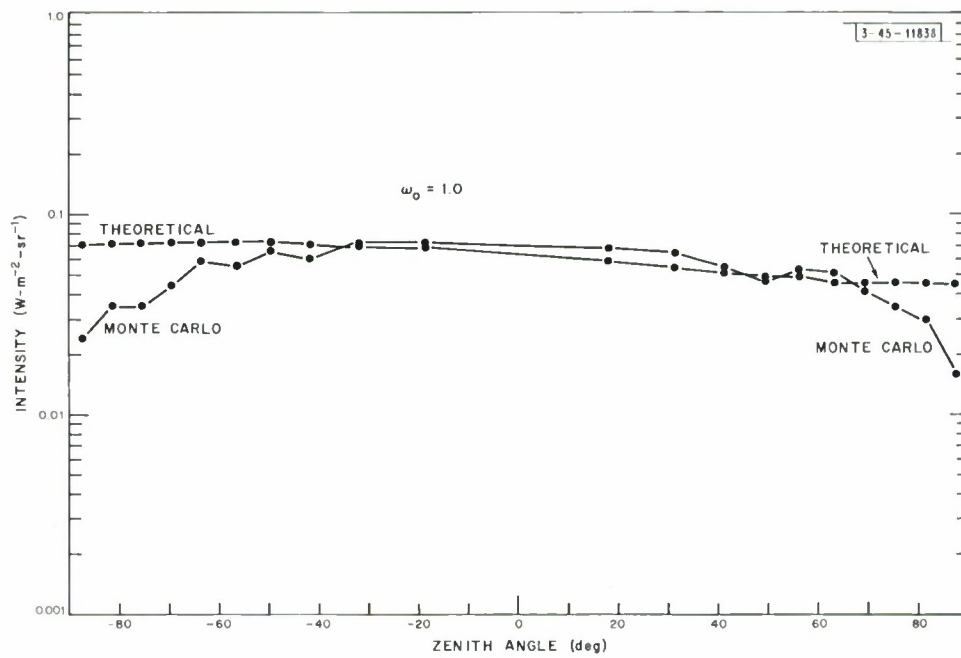Fig. G-3. Vertical incidence, $N_e = 30$, $\omega_o = 1.0$.

Fig. G-4. Incidence at 60°, $N_e = 10$, $\omega_o = 1.0$.

by a vertically incident uniform plane wave with unit intensity at 0.7-micron wavelength. The assumed particle size distribution was Deirmendjian's cumulus cloud distribution function,[3] which peaks at a particle radius of 4 microns. The single-particle albedo (called ω_o by Plass and Kattawar) was assumed to be unity for this curve, meaning that the particles were nonabsorptive. The curve marked "Monte Carlo" is that of Plass and Kattawar, while the curve marked "Theoretical" was calculated from our results in a manner to be described below.

The assumed conditions for Fig. G-2 were identical to those of Fig. G-1, except that ω_o was given the value 0.9 (upper curves) and 0.5 (lower curves). Thus the particles were assumed to be lossy, with each of them absorbing a fraction $(1 - \omega_o)$ of the power incident upon it. The conditions related to Fig. G-3 were identical to those of Fig. G-1, except that the optical thickness N_e was set equal to 30. The assumed conditions for the curves of Fig. G-4 were the same as in Fig. G-1, but the plane-wave illumination was incident at an angle of 60 degrees relative to the zenith.

We observe an obvious characteristic of all four figures: each pair of curves shows remarkably good agreement near the zenith, but at larger angles the Monte Carlo curves begin to fluctuate and (except for the case with $\omega_o = 0.5$ in Fig. G-2) to fall below the theoretical curves. There are two reasonable explanations for this behavior. First we note (as Plass and Kattawar did in Ref. 19) that fluctuations must necessarily occur in any Monte Carlo simulation, simply because the number of calculations is finite. One expects the fluctuations to be more severe at large angles in the multiple-scattering simulations, because the number of photons which are scattered through large angles is relatively smaller. The second phenomenon which could contribute to the upward deviation of the theoretical curves at large angles relates to the technique we used to solve the (N-1)-fold superposition integral [Eq. (3-56)] for the angular impulse response of the cloud. As we explain in the paragraph immediately below Eq. (3-56), it would be reasonable to set the result of each successive convolution in the equation to zero outside the range.

$$(\alpha^2 + \beta^2) \leqslant (\frac{\pi}{2})^2 \quad , \tag{G-1}$$

in accordance with our assumption that all upward-scattered radiation is lost. But the impulse response [Eq. (3-72)], which we used to calculate the theoretical curves in Figs. G-1 through G-4, was obtained by letting all integration limits be $\pm \infty$ in Eq. (3-56). Had we been willing to include the series of truncations at $\pi/2$ in our solution of Eq. (5-36), the result might have been similar to the slight tailing off at large angles exhibited by the Monte Carlo curves.

As we stated above, the specific result of the present study which corresponds to these curves is the angular impulse response [Eq. (3-72)] of Sec. 3.4,

$$h_I (\alpha, \beta; \ \alpha_o, \beta_o) = \frac{\exp[-N_e(1 - \gamma_f)]}{2\pi\sigma_\alpha^2} \ \exp\left[- \frac{(\alpha - \alpha_o)^2 + (\beta - \beta_o)^2}{2\sigma_\alpha^2} \right] \quad , \tag{G-2}$$

which is the angular intensity distribution function below a cloud illuminated by a single unit-intensity plane wave with angle of arrival (α_o, β_o). The quantity N_e is the optical thickness of the cloud, and the average single-particle forward-scattering efficiency γ_f is the fraction of the power incident on a particle which is scattered through angles less than $\pi/2$. The variance is

$$\sigma_\alpha^2 = \gamma_f N_e W_\alpha^2 \quad , \tag{G-3}$$

in which W_α is the average single-particle scattering pattern width parameter defined by Eq. (3-42). The author has computed the value of W_α for these calculations by numerical integration of the average scattering pattern[3] for the particle size distribution used by Plass and Kattawar; the result is

$$W_\alpha \cong 0.295 \text{ radian}$$

$$= 16.9 \text{ degrees} \quad . \tag{G-4}$$

The value of γ_f obtained from the same data, assuming the particles to be lossless, was

$$\gamma_f = 0.96 \quad . \tag{G-5}$$

The theoretical curves in the first three figures in this appendix represent the function

$$g(\Theta) = \frac{\Theta}{\sin \Theta} \frac{\exp[-N_e(1 - \gamma_f)]}{2\pi\gamma_f N_e W_\alpha^2} \exp\left[-\frac{\Theta^2}{2\gamma_f N_e W_\alpha^2}\right] , \tag{G-6}$$

which is the transformation to polar coordinates of Eq. (G-2) with $\alpha_0 = \beta_0 = 0$. For Fig. G-1, with $N_e = 10$ and W_α and γ_f given by Eqs. (G-4) and (G-5), the value of Eq. (G-6) at $\Theta = 0$ was smaller by a factor of 0.685 than the value obtained by Plass and Kattawar. We are unable to give a reasonable explanation for this problem. The theoretical curve was rescaled to the same height as the Monte Carlo curve, to facilitate comparison of the shapes of the functions.

For the upper curves in Fig. G-2, Plass and Kattawar assumed that each particle scattered a fraction

$$\omega_0 = 0.9 \tag{G-7}$$

of the power incident on it, absorbing the remainder. The appropriate value of γ_f is therefore

$$\gamma_f = 0.96 \, \omega_0$$

$$\cong 0.864 \quad . \tag{G-8}$$

The value of Eq. (G-6) at $\Theta = 0$ in this case was smaller by a factor of 0.582 than the Monte Carlo results.

For the lower curves in Fig. G-2, with $\omega_0 = 0.5$, the correct value of γ_f was 0.48. At $\Theta = 0$ the value of Eq. (G-6) was 0.0235 of the Monte Carlo figure. It would be presumptuous to attribute this severe discrepancy to a possible scale error in the Monte Carlo result. But we remark that the number of photons penetrating to the ground, which is proportional to the transmitted intensity, was much smaller in this case than in the other Monte Carlo simulations.

The theoretical curve in Fig. G-3 corresponds to $N_e = 30$ and $\gamma_f = 0.96$. The value of Eq. (G-6) at the origin was smaller by a factor of 0.215 than the Monte Carlo curve.

In order to compute the theoretical curve of Fig. G-4 the cloud impulse response [Eq. (G-2)] was modified in a rather obvious manner. Since the incident light arrived at an angle 60 degrees below the vertical, the direct rays had to traverse an optical distance

$$\sec 60° = 2.0 \tag{G-9}$$

times greater than the assumed optical thickness of 10 measured vertically through the cloud. We therefore used an effective optical thickness

$$N_e = 10 \sec 60° = 20$$

in Eq. (G-2). As in the previous case with $\omega_o = 1$, we set $\gamma_f = 0.96$. Assuming that the scattered intensity was measured in the plane formed by the vertical line and the incident direction, we set

$$\alpha_o = \Theta_o = -60° \quad ,$$

$$\beta = \beta_o = 0 \qquad\qquad\qquad\qquad\qquad\qquad\qquad\qquad\qquad\qquad (G-10)$$

in Eq. (G-2) and transformed it into polar coordinates, to obtain

$$g(\Theta) = \frac{(\Theta - \Theta_o)}{\sin(\Theta - \Theta_o)} \cdot \frac{\exp[-N_e(1 - \gamma_f)]}{2\pi\gamma_f N_e W_\alpha^2} \exp\left[-\frac{(\Theta - \Theta_o)^2}{2\gamma_f N_e W_\alpha^2} \right] \quad . \qquad (G-11)$$

The value of Eq. (G-11) at $\Theta = \Theta_o$ was smaller by a factor of 0.592 than the corresponding Monte Carlo value in Fig. G-4.

A recent paper by Dell-Imagine[18] addressed the problem of optical communication through clouds. His approach involved approximate numerical solution of Chandrasekhar's equation of radiative transfer. He assumed that a finite beam of light was vertically incident upon the top of an idealized laminar cloud similar to that of the present study, and calculated the measured power as a function of receiver beamwidth at a point on the ground directly below the center of the incident beam. He obtained these results for a variety of incident-beam radii, cloud optical thicknesses, and cloud heights h above the receiver. A set of three curves computed from our results of Sec. 3.5 is compared in Fig. G-5 with corresponding curves from Dell-Imagine's Fig. 17. The optical thickness N_e of the cloud was 5.0, and the assumed particle size distribution was the "haze M" distribution of Deirmendjian.[3] Since the author had not computed W_α for this particle distribution, its value was so adjusted that the uppermost calculated curve in Fig. G-5 coincided with the corresponding one in Dell-Imagine's data.
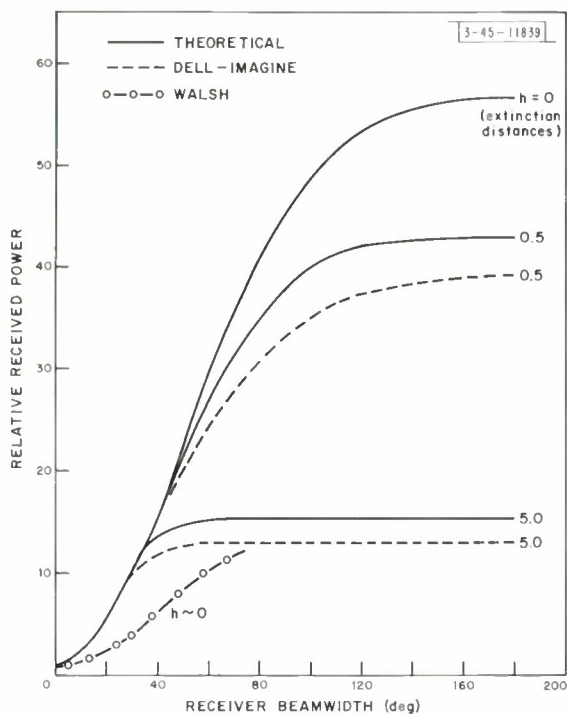

Fig. G-5. Received power vs receiver beamwidth.

These curves can be described in terms of Eq. (5-3) in Sec. 5.1 of this report,

$$P_G(\alpha, \beta, 0, 0) = \exp[-N_e(1 - \gamma_f)] \quad [4\pi^2 \sigma_{\alpha s}^2 \sigma_{xs}^2 (1 - \rho_{\alpha xs}^2)]^{-1}$$

$$\exp\left[-\frac{1}{2(1 - \rho_{\alpha xs}^2)} \frac{\alpha^2 + \beta^2}{\sigma_{\alpha s}^2}\right] , \tag{G-12}$$

in which

$$\sigma_{\alpha s}^2 = \gamma_f N_e W_\alpha^2 \quad ;$$

$$\sigma_{xs}^2 = \sigma_i^2 + \sigma_{\alpha s}^2 (\frac{\tau^2}{3} + \tau h + h^2) \quad ;$$

$$(1 - \rho_{\alpha xs}^2) = \frac{\sigma_{\alpha s}^2 (\tau^2/12) + \sigma_i^2}{\sigma_{xs}^2} . \tag{G-13}$$

The parameters τ and h, the thickness and the height above ground of the cloud, were both normalized by Dell-Imagine to the extinction distance D_e of the cloud. We therefore do the same in these calculations. Equation (G-12) is the scattered intensity at (α, β) below a cloud, at coordinates $x = y = 0$, in response to a unit-power vertically-incident beam at $x_o = y_o = 0$. The incident beam intensity is symmetric and Gaussian in x and y, with "variance" parameter σ_i^2. Dell-Imagine let the incident beam be uniform over a circle of radius 0.5 extinction distances in computing these curves; hence, we set $2\sigma_i$ equal to 0.5. A receiving antenna with uniform gain over a beam of width 2ψ, illuminated by Eq. (G-12), receives

$$\int_{(\alpha^2 + \beta^2) \leqslant \psi} P_G(\alpha, \beta, 0, 0) \, d\alpha \, d\beta = \frac{\exp[-N_e(1 - \gamma_f)]}{2\pi \sigma_{xs}^2}$$

$$\times \left[1 - \exp\left(\frac{-\psi^2}{2\sigma_{\alpha s}^2 (1 - \rho_{\alpha xs}^2)}\right)\right] \tag{G-14}$$

watts of power per unit aperture area. This is the equation used to compute the theoretical curves in Fig. G-5. Its dependence upon h enters in via the quantities σ_{xs}^2 and $(1 - \rho_{\alpha xs}^2)$. The vertical axis in Dell-Imagine's graph was labeled "percent transmission," but he did not explain how it was defined; therefore, we simply renormalized (G-14) so that our curve coincided with his for h = 0. The curve labeled "h ~ 0" in Fig. G-5 represents experimental data measured by Walsh[49] in an endeavor to substantiate Dell-Imagine's results.

While the curves of Fig. G-5 show substantial agreement, certain other results of Dell-Imagine depart drastically from ours. In his Figs. 18 through 26, he plots time step responses of the cloud, corresponding to the power measured by a receiver below the cloud when the incident illumination is turned on at some instant of time. He computes the rise time of the power transported to the receiver by single-scattered light, and then uses a rather tenuous argument to conclude that the rise time of the multiple-scattered power is of the same order. As an example of these results, he indicates in his Fig. 20 that the rise time is about 0.002 of the time required to propagate through the cloud, for an optical thickness of 5.0 and a receiver beamwidth of 5 degrees. Now, we showed in Sec. 4.4 and Appendix E that the range scattering function $\sigma(t)$

under similar circumstances (for an upward-pointing narrow-beam antenna) had a multipath spread

$$L \cong \frac{D_e}{c} [1 + 2 \sqrt{N_e}] \quad . \tag{G-15}$$

The function $\sigma(t)$ can be interpreted as an impulse response; the step response is the integral of $\sigma(t)$, and its rise time is roughly equal to L. As a fraction of the time

$$\frac{\tau}{c} = \frac{D_e N_e}{c} \tag{G-16}$$

required to propagate through the cloud, the rise time is roughly

$$\frac{1 + 2\sqrt{N_e}}{N_e} = 1.1 \quad . \tag{G-17}$$

This is in sharp contrast to Dell-Imagine's result. Note also that Plass and Kattawar[19] found that the average total path length traversed by transmitted photons was comparable to or greater than twice the vertical distance through the cloud.

It is worthwhile to list some numerical values for typical cloud parameters. As we shall see below, they indicate that the results of this study are valid for a broad range of naturally occurring clouds. Table G-1 is a rough composite of cloud data obtained from four references,[50-53] each of which includes material from a variety of sources. The clouds of type 1 are fair-weather cumulus, the woolly individual masses usually associated with "partly cloudy" weather. Type 2 clouds are the medium-height widespread overcasts (including cirrus, cirrostratus, altostratus and altocumulus) which often foreshadow prolonged precipitation. The clouds of type 3 include stratus and stratocumulus, the low watery overcast which becomes fog when it touches the ground. In view of Eq. (2-2) et seq. in Sec. 2.2, we calculate approximate values for the extinction distances D_e in these clouds by means of the formula

$$D_e = (2\pi a_m^2 d_v)^{-1} \quad , \tag{G-18}$$

in which a_m is one of the particle radii in Table G-1. We find that typical values for D_e lie in the range of about 20 to 100 meters. The larger particle sizes are generally associated with the smaller volume concentrations, tending to decrease the range of D_e. Thus the clouds of types 2 and 3, presumably the ones of greatest interest in optical communication applications, have optical thicknesses N_e ranging from perhaps 5 to 50, with the larger values being rather less common.

TABLE G-1 CLOUD DATA				
Cloud Type	Particle Concentration d_v (cm^{-3})	Mode Radius a_m (microns)	Thickness (meters)	Height above Ground (meters)
1	100 to 300	4 to 10	700 to 2000	100 to 2000
2	100 to 400	5 to 10	~1000	>1000
3	100 to 300	4 to 6	<1000	100 to 2000

It must be emphasized that the above numerical values are quite crude, being intended only as guidelines. The design of a receiver for optical communication through clouds in a particular locality will naturally depend upon extensive knowledge of local meteorological data.

The single-particle scattering pattern width parameter W_α appears to be almost invariant to particle size, for particles typically found in clouds. Using precise numerical computations[54] of the Mie scattering pattern of water droplets, the author has calculated W_α in accordance with Eq. (3-42) for ten different radii, ranging from about 3 to 12 microns. Following no discernible pattern, W_α varied within 6 to 7 percent of the 16.9-degree value used in the earlier calculations in this appendix. Similarly, values calculated for γ_f fell within about 0.008 of the value 0.96, for the same range of particle sizes. To be sure, the half-power beamwidths of the scattering patterns decreased with increasing radius, but this had little effect on γ_f or the "standard deviation" parameter W_α.

REFERENCES

1. H.C. van de Hulst, _Light Scattering by Small Particles_ (Wiley, New York, 1957).

2. E. Reisman, et al., "Comparison of Fog Scattered Laser and Monochromatic Incoherent Light," Appl. Opt. 6, No. 11, 1969-1972 (November 1967).

3. D. Deirmendjian, "Scattering and Polarization Properties of Water Clouds and Hazes in the Visible and Infrared," Appl. Opt. 3, No. 2, 187-196 (February 1964).

4. R.S. Kennedy, private communication.

5. H.C. van de Hulst, op. cit.

6. G. Mie, Ann. Physik 25, 377 (1908).

7. R.G. Newton, _Scattering Theory of Waves and Particles_ (McGraw-Hill, New York, 1966).

8. S. Chandrasekhar, _Radiative Transfer_ (Clarendon Press, Oxford, 1950).

9. V.V. Sobolev, _A Treatise on Radiative Transfer_, Transl. by S.I. Gaposchkin (Van Nostrand, New York, 1963).

10. S. Fritz, "Scattering and Absorption of Solar Energy by Clouds," Sc.D. Thesis, Massachusetts Institute of Technology, Cambridge (1953).

11. _____, "Scattering of Solar Energy by Clouds of Large Drops," J. Meteorol. 11, 291-300 (August 1954).

12. _____, "Illuminance and Luminance under Overcast Skies," J. Opt. Soc. Am. 45, 820-825 (October 1955).

13. L.W. Carrier and L.J. Nugent, "Comparison of Some Recent Experimental Results of Coherent and Incoherent Light Scattering with Theory," Appl. Opt. 4, 1457-1462 (November 1965).

14. E. Reisman, et al., loc. cit.

15. C. Smart, et al., "Experimental Study of Multiple Light Scattering," J. Opt. Soc. Am. 55, No. 8, 947-955 (August 1965).

16. D.H. Woodward, "He-Ne Laser as Source for Light Scattering Measurements," Appl. Opt. 2, 1205-1207 (November 1963).

17. _____, "Multiple Light Scattering by Spherical Dielectric Particles," J. Opt. Soc. Am. 54, 1325-1331 (November 1964).

18. R.A. Dell-Imagine, "A Study of Multiple Scattering of Optical Radiation with Applications to Laser Communication," in _Advances in Communication Systems_, Vol. II, Ed. by V.A. Balakrishnan (Academic Press, New York, 1966), pp. 1-50.

19. G.N. Plass and G.W. Kattawar, "Influence of Single Scattering Albedo on Reflected and Transmitted Light from Clouds," Appl. Opt. 7, 361-367 (February 1968).

20. _____, "Monte Carlo Calculations of Light Scattering from Clouds," Appl. Opt. 7, 415-419 (March 1968).

21. _____, "Radiant Intensity of Light Scattered from Clouds," Appl. Opt. 7, 699-704 (April 1968).

22. G.W. Kattawar and G.N. Plass, "Influence of Particle Size Distribution on Reflected and Transmitted Light from Clouds," Appl. Opt. 7, 869-878 (May 1968).

23. J.A. Stratton, _Electromagnetic Theory_ (McGraw-Hill, New York, 1941).

24. H.C. van de Hulst, op. cit., p. 423.

25. Ibid., pp. 231-232.

26. H.J. Aufm Kampe and H.K. Weickmann, "Physics of Clouds," Meteorol. Mono. 3, 182-225 (July 1957).

27. W. Feller, _An Introduction to Probability Theory and Its Applications_, Vol. I, (Wiley, New York, 1957), p. 143.

28. J.A. Stratton, op. cit.

29. W. Hartel, Licht 10, 141 (1941).

30. J.S. Zaborowski, S.M. Thesis, Department of Electrical Engineering, Massachusetts Institute of Technology, Cambridge (1968).

31. W. Feller, op. cit., Vol. II, p. 254.

32. Ref. 4.

33. H.L. VanTrees, Detection, Estimation, and Modulation Theory, Part 2 (Wiley, New York, to be published in 1969).

34. E.V. Hoversten, private communication.

35. C.W. Allen, Astrophysical Quantities (Athlone Press, University of London, 1955).

36. R.S. Kennedy, Performance Limits for Fading Dispersive Channels, (Wiley, New York, to be published in May 1969).

37. B.M. Oliver, "Signal-to-Noise Ratios in Photoelectric Mixing," Proc. IRE 49, No. 12, 1960-1961 (December 1961).

38. C.W. Helstrom, "Detectability of Coherent Optical Signals in a Heterodyne Receiver," J. Opt. Soc. Am. 57, No. 3, 353-361 (March 1967).

39. L.I. Bluestein and R.L. Greenspan, "Efficient Approximation of Orthogonal Waveforms," Group Report 1964-48, Lincoln Laboratory, Massachusetts Institute of Technology (3 November 1964), DDC 451755, H-616.

40. W.W. Peterson, Error-Correction Codes (Massachusetts Institute of Technology Press, Cambridge, 1961).

41. G.W. Kattawar and G.N. Plass, loc. cit.

42. Ref. 4.

43. J. W-S. Liu, "Reliability of Quantum-Mechanical Communication Systems," Sc. D. Thesis, Department of Electrical Engineering, Massachusetts Institute of Technology, Cambridge (September 1968).

44. J.M. Wozencraft and I.M. Jacobs, Principles of Communication Engineering (Wiley, New York, 1965) pp. 111-114.

45. H.M. Heggestad, "Angle-of-Arrival Dispersion of a Plane Wave Traversing a Two-Dimensional Cloud," Quarterly Progress Report No. 90, Research Laboratory of Electronics, Massachusetts Institute of Technology (15 July 1968), pp. 169-174.

46. W. Feller, loc. cit.

47. P.M. Morse and H. Feshbach, Methods of Theoretical Physics (McGraw-Hill, New York, 1953), p. 1323.

48. G.N. Plass, private communication.

49. D.H. Walsh, "Laboratory Measurement of Multiple Scattering of Coherent Optical Radiation by a Nonabsorbing Aerosol," Appl. Opt. 7, No. 6, 1212-1219 (June 1968).

50. B.J. Mason, The Physics of Clouds (Clarendon Press, Oxford, 1957).

51. N.H. Fletcher, The Physics of Rainclouds (University Press, Cambridge, 1962).

52. W.G. Durbin, "Droplet Sampling in Cumulus Clouds," Tellus 11, No. 2, 202-215 (1959).

53. F. Singleton and D.J. Smith, "Some Observations of Drop-size Distributions in Low Layer Clouds," J. Roy. Meteorol. Soc. 86, 454-467 (1960).

54. A. Holland, private communication.

DOCUMENT CONTROL DATA - R&D

(Security classification of title, body of abstract and indexing annotation must be entered when the overall report is classified)

1. ORIGINATING ACTIVITY *(Corporate author)*	2a. REPORT SECURITY CLASSIFICATION
Lincoln Laboratory, M.I.T.	Unclassified
	2b. GROUP
	None

3. REPORT TITLE

Optical Communication Through Multiple-Scattering Media

4. DESCRIPTIVE NOTES *(Type of report and inclusive dates)*

Technical Report

5. AUTHOR(S) *(Last name, first name, initial)*

Heggestad, Harold M.

6. REPORT DATE	7a. TOTAL NO. OF PAGES	7b. NO. OF REFS
22 November 1968	120	54

8a. CONTRACT OR GRANT NO.	9a. ORIGINATOR'S REPORT NUMBER(S)
AF 19(628)-5167	TR-454
b. PROJECT NO. 649L	
c.	9b. OTHER REPORT NO(S) *(Any other numbers that may be assigned this report)*
d.	ESD-TR-68-354

10. AVAILABILITY/LIMITATION NOTICES

This document has been approved for public release and sale; its distribution is unlimited.

11. SUPPLEMENTARY NOTES	12. SPONSORING MILITARY ACTIVITY
None	Air Force Systems Command, USAF

13. ABSTRACT

A model is developed for the effects of multiple scattering upon optical-frequency radiation. Attention is focused upon situations in which the scattering particles are large compared to the carrier wavelength, so that forward-scattering predominates. This is the case for atmospheric clouds at visible-light wavelengths, the physical framework within which the analysis is carried out. The objectives served by the model are those of a communications engineer desiring to design a system for optical communication through clouds.

Light traversing optically dense clouds suffers dispersion in space, time and frequency. These effects are considered both separately and in a compact unified formulation. The spatial variation of the intensity of light beneath a cloud subjected to continuous-wave illumination is modeled as the output of a multidimensional linear system. The approximate impulse response of the system is determined, in two complementary forms, and the approximate response below the cloud under arbitrary illumination is shown to be given by a linear superposition integral. In general, the spatial behavior is representable as a joint function of angle of arrival and horizontal coordinates over the ground.

The field on the ground is shown to be representable in terms of a complex Gaussian random process. A complete statistical description of the process is therefore provided by its mean (which is zero) and its correlation function. The time-space correlation function $K(t_1, t_2, \vec{r}_1, \vec{r}_2)$ is written in terms of a generalized scattering function $\sigma(\tau, f, \vec{v})$, combining all the time, frequency and spatial information. The spatial impulse responses are shown to be special cases of the scattering function. Expressions are derived for the spatial correlation function of the received field over the ground, for both omnidirectional and directive antennas. The conventional range-Doppler scattering function $\sigma(\tau, f)$ is derived for an upward-pointing narrow-beam antenna. Polarization effects are not included in any of the analysis.

Some of the implications of these results are considered with respect to communications system design and performance. A system is proposed and analyzed to provide an indication of the rates and error performance that can be achieved with optical signaling through a cloud.

14. KEY WORDS

optics
optical communications
optical-frequency radiation
optical systems

multiple scattering
fading dispersive channels
time-frequency scattering function